Aus der

Medizinischen Klinik und Poliklinik V

Klinikum der Ludwig-Maximilians-Universität München

Direktor: Prof. Dr. med. Jürgen Behr

Neutrophils drive fascia matrix mobilization and regulate wound healing through ferroptosis

Dissertation

Zum Erwerb des Doktorgrades der Humanbiologie

an der Medizinischen Fakultät der

Ludwig-Maximilians-Universität München

Vorgelegt von

Jiakuan ZHAO

aus

Jining, China

Jahr

2024

Mit Genehmigung der Medizinischen Fakultät der

Ludwig-Maximilians-Universität München

Erstes Gutachten:	Prof. Dr. med. Jürgen Behr
Zweites Gutachten:	Prof. Dr. Anne Hilgendorff
Drittes Gutachten:	PD Dr. Andreas Ohlmann
Dekan:	Prof. Dr. med. Thomas Gudermann
Tag der mündlichen Prüfung:	30.10.2024

Table of content

Zusammenfassung **9**

Abstract **11**

1 Introduction **13**

1.1 Skin Structure and Function 13

1.1.1 Animal Models for Skin Research 14

1.1.2 Novel Approaches to Study Skin Biology in Vitro. 14

1.2 Wound Healing Phases 15

1.2.1 Wound Healing Process 15

1.2.2 Chronic and Non-Healing Wounds 17

1.2.3 Scarring 18

1.3 Neutrophil Function in Wound Healing 18

1.3.1 The Dynamics of Immune Cells during Wound Healing 18

1.3.2 The Contribution of Neutrophils 19

1.4 Ferroptosis 20

1.4.1 Ferroptosis in Skin Neutrophils 21

1.4.2 Ferroptosis in Other Skin Cells 21

2 Methods **25**

2.1 Human Samples 25

2.2 ER-Hoxb8 Cells Culture 25

2.3 Mice 25

2.4 Genotyping 26

2.5 Mouse Model of Full-thickness Excisional Wounds 27

2.6 Fascia Explant Assay 28

2.7 Flow Cytometric Analysis of Bone Marrow Cells 28

2.8 Flow Cytometry-based Cell Viability Assay 30
2.9 Cell Viability Quantification with CytoTox-One 31
2.10 Cellular Lipid Peroxide Detection with BODIPY 32
2.11 Masson's Trichrome Staining 33
2.12 Immunostaining 33
2.13 Matrix Mobilization assay 34
2.14 Image Analysis 34
2.15 Western blot Analysis 35
2.16 Re-analysis of RNA Sequencing Data 35
2.17 Single Cell RNA Sequencing 35
2.18 scRNA-seq Data Analysis 36

3 Results 41

3.1 Ferroptosis in Neutrophil 41
3.1.1 Neutrophil Culture from Immortal Progenitors 41
3.1.2 Phenotype of Differentiated ER-Hoxb8 Cells 42
3.1.3 The Maturation of Differentiated ER-Hoxb8 Cells 42
3.1.4 Ferroptosis in Neutrophils 45
3.2 Functional consequences of Ferroptotic Neutrophil in wound healing 47
3.2.1 Matrix Mobilization is Impaired by Ferroptosis Neutrophil. 47
3.2.2 Matrix Migration Caused by Primary Neutrophils. 48
3.2.3 Granular Proteins Dynamic Post Maturation 49
3.3 Neutrophil Ferroptosis in Wound Repair and Surgical Adhesion 50
3.3.1 Ferroptosis Activity at Skin Wound. 50
3.3.2 Neutrophil Ferroptosis in Diabetic Foot Ulcers 51
3.3.3 Neutrophil Ferroptosis in Mouse Wound Model 52
3.4 Immune Cells at Murine Wound 53

3.4.1 Immune Cells Recruited into Wound. 53
3.4.2 Quality Control and Filtering of Single Cells 54
3.4.3 High Variable Gene and Dimensional Reduction 55
3.4.4 Characteristics of Immune Cells at The Wound 56
3.4.5 scRNA-seq analysis of Ferroptosis of Wound infiltrated Immune Cells 57
3.5 Ferroptosis in Neutrophils 59
3.5.1 Neutrophil Subsets in Wounds 59
3.5.2 Dynamics of Neutrophil Subset Maturation 60
3.5.3 Interaction Between Neutrophils and Fibroblasts 61
3.6 Ferroptosis in Neutrophils regulates Fascia Mobilization 61
3.6.1 Fascia Contraction with Neutrophil ferroptosis 61
3.6.2 The Effect of Ferroptosis Inhibition on Wound Healing 64
3.6.3 Matrix Remodeling at Wound Site 65
4 Discussion 67
4.1 Maturation and Development of Neutrophils in Peripheral Tissue 67
4.2 Interaction between Neutrophils and Fibroblasts 67
4.3 Heterogeneity of Neutrophils in Tissue 69
4.4 Ferroptotic Neutrophil in Wound healing 70
5 Reference 71
6 Abbreviations 83
Acknowledgment 87
Publications 89
Affidavit 90

Zusammenfassung

Die Wundheilung der Haut ist ein komplexer Prozess, der mehrere Phasen umfasst, die jeweils aus unterschiedlichen Zelltypen und molekularen Mechanismen bestehen. Die subkutane Faszie, die die obere Schicht der Dermis mit dem darunter liegenden Muskel verbindet, dient als Hauptquelle für narbenbildende Fibroblasten und Narbengewebe. Bei einer Verletzung wird die subkutane Faszie, die eine extrazelluläre Bindegewebsmatrix, Neutrophile, Nerven und Blutgefäße enthält, in das Wundbett transportiert. In dieser Studie identifizieren wir einen Zusammenhang zwischen der Anwesenheit von Neutrophilen und der Aktivierung und dem Transport von Faszien, wodurch eine Schlüsselrolle für Neutrophile bei der frühen Wundheilung aufgedeckt wird. Hier haben wir ER-Hoxb8-Zellen, eine immortalisierte Vorläuferzelllinie für Granulozyten-Monozyten, verwendet, um differenzierte Neutrophile in vitro zu erzeugen. ER-Hoxb8-Zellen durchlaufen denselben Differenzierungsprozess wie bei der Neutrophilenvorläuferdifferenzierung, die aus dem Knochenmark isoliert wurde. Wenn sie mit Faszienexplantaten kokultiviert werden, induzieren die reifen Neutrophilen, aber nicht die unreifen, die Matrixmigration ex vivo. Wir zeigen, dass die Anzahl der reifen Neutrophilen durch intrinsische ferroptotische Wege streng reguliert wird. Während die Blockierung der Ferroptose in Neutrophilen den ferroptotischen Stress lindert und die Faszienkontraktion ex vivo verlangsamt, beschleunigt die Ferroptoseinduktion den Wundverschluss bei exzisionellen murinen Wunden in vivo. Zusammenfassend unterstützen unsere Daten einen Mechanismus, bei dem die Schwellenwerte, Differenzierungsstadien und Aktivierungsstatus der Neutrophilen in Wunden durch ferroptotische Signale gesteuert werden, die wiederum die Faszienmobilisierung und die Wundheilung initiieren.

Abstract

Skin wound healing is a complex process involving multiple phases, each of which is choreographed by distinct cell types and molecular mechanisms. The subcutaneous fascia, which connects the upper layer of the dermis to the underlying muscle, serves as a main source of scar-forming fibroblasts and scar tissue. When wounded, the subcutaneous fascia, containing extracellular connective tissue matrix, neutrophils, nerves, and blood vessels, is transported into the wound bed. In this study, we identify a link between the presence of neutrophils and fascia activation and transportation, unravelling a key role for neutrophils in early wound healing. Here, we utilized ER-Hoxb8 cells, an immortalized granulocyte-monocyte progenitor cell-line, to generate differentiated neutrophils in vitro. ER-Hoxb8 cells undergo the same differentiation process as seen in neutrophil progenitor differentiation isolated from the bone marrow. When cocultured with fascia explants, the mature neutrophils, but not immature ones, induce matrix migration ex vivo. We show that the numbers of mature neutrophils are tightly regulated by intrinsic ferroptotic pathways. Whereas blocking ferroptosis in neutrophils alleviates ferroptotic stress and slows down fascia contraction ex vivo, ferroptotic induction accelerates wound closure in excisional murine wounds in vivo. In conclusion, our data supports a mechanism whereby neutrophil thresholds, differentiation stages, and activation statuses, in wounds are governed by ferroptotic signals, that in turn initiate fascia mobilization and wound healing.

1 Introduction

1.1 Skin Structure and Function

The skin is a well-organized multilayered and the largest organ in mammalian and human body. It consists mainly of the outermost epidermis, underlying dermis and innermost fascia connective tissue (Correa-Gallegos et al., 2023). The epidermis is composed of keratinocytes which form a barrier to external microorganisms and chemicals (Brohem et al., 2011). The underlying dermis provide mechanical and structural support for physiological homeostasis and is composed mainly of fibroblasts and extracellular matrix. The dermis also provides various nutrition for epidermis and circulating cells, which support thermal regulation, and immune response (Brohem et al., 2011). Beneath the dermis lies the subcutaneous fat, which contains several layers of superficial fascia (Jiang & Rinkevich, 2021), a specialized viscoelastic sheet of connective tissue that assists with mechanical support and facilitate the gliding between the skin and underlying skeleton muscle.

Similar to human skin, the skin of mice is also organized into multiple layers, including epidermis, dermis, subcutaneous fat, panniculus carnosus muscle and subcutaneous fascia, and it provides the same barrier function to protect body from external factors, for example pathogens, UV radiation (Guénet et al., 2012). Both mice and humans have a similar epidermal structure, with a stratum corneum consisting of corneocytes bound to the corneodesmosomes and lamellar lipids to provide the main barrier function (Proksch et al., 2008). The dermis of both species contains fibroblasts, collagen, and elastin fibers, together with vessels and nerves.

However, many differences exist in the skin structure and functions between humans and mice, in various aspects. For example, skin in humans is much thicker than in mice, especially its epidermis and dermis (Duverger & Morasso, 2014). Another part, hair morphogenesis and pattern distribution in mice is different than in human skin (Duverger & Morasso, 2014), as well as hair follicle cycle (Teichert et al., 2011). Furthermore, rete ridges, the epithelial extensions projecting into dermis, create a growth environment for epidermal stem cells, a feature absent in mouse skin (Lin et al., 2019). Moreover, the subcutaneous fascia, a loosely areolar connective tissue serving as a matrix scaffold for vessels and nerves beneath dermis, located underneath the adipose tissue and panniculus carnosus muscle layers in rodents, contrasting with the tightly interlaced subcutaneous fat found in human (Jiang & Rinkevich, 2021).

1.1.1 Animal Models for Skin Research

Animal models are commonly utilized to study skin development, wound healing, and pathogenesis of skin-related diseases. Among all animal models, mouse models are most popular because of its genetic similarity to humans and feasibility of transgenic modifications. However, several factors should be taken into consideration before considering mouse models for skin research (Quigley et al., 2009). Firstly, as stated above, the structure and function of mice do not perfectly resemble that of humans; secondly, genetic background of mice can vary, which may affect the reverence of finding to human skin (Quigley et al., 2009).

To overcome these limitations, a common approach uses humanized mice, where functional human immune cells are engrafted into mice (Brehm et al., 2013). This technique has been already widely used in small pre-clinical animal models for studying human diseases. However, it is important to note that immunocompromised mice do not represent the exact bacterial microenvironment and cellular complexity as in humans (Youn et al., 2020).

Besides murine models, porcine skin has also been extensively employed for investigation (Jiang et al., 2018; Khiao In et al., 2019; Ranamukhaarachchi et al., 2016). Histological and ultrastructural assessments of epidermis and dermis of porcine skin have demonstrated remarkable similarities to human skin, which is beneficial for the evaluation of various treatments for wound healing and skin barrier function (Khiao In et al., 2019). Additionally, porcine skin has been instrumental in developing skin substitutes for tissue engineering and regenerative medicine applications (Halim et al., 2010).

1.1.2 Novel Approaches to Study Skin Biology in Vitro.

Taking full advantage of in vitro and in vivo models is critical to fully understanding of the biology of mammalian skin and to develop effective therapies for skin abnormalities. The architecture of human skin can be synthesized through tissue engineering techniques. For example, 3D bioprinting allows fabrication of synthetic skin by incorporating keratinocytes, the main cells in the epidermis, and fibroblasts, the main cells in the dermis, as well as collagen to mimic dermal matrix (Ng et al., 2018). Moreover, human skin substitutes, created by mixing fibrin-agarose biomaterials and human cells obtained from skin biopsies in vitro, were used for infrared microspectroscopy imaging (Ionescu et al., 2020).

One such model is termed SCAD, standing for “scar-like tissue in a dish”. In SCAD, ex vivo skin explant includes all skin layer down to the subcutaneous fascia and is cultured outside of the body over 5 days (Correa-Gallegos et al., 2023; Jiang et al., 2020). SCAD formed a

plug of scars originated from fascia fibroblast were enhanced when inducing with TGF-β1 (Wan et al., 2021). In addition, fascia, a connective tissue that is present in the deepest compartments of skin, maintains organ structure and integrity strictly (Jiang et al., 2020). Ex vivo fascia culture has been used to investigate the behaviors of cells and ECM in real time over the days, providing a valuable model into wound healing (Correa-Gallegos et al., 2023). Fascia cultures enable tracking the dynamics of single cells and the dynamics of fascia ECM over days relative to SCAD maintaining most skin structure and cell types (Correa-Gallegos et al., 2023; Jiang & Rinkevich, 2021). Using these methods, our lab revealed that RUNX2 fibroblasts are associated with ECM production and remodeling, suggesting a role for mechanical loading in fascia tissue with repair (Correa-Gallegos et al., 2023). Overall, ex vivo fascia cultures have the potential to provide valuable insights into the properties and behavior of fascia tissue, as well as to facilitate the development of new treatments for fascia-related disorders.

1.2 Wound Healing Phases

Skin wound healing encompasses several distinct but overlapping stages or phases to facilitate explanation in context, which includes hemostasis at early beginning, inflammation, proliferation, and remodeling (Gurtner et al., 2008).

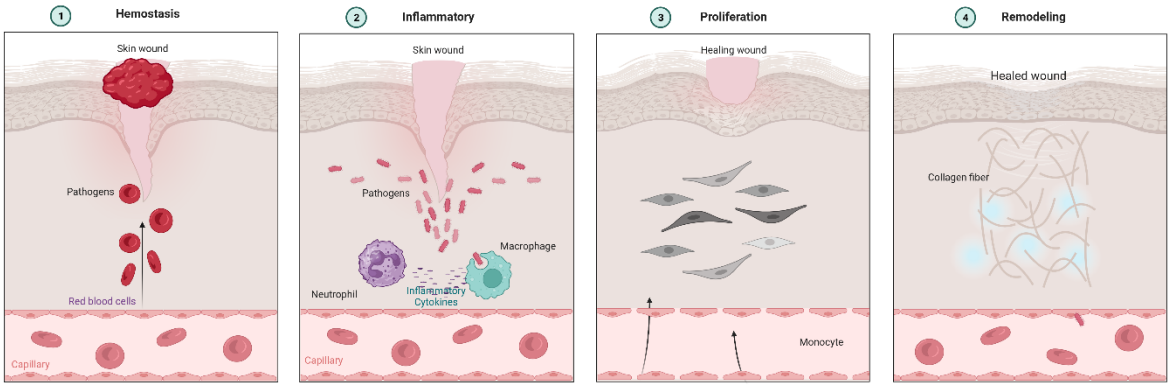

Figure 1.1 Illustration of wound healing phases. Wound healing processing includes four stages: hemostasis, inflammation, proliferation, and remodeling.

1.2.1 Wound Healing Process

Wound healing is initiated with a hemostasis phase by abundant fibrin clot formation at injury. The clot provides a provisional scaffold for recruiting inflammation cells from distal vessels to wound bed (Gurtner et al., 2008).

Next, the wound started into an inflammatory phase. Wherein damaged tissues release chemokines attracting white blood cells to the wound bed and fascia (Guo & Dipietro, 2010;

Gurtner et al., 2008). These cells combat bacterial and fungal infections and eliminate debris of apoptotic or necrotic cells from the wound bed. Additionally, vessels in the vicinity of the wound contract in order to limit bleeding, and subsequently dilate to enhance blood flow into the wound, bringing oxygen and nutrients to support healing (Guo & Dipietro, 2010). This phase is vital for tissue repair, which promote cell proliferation and regeneration during the healing stages (Guo & Dipietro, 2010). However, absence of inflammatory effectors or prolonged inflammation can result in delayed wound healing and the development of nonhealing chronic wounds because of wound microbiome, the microorganisms that reside within a wound after injury (Gay et al., 2020; Misic et al., 2014). Studies revealed that chronic wounds harbor an abundance of bacteria, including *Staphylococcus aureus*, *Pseudomonas aeruginosa*, and *Enterococcus faecalis,* which challenges for antibiotic treatment *(Johnson et al., 2018)*. Utilization of antibiotics disrupts the microbial balance, providing chance of overgrowth for antibiotic-resistant bacteria and biofilm formation (Fulton et al., 1997).

In the second proliferative phase that follows or overlaps with inflammation, new tissue propagates to the wound bed and fills in damaged region (Guo & Dipietro, 2010) Specially, fibroblasts produce collagen that imparts strength and structural support. Blood vessels extend and stretch into the wound depth, supply abundant oxygen and nutrients for new emerging tissue, and facilitate new connective tissue development (Guo & Dipietro, 2010).

Subsequently, the third phase involves tissue remodeling. The newly connective tissue undergoes remodeling and reinforcement (Guo & Dipietro, 2010). Immature collagen fibers are rearranged under physical forces and cross-link with each other to enhance tissue integrity, while excess cells are eliminated from the wound (Guo & Dipietro, 2010). The resulting tissue usually does not exhibit the same biomechanical strength as the original tissue but restores skin function. Overall, the process of wound healing involves interplay of various cells and chemical signals.

Following skin injury, the ECM undergoes significant remodeling to facilitate proper tissue repair and regeneration (Tang et al., 2022). During ECM remodeling, myofibroblasts, which are the main executors of ECM synthesis and remodeling, are essential components contributing to wound healing and fibrosis (Correa-Gallegos et al., 2023). The remodeling of ECM involves intricate communication between various molecules, such as integrins, growth factors, and matrix metalloproteinase (MMPs) like MMP14, enzymes actively degrade and remodeling ECM (Tang et al., 2022). One key player in wound healing is fibronectin, an adhesive molecule that participates in ECM formation and re-epithelialization (Grinnell, 1984). Additionally, WNT, which serves as signaling molecules, contributes to ECM

remodeling throughout the wound healing process (Diller & Tabor, 2022). The activation of fibroblasts is stimulated by inflammatory cytokines, resulting in the synthesis of fibrillary collagen—a structural protein of the wound (Whyte et al., 2012). The interplay between inflammatory factors, ECM composition, and mechanical stress determines the wound's phenotype after injury (Whyte et al., 2012). It is worth noting that disordered ECM were common mechanisms in both wound healing defects and cancers, which is clearly reflected from specific proteomic analysis on ECM (Ljubimov & Saghizadeh, 2015). In summary, proper ECM remodeling is necessary for successful tissues repair and regeneration.

Therefore, deep understanding of the cellular and molecular events in each wound healing phase will pave the way to develop effective therapeutic strategies that optimize wound healing outcomes.

1.2.2 Chronic and Non-Healing Wounds

Chronic and non-healing wounds pose significant challenges in healthcare, which are characterized by a prolonged inflammatory phase, impaired angiogenesis, and abnormal extracellular matrix remodeling, resulting in chronic wounds that are not fully closed over three months (Misic et al., 2014). Several factors, like dysregulated immune responses, high level of blood glucose, peripheral vascular disease, bacterial biofilms, and disrupted growth factor signaling, contribute to the development of chronic and non-healing wounds, and associated complications (Misic et al., 2014). For example, insulin resistance, resulting to metabolic disorders like type 2 diabetes and obesity, negatively affects wound healing by disrupting glucose and lipid metabolism, inducing chronic inflammation, and altering adipokine secretion and adipocyte function (Abdelsaid et al., 2022). Topical application of insulin cream can activate AKT and ERK signaling pathways, leading to accelerated wound healing in diabetic patients (Lima et al., 2012). Furthermore, the use of a hydroalcoholic extract of Teucrium polium has been found to improve wound healing in diabetic rats (Ardestani et al., 2008). Moreover, zinc deficiency has also been identified as a factor that delays wound healing, highlighting the significance of zinc in the metabolic response during wound healing (Lansdown et al., 2007).

Hence, managing chronic and non-healing wounds requires a multidisciplinary approach. It involves strategies such as wound debridement to remove nonviable tissue, infection control, and the use of advanced wound dressings and therapies like growth factors, stem cells, and matrix metalloproteinase inhibitors (Nowak et al., 2022). In conclusion, wound healing is a complex process with several challenges and addressing underlying medical conditions and optimizing therapeutic approaches are also important in promoting wound healing.

1.2.3 Scarring

Scarring is a natural part of the healing process that occurs when tissues or organs experience trauma, injury, or undergo surgery (Jagdeo & Shumaker, 2017). Scars form when the skin or other tissues need to heal at a faster rate than normal skin growth (Jagdeo & Shumaker, 2017). Although scarring is commonly associated with the skin, it can affect various organs throughout the body (Jagdeo & Shumaker, 2017). However, the mechanisms that govern scar formation are still largely unknown.

In the context of skin, scars are an undesired outcome of wound healing. Human skin transplanted onto mice can result in proliferative scars that exhibit morphological and histological characteristics like human hypertrophic scars (Alrobaiea et al., 2016). Skin scarring has functional and aesthetic implications, brings a major psychological and physiological concern to the patients and brings huge socioeconomic burdens to the healthcare systems (Paratz et al., 2012). Further research requires a deeper understanding of the mechanisms involved in tissue fibrosis and scarring to develop more effective treatments for scar prevention and/or reduction.

1.3 Neutrophil Function in Wound Healing

1.3.1 The Dynamics of Immune Cells during Wound Healing

Immune cells are a crucial component in the initiation and development of wound healing. The initial inflammatory phase involves migration of neutrophils and macrophages, towards the injury sites (Devalaraja et al., 2000). Moreover, innate immune cells express Toll receptors (TLRs) recognizing pathogen-associated molecular patterns (PAMPs) as well as damage-associated molecular patterns (DAMPs) released from injured tissues, which removes pathogenic and damaged cells (Leoni et al., 2015). Dysfunction of innate immune cells results in delayed wound closure or excessive scar formation (Leoni et al., 2015).

Macrophages, accumulating at the wound site during the acute phase of wound healing, plays a dual role (Gay et al., 2020). Macrophages activate inflammatory responses, but they also act as scavengers, clearing away proinflammatory cellular debris and promoting tissue regeneration (Gay et al., 2020). The versatility of macrophages is evident as they adapt their functions in immunity, metabolism, and wound healing based on their specific location within tissues and the surrounding inflammatory environment (Gay et al., 2020). Predominant macrophage phenotype switching from a pro-inflammatory state to a pro-reparative state facilitate wound healing (Kotwal & Chien, 2017). In addition, macrophages also produce growth factors, such as VEGF, contributing to the formation of fibrovascular scars (He &

Marneros, 2013). In addition to macrophages, innate lymphoid cells (ILCs) also play a vital role in wound healing and tissue repair (Boothby et al., 2020).

Though, inflammation, fibrogenesis, and proteolysis remodels of the extracellular matrix and increases of tensile strength during the process of cutaneous wound healing, the inflammatory response may lead to an excessive production of inflammatory mediators by immune cells that fail to respond to the initial triggers (Gay et al., 2020). This dysregulation becomes problematic and hinders the resolution of wound healing.

1.3.2 The Contribution of Neutrophils

Neutrophils, recruited by pro-inflammatory factors such as IL-8, are the rapid response cells that reach the wound site in the first wave, eliminating invasive microorganisms, foreign material, and cell debris (Dovi et al., 2003). However, in the case of diabetic wounds, accumulated neutrophils, initiated by chemokines including IL-8 from keratinocytes, has been demonstrated to delay healing (Hosseini Mansoub, 2021; Hosseini Mansoub, 2022). Hence, it suggests that neutrophils might hinder the wound repair process, if their numbers in wounds are out of control. Neutrophilic inflammation caused by IL-17A, released by $\gamma\delta$ T cells but not Th17 cells, extends the healing process via persistent infiltrating neutrophils in wounds (Takagi et al., 2017). In the absence of commensal microbiota, the accumulation of neutrophils was greatly reduced, resulting in rapid reepithelization, and accelerated and scarless wound healing in germ-free mice. Moreover, the depletion of neutrophils in diabetic mice showed accelerated wound closure by 50% (Canesso et al., 2014; McDaniel et al., 2013).

Neutrophil apoptosis and neutrophil extracellular traps (NETs) are major neutrophil cellular events that greatly impact wound healing process with their unique mechanisms. NETs are decondensed chromatin that are actively throw out by neutrophils. These chromatin networks are decorated with cytotoxic proteins, performing their anti-microbial functions (Martinod & Wagner, 2014). However, uncontrolled excessive NETs formation blocks wound healing by amplifying neutrophilic inflammation, hindering microvascular reperfusion by trapping platelets and increasing fibrin deposition (Korkmaz et al., 2017).

Neutrophils subsequently undergo apoptosis in the wound, which is eventually resolved through macrophage engulfment, allowing the wound to proceed into the next healing phase (Wang et al., 2022). Hence, neutrophil infiltration and resolution in a timely manner is a main determinant of successful wound healing (Jin et al., 2020). Dysregulated neutrophil death, such as impaired apoptosis in aberrant aged neutrophils, contribute to the pathogenesis of chronic or non-healing ulcers, pulmonary fibrosis, and cystic fibrosis (Gray et al., 2018; Hu et

al., 2023). Delayed neutrophil apoptosis may also extend inflammation and fibrosis via NETs formation (Gray et al., 2018). Additionally, the deactivation of AKT signaling in neutrophils causes chronic spontaneous cell death, which proved a way to medullated neutrophil homeostasis and resolution of inflammation (Jia et al., 2007). Hyperbaric oxygen therapy (HBOT) reduces inflammatory cytokines in diabetic ulcers and chronic wounds and significantly decreases neutrophil recruitment which promotes healing in patients (Baiula et al., 2020). Hence, chronic wounds either arise from persistent neutrophil accumulation with chronic inflammation or from insufficient neutrophil activates that are unable to control microbial infection (Gay et al., 2020).

1.4 Ferroptosis

Ferroptosis, distinct form of regulated cell death such as apoptosis and necrosis, is characterized by iron-dependent lipid peroxidation and accumulation of reactive oxygen species (ROS) in the cytoplasm (Lei et al., 2019). Unlike apoptosis and necrosis, ferroptosis is governed by unique molecular mechanisms and exhibits specific morphological features. Emerging evidence implicates dysregulated ferroptosis in the pathogenesis of various diseases, including cancer, ischemia-reperfusion injury, kidney dysfunction, and hematological disorders (Kim et al., 2022; Ma et al., 2022; Yang & Yang, 2022). Notably, in the tumor microenvironment, induction of ferroptosis in cancer cells turned out to be a new way to eliminate and treat tumor resistance (Kim et al., 2022). Consequently, modulating ferroptosis has garnered significant attention as a promising therapeutic approach.

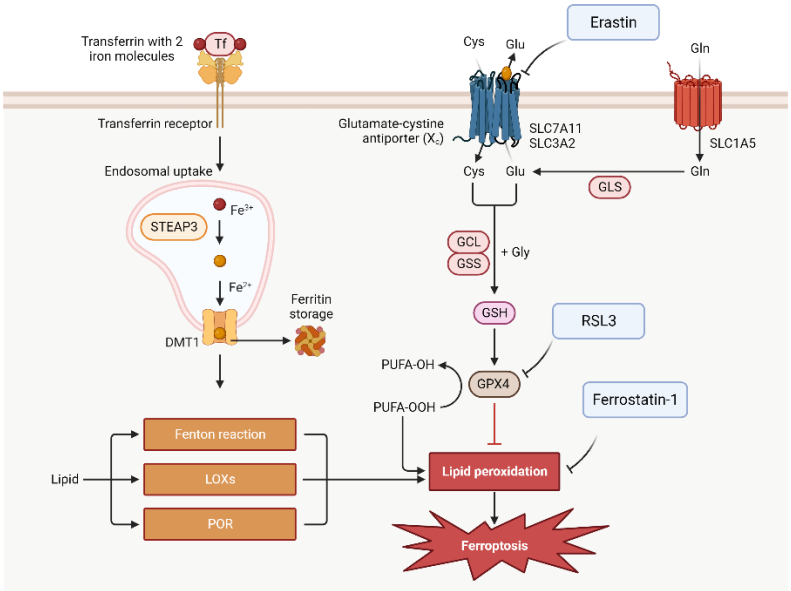

Figure 1.2 General mechanism of ferroptosis pathway. Iron with help from transferrin were transferred into cells then released into cytoplasm after endosomal uptake. Lipid ROS were induced by iron through Fenton reaction or LOXs pathway. Cystine is transported by Xc to cells and reduced into

cysteine. GPX4 reduces lipid ROS production by GSH-GSSG cycle. Ferroptosis inducers, like Erastin and RSL3, block Xc-GPX4 axis, and lead to cellular ferroptosis (Tang et al., 2021).

1.4.1 Ferroptosis in Skin Neutrophils

Neutrophils were demonstrated to undergo ferroptosis in both lupus-prone mouse or patients with systemic lupus erythematosus (SLE), a chronic autoimmune disease characterized by a red rash on the skin (P. Li et al., 2021). In SLE patients, abnormal neutrophils lead to impaired phagocytosis, aggregation of cell debris, and accelerated cell death. Meanwhile, the cell counts, and viability of neutrophils correlated strongly with pathologic activity of SLE patients and SLE mouse model (MRL/lpr and NZB/W F1 mice) (P. Li et al., 2021). The blockage of IFN-α2, one of highly expressed serum cytokines in SLE patients, rescued neutrophil numbers and viability by restoring GPX4 expression in neutrophils (P. Li et al., 2021). Moreover, Liproxstain-1, an efficient inhibitor of ferroptosis, but not inhibitors of NETs with Cl-amidine, improved disease status in line with blocking IFN (P. Li et al., 2021). Therefore, the enhancement of disease through ferroptosis-mediated neutrophils provides a potential avenue for therapeutic treatment.

Interestingly, tumor neutrophils induced lipid peroxides and iron accumulation in tumor cells via transfer myeloperoxidase across cells (Yee et al., 2020). Nonetheless, neutrophils within tumors undergo ferroptosis and manifest immunosuppression, a condition reshaped by the induction of ferroptosis within the tumor environment (Kim et al., 2022). Downregulation of GPX4 in tumor neutrophils caused by the accumulation of PEoX, peroxidized phosphatidylethanolamine, may explain the increased sensitivity of ferroptosis (Kim et al., 2022). In any case, inhibition of ferroptosis will protect neutrophils from immune suppressive factors.

In conclusion, while many theories did not consider the role of neutrophil death, the paradigm of ferroptosis in neutrophils at the core of pathogenesis underscores the significance of targeting ferroptosis in the treatment of skin and other diseases.

1.4.2 Ferroptosis in Other Skin Cells

Skin cells maintain ferroptosis defense functions by expressing GPX4, which regulates the synthesis of glutathione (GSH) to glutathione disulfide (GSSG), and cystine/glutamate antiporter, termed system Xc (M. Liu et al., 2022). Recent studies have shown that ferroptosis serves as an initiating factor of skin inflammation following exposure to ultraviolet B radiation (UVB) (Vats et al., 2021). Apart from UVB irradiation, ferroptosis has been linked to various cutaneous diseases, including neoplastic diseases, genetic skin disease, and autoimmune diseases (L. Liu et al., 2022). In psoriasis vulgaris, ferroptosis activation

induced cell death across all layers of the epidermis and triggered inflammation in keratinocytes (Zhou et al., 2022). Notably, cigarette smoke cause ferroptosis in female skin, activating multiple miRNAs and transcription factors (TFs) associated ferroptosis (Zhang et al., 2022). Moreover, signatures related to ferroptosis have been examined for predicting overall survival in melanoma patients via LASSO Cox regression (Zeng et al., 2021). Overall, these studies suggest that ferroptosis plays a crucial role in skin health and disease.

Although the exact mechanisms of ferroptosis have not yet been fully uncovered, references suggest that ferroptosis has emerged as a potential therapeutic target for various skin diseases (Li et al., 2023; Stockwell, 2022; Wu et al., 2021; Zhang et al., 2023). For example, a recent review reported that ferroptosis acted as potential therapeutic target for inflammatory-associated intestinal diseases, with implications for skin diseases such as psoriasis and atopic dermatitis (Zhang et al., 2023).

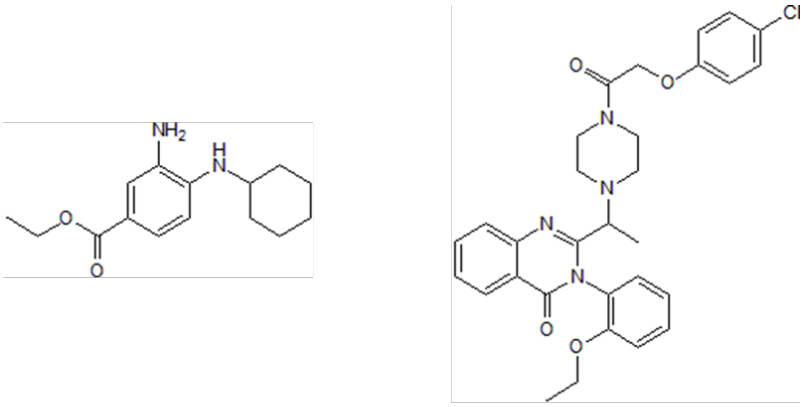

Figure 1.4 Ferrostatin-1 (Fer) is a small molecule compound initially identified through a high-throughput screening process aimed at discovering novel inhibitors of ferroptosis (Dixon et al., 2012). Fer is thought to directly or indirectly interfere with the process of lipid peroxidation and enhance the activity of the System Xc- antiporter, leading to increased glutathione (GSH) levels within cells. Erastin (Era), characterized by a central piperazine ring connected to two phenyl groups, primarily induces ferroptosis by inhibiting the system xc- cystine/glutamate antiporter, leading to decreased GSH levels (Dolma et al., 2003). Consequently, cells become more susceptible to oxidative damage caused by lipid peroxidation. This oxidative stress ultimately triggers ferroptotic cell death.

Clearance of specific cell types through the induction of ferroptosis is one candidate approach for therapy. Frist, inhibiting system Xc is feasible through the application of Glu, Sulfasalazine, and Erastin (Era). Second, targeting GPX4 via inhibition or inactivation molecules, such as genetic knockout of the GPX4 exons or depletion of CoQ_{10}, has been

shown to improve lupus erythematosus disease outcomes (Ohl et al., 2021). Furthermore, intermediate products, such as iron, PUFAs, and lipid peroxidation, that accumulate in the cytoplasm induce ferroptosis and demonstrate beneficial effects (Stockwell, 2022).

Regarding cutaneous diseases, ferroptosis pathway induction via iron metabolism is observed in the epidermis of psoriasis vulgaris, which triggers iron deposition and excess accumulation of lipid peroxidation in skin cells (Li et al., 2023). The transcriptional repressor CREMα was identified as suppressing wound healing through binding of the upstream promoter of GPX4, resulting in aggregation of lipid-reactive oxygen species that, in turn, induce ferroptosis (P. Li et al., 2021). Fibroblast and endothelial cells in vitro respond to high concentrations of ROS, lipid peroxidation products and ferroptosis-associated proteins, which are mainly attenuated by ferrostatin-1 (Fer), the inhibitor of ferroptosis (S. Li et al., 2021). Moreover, Fer application in wound lesions from diabetic rats effectively blocks oxidative stress (S. Li et al., 2021). Additionally, recent studies show that mesenchymal cells from epithelial-mesenchymal transition (EMT) were more vulnerable to ferroptosis induction, suggesting a potential strategy to treat cancer via targeting ferroptosis and EMT together (Ren et al., 2023). Overall, evidence suggests that ferroptosis is a promising therapeutic route in skin diseases.

2 Methods

2.1 Human Samples

Fresh human keloid biopsies were collected from patients aged 18 to 65 years through the Department of Dermatology and Allergology, with ethical approval reference number 85/18S, from Klinikum rechts der Isar, Technical University of Munich. All subjects were informed that their samples will be involved in the study and signed informed consent forms to ensure that they fully understood the study's purpose, procedures, and potential risks. Human specimens were stored in sterile bags embedded in medium for fascia tissue dissection.

2.2 ER-Hoxb8 Cells Culture

ER-Hoxb8 cells were kindly obtained from Dr. David Sykes (Harvard University). The cells were cultured in a complete medium containing RPMI 1640 (Thermo Fisher Scientific), 10% FCS (Thermo Fisher Scientific), 50 μM 2-mercaptoethanol, 1 μM β-estradiol (Sigma E2758), and 5% SCF-conditioned medium. The SCF-conditioned medium was sourced from the supernatant of CHO-SCF cells, which constitutively express SCF and were also provided by Dr. David Sykes.

To induce neutrophil differentiation from ER-Hoxb8 cell, the complete medium containing β-estradiol were replaced with differentiation medium containing RPMI 1640, 10% FCS, 50 μM 2-mercaptoethanol, 20 ng/mL mouse G-CSF (PeproTech), and 5% SCF-conditioned medium.

2.3 Mice

Wild-type mice, C57BL/6J, aged 6~8 weeks, were purchased from Charles River. The Catchup mice, Ly6G-Cre-2A-tdTomato, were granted by the Cardiovascular Physiology and Pathophysiology Department of LMU. These genetically modified Catchup mice did display any abnormal function, neutrophil-associated recruitment, or murine G-CSF-induced mobilization. $Gpx4^{fl/fl}$ mice were provided by Dr. Conrad Marcus from Helmholtz Munich Centre. All mice were housed in the Animal Facility of Helmholtz Munich Centre, which maintains constant temperature, humidity, and 12-hours light cycle automatically. All mouse experiments were approved by the Government of Upper Bavaria State under projects ROB-55.2-2532-02-21-153 and ROB-55.2-2532.Vet_02-19-23 and were conducted under strict guidelines and relevant ethical regulations of Helmholtz Munich Centre and Government.

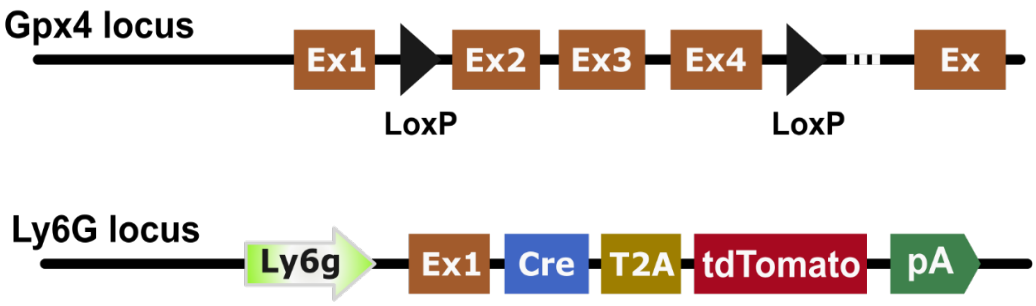

Figure 2.1 Genetic structure for Gpx4 and Ly6G mice. Upper panel represents LoxP flanked Gpx4 mice between Exon 2 to Exon4. Bottom panel represents Catchup mice, which Cre-T2A-tdTomato was inserted downstream of Ly6G promoter.

2.4 Genotyping

Genotype of transgenic mice were identified with PCR. Briefly, genomic DNA from the surplus ear clips was extracted by incubating samples with Quick Extract DNA extraction solution (Lucigen) at 65 °C for 10 min with vortexing at 300 rpm, following the manufacturer's guidelines. Samples were then cooled for 2 min and spun down to remove pellets and cell debris. Typically, 1 µL cleaned DNA was added to a reaction buffer containing 2x GoTaq ® Green Master Mix (Promega), forward primer, and reverse primer according to the genotype of the mice, and water to a final volume of 20 µL.

PCR reactions began with an initial denaturation at 95 °C for 5 min, followed by 30 amplification cycles. Each cycle consisted of denaturation at 95 °C for 30 sec, annealing at 60 °C for 30 sec, and extension at 72 °C for 1 min, with a final extension at 72 °C for 5 min. At the end, samples were held at 4 °C for gel electrophoresis.

After amplification, a 2% agarose gel was prepared using TAE buffer and SYBR Safe Master Mix. Following the loading of 8 µL PCR products and 100 bp DNA ladder, electrophoresis was run at a constant voltage of 120 V for 15 min. Finally, agarose gel was imaged under a UV trans-illuminator (Bio-Rad ChemiDoc).

Table 2.1 Primers list for genotyping

Line	Primer	Sequence 5' -> 3'	Concentration
Ly6gCreTd	Ly6g-Cre_F	ATT GCT GTC ACT TGG TCG TGG C	10nM
	Ly6g-Cre_R	GGA AAA TGC TTC TGT CCG TTT GC	10nM
Gpx4$^{fl/fl}$	Gpx4_F	CGT GGA ACT GTG AGC TTT GTG	10nM
	Gpx4_R	AAG GAT CAC AGA GCT GAG GCT G	10nM

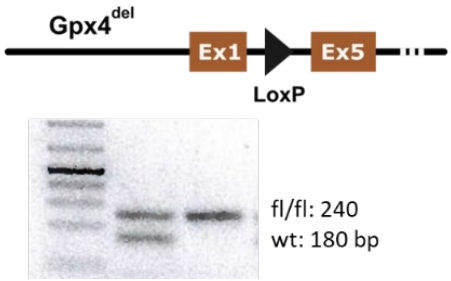

Figure 2.2 Genetic structure for Gpx4^{del} mice. The upper panel shows flanked exons between Exon 2 and Exon 4 in Ly6gCreTd x Gpx4 mice, which are excised by Cre when Ly6g promoter is activated. The bottom panel shows PCR products for Gpx4$^{del/fl}$ and Gpx4$^{del/del}$ mice.

2.5 Mouse Model of Full-thickness Excisional Wounds

Around 8-week-old mice were anesthetized with medetomidine, midazolam, and fentanyl (MMF), provided by the Pharmacy of the Animal facility of Helmholtz Centre Munich. Tow full-thickness excisional wounds with a diameter 5 mm were punched under analgesia condition. For following 3 days, drinking water was mixed with medetomidine to potentially alleviate pain. Whole wound skin, including limbs and spinal cord, was harvested on days 3, day 5, day 7 post-operation after euthanasia by cervical dislocation. All tissues were briefly washed with DPBS and then fixed in 4% PFA at 4 °C overnight. Wound skins were sliced into two equal parts prior to dehydration in 15 % and 30% sucrose in PBS. Subsequently, tissues were embedded into OCT for 24 h before cryotome cutting at 7 um per section. Cut slides were dried at room temperature for 1 h, then stored at -20 °C until Masson's trichrome or immunofluorescence staining.

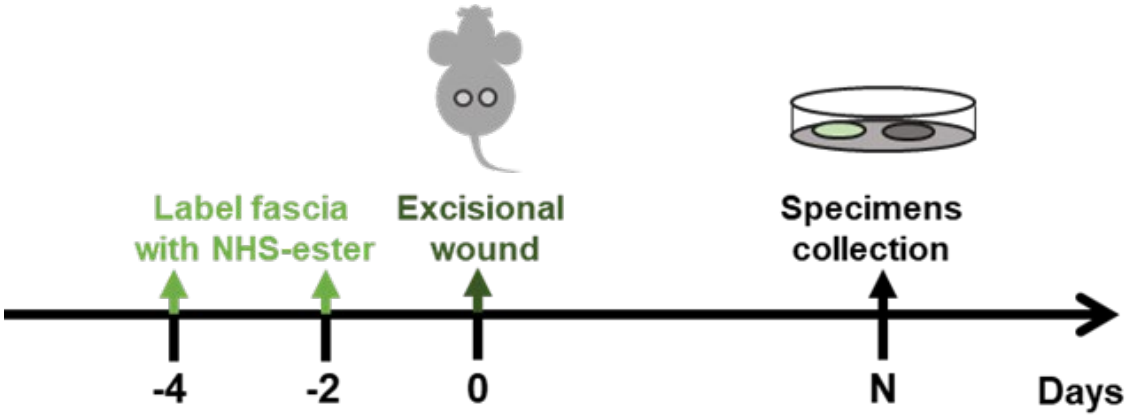

Figure 2.3 Experiments design to perform fascia labelling under murine skin. To achieve experiments, wild-type mice were injected with NHS-ester to label fascia twice prior to surgical wounding. Mice are sacrificed for sample collection at the indicated planned time points.

2.6 Fascia Explant Assay

Dorsal skin was dissected from dead mice following ethanol disinfection and hair removing. Whole skin, along with under deepest underlying fascia, was washed in cold DPBS to remove blood, debris, and any remaining hairs. The fascia was grasped with a forceps and sliced into 2~3 mm block, with the fascia facing up and epidermis down. All of explants were floated into DMEM/F-12 medium (Thermo Fisher Scientific, 11039021) containing 10% FCS, 1x Penicillin/streptomycin (Thermo Fisher Scientific). The media was refreshed every two days, with or without compounds or immune cells, as appropriate. Culturing was performed at 37 °C in a 5% CO_2 incubator for 6 days. The shape of the fascia was captured each day using a stereomicroscope (Leica M50) under bright field. Finally, all floated fasciae were embedded into OCT for cryotome sectioning.

2.7 Flow Cytometric Analysis of Bone Marrow Cells

The hip bones, femur, and tibias from sacrificed mice were carefully dissected following cervical dislocation. They were stored in DPBS containing 2 mM EDTA and 2% FCS for cell isolation. After removing muscle tissue, bone marrow cells were flushed out with a 23-gauge needle connected to a 10 mL syringe filled with cold DPBS buffer. Subsequently, the bone marrow cells were then dissociated by passing through a mash with a syringe plunger and filtered through a 40 μ m PP strainer. Trypan blue-stained cells were pipetted onto Neubauer slides for counting live cells.

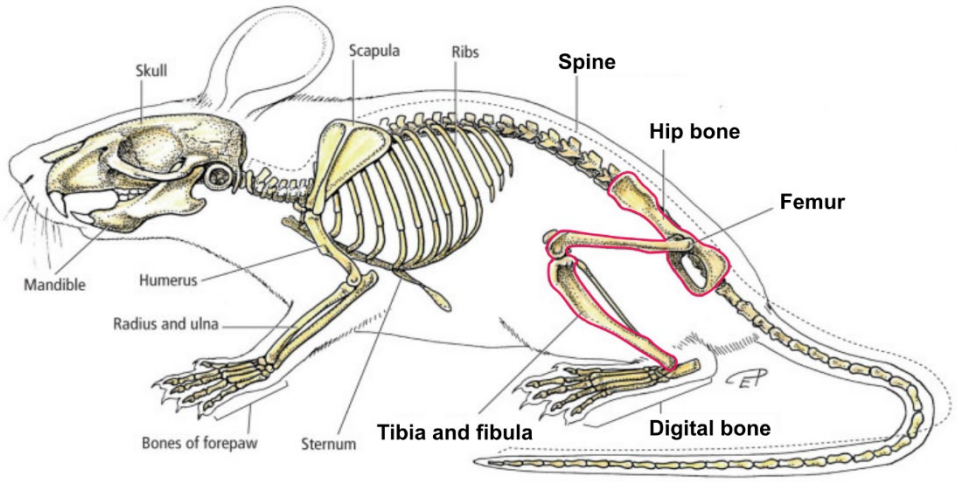

Figure 2.4 Skeleton of the mouse. Both hip bone, femur, and tibias from mice were carefully incised to extract bone marrow.

The counted cells were washed and incubated with primary fluorophore-conjugated antibodies for 15 min at 4 °C. Live/Dead™ Fixable Near IR 780 dye (Invitrigen) was used to stain dead cells following washing with DPBS buffer.

Cell acquisition was performed on a 4-laser BD LSRII using FACSDiva software. Data in FCS 3.1 format was subsequently exported into FlowJo software (BD). Sorted bone marrow neutrophil subsets were obtained using a 4-laser BD FACSAria II to achieve > 98% purity.

At the beginning of each protocol, UltraComp eBeads Plus Compensation Beads (Thermo Fisher, 01333342) were incubated with primary antibody to establish basic compensation via AutoSpill, a web-based tools for calculating spillover coefficients (Roca et al., 2021).

Table 2.2 Primary antibodies for cytometry

Target	Conjugated	Isotype	Clone	Cat.	Company
Ly6G	PB	Rat IgG2a, κ	1A8	127612	Biolegend
CD11b	BV510	Rat IgG2b, κ	M1/70	101263	Biolegend
B220	FITC	Rat IgG2a, κ	RA3-6B2	103206	Biolegend
CD90	FITC	Rat IgG2a, κ	53-2.1	140304	Biolegend
NK-1.1	FITC	Mouse IgG2a, κ	PK136	108706	Biolegend
CXCR4	PerCP/Cy5.5	Rat IgG2b, κ	L276F12	146510	Biolegend
c-Kit	PE/Cy7	Rat IgG2b, κ	2B8	105814	Biolegend
CXCR2	AF647	Rat IgG2a, κ	SA044G4	149305	Biolegend
Gr1	AF700	Rat IgG2b, κ	RB6-8C5	108422	Biolegend
CD16/32	BV421	Rat IgG2a, λ	93	101331	Biolegend
CD34	AF647	Rat IgG2a, κ		560233, RRID: AB_1645199	BD

2.8 Flow Cytometry-based Cell Viability Assay

Blood cells were harvested via heart puncture. Red blood cells were lysed twice with 1x Red Blood Cell Lysing Buffer (BD Pharm Lyse™), each time for 5 min. The cell suspension was washed with DPBS containing 2% FCS for 5 min at 350 G. Neutrophils were treated with different concentrations of Erastin (100 nM, 500 nM, 2 μM, and 10 μM), Ferrostatin (100 nM, 500 nM, 1μM, 5 μM), Lipoxin (50 nM, 100 nM, 500 nM, and 1 μM), Rosiglitazone (50 nM, 100 nM, 500 nM, 1 uM), RSL3 (100 nM, 500 nM, 1 μM, and 5 μM) and aTOC (100 nM, 500 nM 2 μM, and 10 μM) for 16 h in an incubator.

Cell viability was evaluated using the Live/Dead Fixable 780 (Invitrogen) and Ly6G to gate out neutrophil. Briefly, the cell suspension was pass through a 35 μm mesh and loaded into LSRII flow cytometer with FSC-A, SSC-A, FITC-A, APC-A and APC-Cy7-A channels. All cells were gated based on FSC-A and SSC-A to exclude debris. Live cells were identified as negative in the APC-Cy7-A channel for subsequent analysis.

Table 2.3 Chemical Regulators of Ferroptosis

Chemicals	Source	Identifier
Erastin	Sigma-Aldrich	329600
Alpha-Tocopherol	Sigma-Aldrich	258024
Ferrostatin	Merck Millipore	341494
Rosiglitazone	Sigma-Aldrich	R2408
Liproxstatin-1	Sigma-Aldrich Chemie	SML1414
1S,3R-RSL3	Tocris Bioscience	6118/10

2.9 Cell Viability Quantification with CytoTox-One

Cytotoxicity was assessed by evaluating the membrane integrity of neutrophil using the CytoTox-ONE™ Assay (Promega). This assay quantifies fluorescence intensity of a substrate generated by lactate dehydrogenase released from viable cells. The kit provides a CytoTox-ONE Reagent mix, allowing for easy and quick measurement of LDH in culture medium within a 10 min enzymatic assay, which converts resazurin into resorufin without damaging healthy cells.

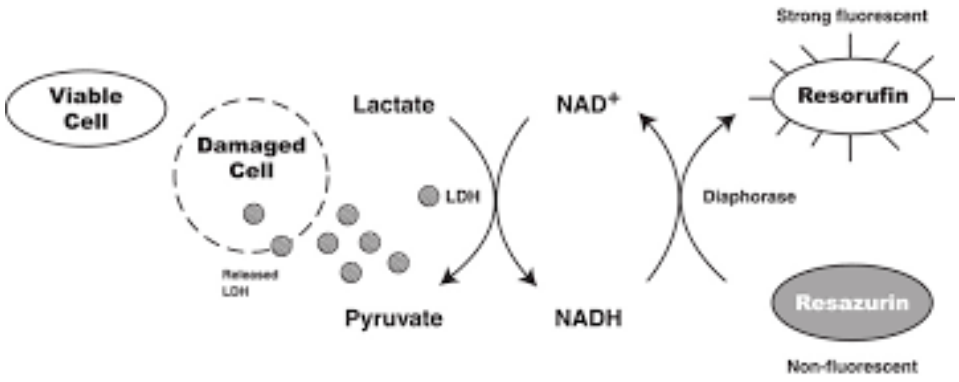

Figure 2.5 LDH cytotoxicity assay based on cellular membrane integrity. (C. Bueno et al., Photochem.Photobiol. 76, 385-390, 2002).

Prior to measurement, lyophilized substrate mixes were equilibrated at room temperature. CytoTox-ONE Reagent was prepared by adding it to the “Substrate Mix” with “Assay Buffer” under dark environment. For the assay, cells, including progenitors and subset of neutrophils, were plated at 2×10^4 cells/well in a black 96-well plate. Regarding to experimental design, we included a no-cell control as background, a positive control with

cells treated with 2 µL of lysis solutions, and assay cells. The final volume of culture medium in each well should be 100 µL. The cells were cultured for desired exposure period of 2 h. Black 96-wells plates were then removed from the incubator and equilibrated at room temperature for approximately 20 to 30 min. At the same time, the CytoTox-ONE substrate was also left at room temperature. Positive controls were constituted by adding 2 µL of lysis solution per 100 um or original medium to generate maximum LDH release. Then, 100 µL CytoTox-ONE substrate, which is equal to the volume of cell culture medium, were added to each well and mix for 30 sec. The assay plate was incubated at room temperature for 10 min prior reading. After incubation, 50 µL of stop solution were added and mixed at 500 rpm for 10 sec to terminate the color reaction. The fluorescence signal was measured using a Microplate Reader with an excitation wavelength of 560 nm and an emission wavelength of 590 nm (Molecular Devices, SpectraMax i3x). Background fluorescence was determined using negative controls, and vehicle control was used for untreated cells.

Relative fluorescence units were calculated by subtracting the medium background from experimental assay and then normalizing by dividing by the maximum LDH release assay corrected for medium background.

$$\boldsymbol{RLU = 100 \times \frac{Experimental\ wells - Meidum\ background}{Maximum\ LDH\ control - medium\ background}}$$

2.10 Cellular Lipid Peroxide Detection with BODIPY

To measure intracellular levels of lipid peroxide, 10 mM BODIPY diluted in DMSO was added to treated neutrophils ex vivo. Approximately 1 x 10^5 cells per well were plated in a 6-well plate and stained in the dark at 37 °C for 15~20 min. Harvested cells were washed with DPBS and centrifuged at 250 g for 5 min at 4 °C. After washing the cells with HBSS/media solution, the cell pellet was resuspended in 300 µL HBSS for detection by flow cytometry after passing the cell suspension through a 35 µ m mesh into a FACS tube.

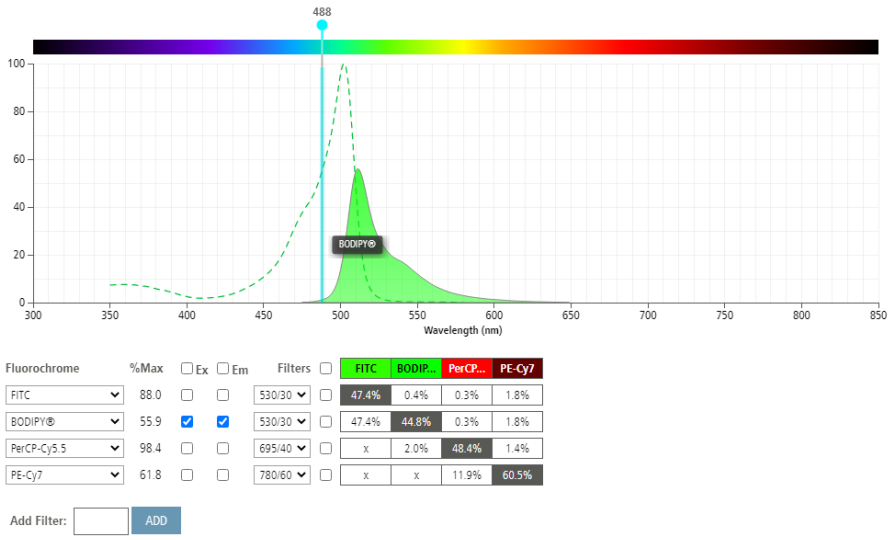

Figure 2.6 BODIPY spectrum provided by BD spectrum viewer online.

2.11 Masson's Trichrome Staining

Fixed tissues were subjected to Masson's trichrome staining using 4% PFA following the manual (Sigma-Aldrich, HT15). Initially, all tissues were dehydrated in 30% Sucrose for 1 day, then embedded in OCT. Frozen tissues were sectioned into 7 µm slices using a cryotome NX70 (Thermo Fisher Scientific) and stored at -20 °C until staining. Prior to staining, slides were incubated at 60 °C for 2 h to prevent section detachment and then re-fixed with preheated Bouin's solution (Sigma Aldrich, HT10132-1L) at 56 °C for 15 min. Staining was performed by immersing slides in a trichrome stain solution (Sigma Aldrich, HT15-1KT) through several consecutive dyes, including Weigert's Iron Haematoxylin, Biebrich scarlet-acid fuchsin solution, and Aniline Blue solution. Excess stain, particularly Biebrich scarlet-acid fuchsin solution, was removed from sections by immersing slides in 1% acetic acid for 5 min which enhance the differentiation of tissue components and produce distinctive colour patterns. Stained slides were dehydrated in a series of ethanol solutions (typically 70%, 95%, and 100% ethanol) and mounted with ROTI Histokitt (Roth 6638) before clearing with ROTI® Histol (Roth 6640) to achieve transparency.

Once dried in a fume hood, sections were observed under bright-field microscope, using an Axio Imager Z1 (Zeiss) to examine skin structures and cellular components. Nuclei appeared dark, cell plasma stained red, and collagen appeared cyan.

2.12 Immunostaining

The slides were initially chosen at -20°C after optical inspection of their structure, then equilibrated at room temperature for several minutes. Prior to immunostaining, all sections

were washed 3 times for 5 min each with PBS to remove any remaining OCT. For cellular antigens, 0.1 % Triton X-100 in PBS, a strong detergent, was used to permeabilize cell membranes, facilitating the access of antibodies and other reagents to intracellular organelles and nuclei. Subsequently, sections were incubated with 5% donkey serum in PBS for 1 h at room temperature to block non-specific binding sites for primary antibodies. Following this, primary antibodies diluted in 5% blocking solution were carefully applied to the sections and left to incubate overnight at 4 °C in humidity. The next day, sections were washed 3 times with PBST and then incubated with fluorescein-conjugated antibodies (Life technologies, usually at 1:1000) against primary antibodies respectively for 2 h at room temperature. Finally, sections were mounted using fluorescent mounting media containing DAPI (Thermo Fisher, 00495802). Images were captured under Zeiss Axio Imager Z1.

2.13 Matrix Mobilization assay

Murine lung tissue biopsies were obtained through lung puncture following perfusion with DPBS (Thermo Fisher Scientific). To assess matrix dynamics, lung biopsies were surface labelled with NHS-FITC (Thermo Fisher Scientific, 46410) for 1 min and subsequently cultured in vitro for 24 or 48 hours. To investigate the influence of neutrophils on matrix dynamics, lung biopsies were co-cultured with neutrophils with specified chemicals. Matrix dynamics were quantified by measuring the ratio of NHS-FITC-labelled area to biopsy section length using Fiji.

2.14 Image Analysis

All microscopy images were viewed, processed, and analysed with Fiji (version 1.53f).

For measuring tissue area, images are calibrated based on microscope settings. Selecting tools were used to define regions of interest (ROI) and recorded in the ROI manager.

To analyse immune labelling cells, whole mount-stained tissues were prepared for imaging. White balance was corrected for each bright field imaging session. For immunofluorescence staining, dark field images were acquired to minimize background. In cases where tissues were not on a flat plane, image stacks from the microscope were used to enhance depth of focus. To segment labelled cells, cell detection was performed using Stardist with a nuclei model, ensuring precise and reliable detection of cells (Casanova-Acebes et al., 2021). Mean intensities of the detected cells were then measured to extract the maximum possible frequency.

2.15 Western blot Analysis

Differentiated neutrophils from ER-Hoxb8 cells were collected and subjected to Western-blotting analysis. Round $1x10^6$ cells were harvested for each treatment and lysed in 100 µL RIPA buffer supplemented with protease inhibitors (complete protease inhibitor cocktail, Pierce). Following protein denaturation, 20 µL of each sample was loaded onto 10% Precast Protein Gels (Bio-Rad). After transferring to PVDF membranes, anti-Cathepsin B (CSTB) (Cell Signalling, 31718), and anti-β-actin (Bio-Rad, AHP2417) were incubated and followed by Anti-rabbit-HRP secondary antibody (Bio-Rad). To acquire blotting image, protein bands were visualized using Chemiluminescent substrate (Thermo Fisher Scientific, 34580) on a Bio-Rad ChemiDoc imaging system. Proteins intensities were quantified with Gels and Analyzer model of Fiji. Relative pro-CSTB and CSTB expression were normalized to β-actin.

2.16 Re-analysis of RNA Sequencing Data

Bulk neutrophils and progenitors' transcriptomic raw counts were retrieved from the NCBI Sequence Read Archive database (SRA) under accession numbers PRJNA431153 (GSE109467) and PRJNA636821 (GSE151682) (Evrard et al., 2018; Kwok et al., 2020). Upstream analysis was conducted using usegalaxy.eu, a web toolkit for bioinformatics. Briefly, reads in fastq files were downloaded using SRA toolkits v3.0.3, fastq-dump command, and spit into paired-end collections. Trim Galore v0.6.7 was employed to remove sequencing adapters and reads with quality score lower than 20. Additionally, approximately 30 base pairs were trimmed from the 5' end of reads if no adapters were detected with default setting. The quality controlled paired-end reads were then aligned to the mouse reference genome (mm10) using RNA STAR v2.7.2b with an index built from the respective gene model. The reads alignment in BAM files were processed using FeaturesCounts from subread v2.0.3 package, which counted paired-end reads as a single fragment. The counts matrix, with ensemble gene IDs as row names, was exported into R (R, v4.2) for downstream analysis. Differential gene expression analysis was performed using DESeq2, with the experimental design specified as "*~ project_id + cell_type"*. A general threshold was set, considering an adjusted p-value < 0.05 and a fold change > 2, to identify differentially expressed genes. Cluster Profile was used to compute Gene Ontology enrichment and pathway analysis (Wu et al., 2021).

2.17 Single Cell RNA Sequencing

Skin biopsies from excisional wound were dissected on days 0, 1, 3 post-surgeries. The tissue was minced into tiny pieces by scalpels and digested with a mixture of Collagenase (Roche), DNase (Sigma), and hyaluronidase (Sigma) at 37 °C for 30 min with shaking. Digestion was stopped by topping PBS buffer containing 10% FCS to a final volume of 10

mL. The cell suspension was passed through 70 µm cell strainers to remove debris. Cell pellets were washed twice with FACS buffer containing 2% BSA and 2 mM EDTA in PBS. To sort immune cells, primary antibody APC-CD45 antibody (Biolegend) were incubated with cell suspension for 30 min at 4 °C. Finally, labelled cells were sorted on a DB FACSAria II with a 100 µm nozzle and 30 psi, preserving maximum cell viability under this condition. Before preparing RNA for the library, we measured cell viability and yield via staining trypan blue staining and counting unstained cells.

Chromium Next GEM Single-cell 3' v2 (10x Genomics) were used for single-cell RNA-seq libraries preparation according to manual. Approximately 8,000 cells from each sample were loaded onto Chips for mRNA capture, barcoding and reverse transcription, finally creating RNA-seq libraries. The single cell RNA-seq libraries were accessed for quality using a Qubit fluorometer (Thermo Fisher Scientific). Samples were paired-end sequenced on Illumina platform at the core facility of Helmholtz Munich Center.

2.18 scRNA-seq Data Analysis

Sequenced reads, in fastq format from platform, were aligned to the mouse genome, mm10, pre-indexded by 10x Genomic, using the scRNA workflow adapted from NF-Core. Cellranger pipelines (v7.2) were chosen for alignment, mapping reads, and counting reads per gene. Unfiltered raw counts, exported from Cellranger, were read into R by read_10x function, and created as a Seurat object for downstream analysis, with parameters min.cells = 3 and min.feature = 200 to exclude any cell debris. Metadata of mice, including sample status, days post excisional and tissue, were added to meta slot via AddMetaData function.

Table 2.4 QC report of 10x Genomics sequencing files (CellRanger).

Sample	*Reads*	*Q30 Bases in Barcode*	*Q30 Bases in RNA Read*	*Q30 Bases in UMI*	*Confident Mapping to Genome*	*Confident Mapping to Transcriptome*
MUC13960	346,451,542.00	96.2%	93.7%	96.2%	86.1%	51.5%
MUC13961	649,647,763.00	96.3%	94.1%	96.2%	90.9%	56.9%
MUC13962	560,666,961.00	96.3%	94.0%	96.2%	91.6%	58.8%
MUC13963	593,021,400.00	96.3%	93.9%	96.2%	90.7%	53.9%
MUC13964	540,646,590.00	96.3%	93.8%	96.3%	91.5%	54.9%
MUC13965	431,347,371.00	96.3%	94.0%	96.3%	92.0%	56.9%

Table 2.5 CellRanger statistics of samples

Sample	*Estimated Number of Cells*	*Mean Reads per Cell*	*Median Genes per Cell*	*Median UMI per Cell*	*Fraction Reads in Cells*	*Sequencing Saturation*
MUC13960	3167	109394	1304	2909	87.7%	81.4%
MUC13961	5413	120016	1254	5770	94.1%	84.9%
MUC13962	7187	78011	2428	7316	94.1%	76.3%
MUC13963	7123	83254	1873	4673	90.5%	80.5%
MUC13964	6268	86255	1203	5168	92.2%	81.7%
MUC13965	7494	57559	1352	5500	94.2%	73.1%

Table 2.6 QC and information for neutrophils of samples.

Sample	*QC Neutrophils*	*Median Genes per Neutrophil*	*Median UMI per Neutrophil*	*Mean Mitochondrial Reads percentage*	*Mean Ribosomal Reads percentage*	*Mean hemoglobin Reads percentage*
MUC13960	*500*	*2183.5*	*4764.5*	*11.234.761*	*9.844.796*	*0.003534536*
MUC13961	*1655*	*2763.0*	*9756.0*	*3.703.024*	*11.195.666*	*0.033343709*
MUC13962	*3338*	*2989.0*	*9073.5*	*4.342.217*	*11.019.786*	*0.023081253*
MUC13963	*1594*	*2496.0*	*6541.5*	*6.971.326*	*12.173.607*	*0.008442159*
MUC13964	*1966*	*2415.5*	*8029.5*	*5.049.306*	*11.217.333*	*0.006369665*

To quality control cells and RNA, the percentage of mitochondrial, ribosomal and hemoglobin genes were calculated using an internal function based on gene name pattern. Reads were filtered under the condition that gene counts greater than 200, percentage of mitochondrial genes less than 20%, percentage of ribosomal genes greater than 5%, and percentage of hemoglobin genes less than 5%. After quality control, we removed mitochondrial, ribosomal, and hemoglobin genes to avoid any side effects during gene selection.

For doublet detection, we applied to the DoubletFinder library of R to score doublets (Clarke et al., 2021). Singlets were retained for normalization and dimensional reduction. Prior to clustering, RNA counts were normalized to 10,000 and scaled with regression to remove unwanted variation due to gene number and mitochondrial gene percentage. High variable genes were set to 2,000 for principal components analysis (PCA) and further Uniform Manifold Approximation and Projection (UMAP) using 30 PCs of PCA.

To annotate cell cluster segmented by FindClusters with multi-resolutions using the Louvain algorithm, gene expression of canonical markers from the literatures were plotted. Additionally, the Celltypist algorithm with an embedded model were used to predict cell type (Dominguez Conde et al., 2022). Singlets annotated as neutrophils were included for pathway analysis and RNA velocity.

Table 2.7 Murine canonical markers for annotation

Cell type	*Canonical Markers*
Melanocyte	*DCT, MLANA, PMEL, TYR, TYRP1*
Keratinocytes	*KRT1, KRT10, KRT5, KRT14*
Fibroblast	*PDGFRA, PDGFRB, COL1A1, COL1A2, COL3A1, LUM*
Myocyte	*ACTA1, DES, MYL1, TTN, NEB*
Neurons	*ENO2, RBFOX3*
Endothelial cells	*VWF, CDH5, CLEC14A, CLDN5, ADGRL4*
Lymphovascular cells	*CCL21, TFF3*
Epithelial cells	*EPCAM, KRT7, MUC1*
Mesothelial cells	*KRT19, UPK3B, MSLN, WT1, PDPN*
Pericyte	*RGS5, ESAM, MEF2C*
Erythrocyte	*HBA1, HBA2, HBB*
Immune cells	*PTPRC,*
T cells	*CD2, CD3D, CD3E*
B cells	*MS4A1, CD79A, CD79B, CD19*
Plasma cells	*JCHAIN, MZB1, TNFRSF17, SDC1, IGHG1*
Monocyte	*CCR2, CSF1R*
Macrophage	*AIF1, CD14, CD163*
Neutrophil	*LY6G, S100A8, S100A9, MMP9, ELANE, MPO, CXCR2, CD33*
Mast cells	*CPA3, MS4A2, TPSB2, TPSAB1*
NK cells	*NKG7, KLRD1, GZMB, KLRF1*
DC1	*CLEC9A, XCR1, WDFY4*
DC2	*ITGAX, SIRPA, CD209A*
DCs	*CCR7, CD86, CLEC10A, IRF8*

3 Results

3.1 Ferroptosis in Neutrophil

3.1.1 Neutrophil Culture from Immortal Progenitors

While neutrophils are abundant at their origin, genetic editing was impossible due to its short lifespan. Therefore, conditionally immortalized myeloid progenitors, ER-Hoxb8 cells, were created by activating Hoxb8, a transcription factor in the Hox gene family that regulates the growth and differentiation of myeloid cells, under the control of estrogen receptor (ER) (Wang et al., 2006). With the supplement of Estradiol and SCF, ER-Hoxb8 cells maintains their progenitor status (Wang et al., 2006). Due to the heterogeneity of neutrophil development from multipotent progenitors to mature neutrophils, ER-Hoxb8 cells were cultured with GM-CSF for 4 days to synchronize their differentiation into mature neutrophils. Each day during culture, cells were harvested and stained with Giemsa staining to examine the morphology of their nuclei. On day 0, ER-Hoxb8 cells showed a large uncondensed, intact nucleus with little cytoplasm. In following days, nuclei were progressively condensed from a “doughnut” shape at day 1 to a poly-segmented nucleus at day 4. Here, we demonstrated the subsets of neutrophils through ER-Hoxb8 differentiation.

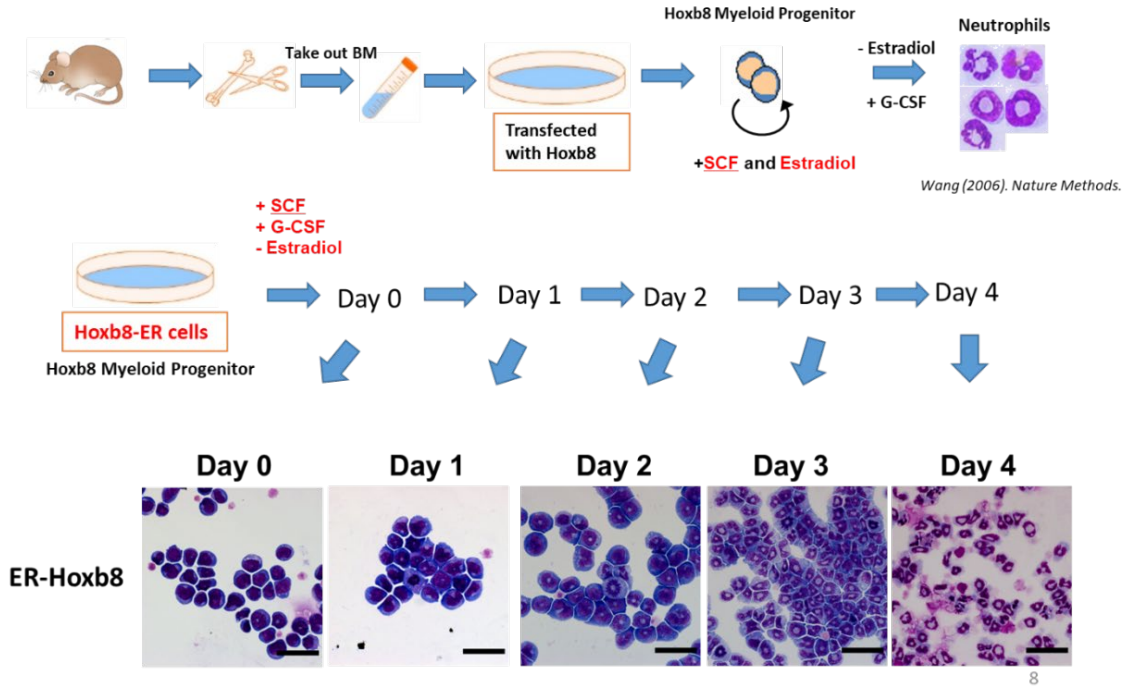

Figure 3.1.1 ER-Hoxb8 cells culture and induction in dish. ER-Hoxb8 cells were generated from murine bone marrow by knocking in the ER-Hoxb8 fragment in vitro in Dr. David Sykes’s lab. The genetically modified ER-Hoxb8 cells were cultured with RPMI 1640 medium containing SCF and estradiol, an analog that binds to the estrogen receptor. When estradiol is removed from medium, ER-Hoxb8 gradually differentiate into neutrophils.

3.1.2 Phenotype of Differentiated ER-Hoxb8 Cells

To verify the cellular identity of differentiated progeny of ER-Hoxb8 cells, we inspected the expression of classic surface receptors of neutrophils on day 4 by flow cytometric analysis. The differentiated cells were harvested and labeled with antibodies against a mature neutrophil marker Ly6G, as well as integrin Cd11b, Cd18, selectin Cd62L, and chemokine receptor Cxcr2. Isotype antibodies corresponding to these markers were used as background controls, and neutrophils from murine bone marrow served as positive sample controls. Integrins, Cd11b (integrin α_M) and Cd18 (integrin β_2), were expressed on more than 90% cells, similar to primary neutrophils. However, due to the complexity of bone marrow cells, the expression of Cd62L and Cxcr2 was not at the same level as differentiated ER-Hoxb8 cells, indicating cell heterogeneity post-induction of neutrophil maturation. Together, our data confirmed that ER-Hoxb8 cells, the myeloid progenitors, are immortalized and able to be induced into neutrophils with the treatment of GM-CSF and SCF in vitro.

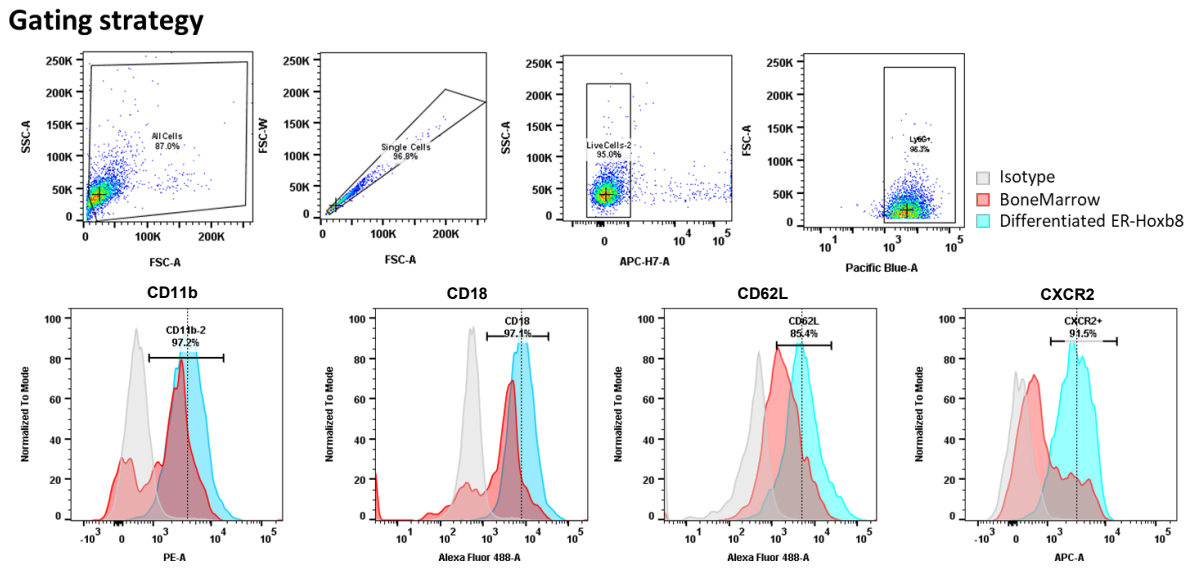

Figure 3.1.2 Phenotype of differentiated neutrophils from ER-Hoxb8 cells. ER-Hoxb8 cells were cultured with RPMI 1640 medium containing SCF and G-CSF to induce neutrophil maturation. On day 4, cells were harvested for analysis of Cd11b and Cd18, Cd62L, and Cxcr2 via flow cytometry. Dead cells were excluded from the analysis by LIVE/DEAD™ Fixable Near IR (780) dye.

3.1.3 The Maturation of Differentiated ER-Hoxb8 Cells

It is known that neutrophils develop in the bone marrow, undergoing a series of sequential stages from myeloblasts to promyelocytes, myelocytes, metamyelocytes, and finally reaching fully functional, mature circulating cells (Hidalgo et al., 2019). However, it is unclear whether the differentiation of ER-Hoxb8 cells mimics this natural maturation process in vivo. To investigate this, ER-Hoxb8 cells were harvested daily and stained with maturation

markers, including c-Kit, Cd11b, Cxcr4, Cxcr2, and Ly6G, for flow cytometric analysis. We observed the high expression of progenitor marker c-Kit in ER-Hoxb8 progenitors on day 0. As differentiation proceeded, ER-Hoxb8 cells gradually lost their c-Kit expression and began to express Cd11b, interacting with ICAM-1. While Cxcr4, a G protein-coupled receptor binding to Cxcl12 that is highly expressed in bone marrow progenitors, showed reduced expression by day 2. Conversely, Cxcr2, which binds to chemokines such as Cxcl1/2, exhibited increased expression. After 4 days of culture, we observed 39% of $Ly6G^{+}Cxcr2^{+}$ mature neutrophils, and 60% of $Ly6G^{hi/mid}Cxcr2^{-}$ immature neutrophils in dish. Our data demonstrated that ER-Hoxb8 cells undergo a differentiation process similar to that of bone marrow progenitors.

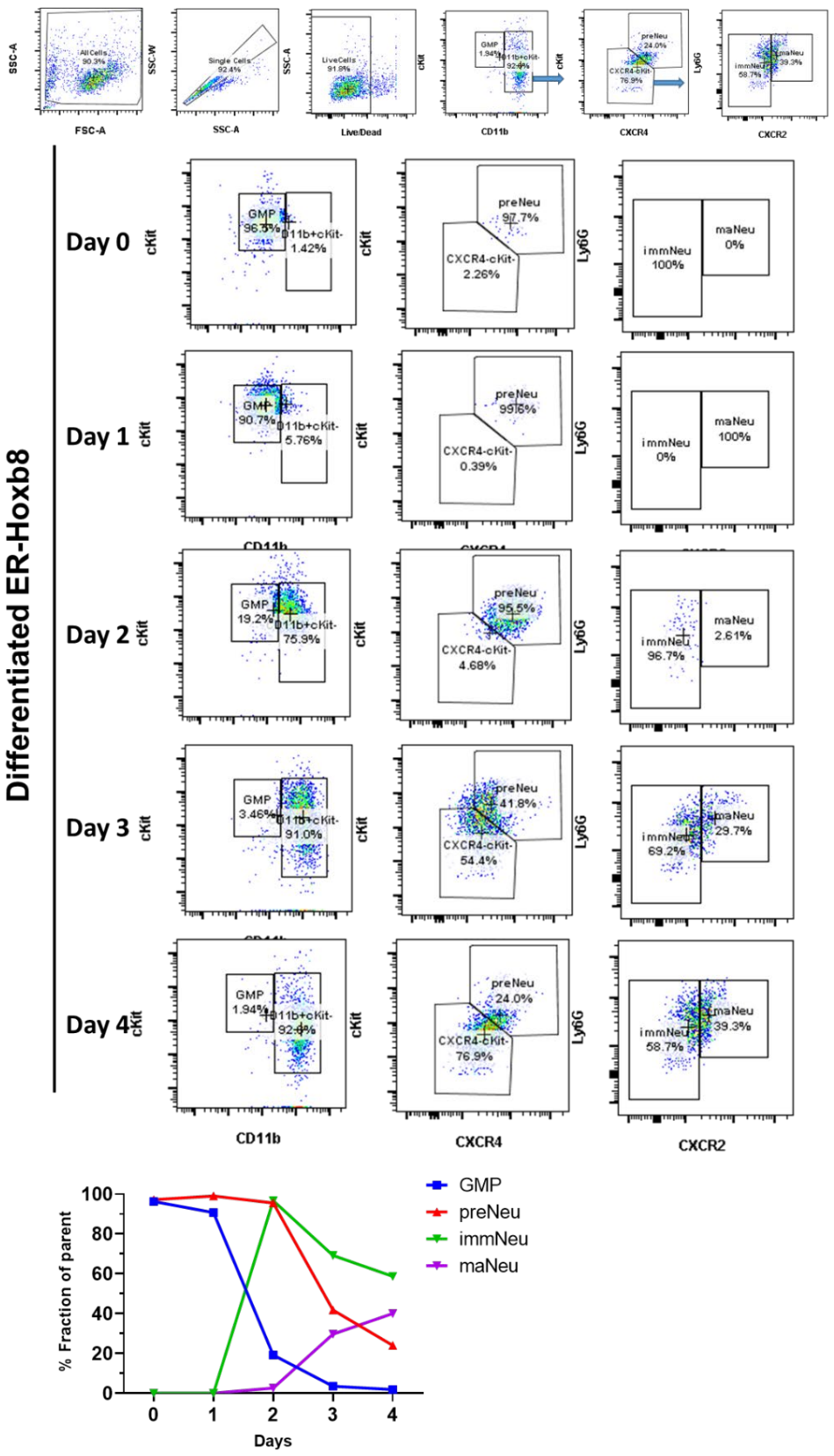

Figure 3.1.3 Maturation of differentiated neutrophils from ER-Hoxb8 cells. ER-Hoxb8 cells were collected daily and stained with maturation surface markers c-Kit, Cd11b, Cxcr4, Cxcr2, and Ly6G for flow cytometry detection. Dead cells were excluded from the analysis using LIVE/DEAD™ Fixable Near IR (780) dye.

3.1.4 Ferroptosis in Neutrophils

As short-lived cells in circulation and the local environment, neutrophils have been debated for their longevity for a long time (Kolaczkowska & Kubes, 2013). Many factors, such as cytotoxic complexes and infections, trigger neutrophil death. Here we explored neutrophil ferroptosis, a newly defined programed cell death relative to apoptosis (P. Li et al., 2021). One common method used to evaluate lipid peroxidation and ferroptosis is BODIPY staining, a lipid peroxidation-sensitive dye (Martinez et al., 2020). Oxidized BODIPY, induced during ferroptosis, leads to enhanced fluorescence intensity that can be detected by sensor. This technique has been utilized to detect lipid peroxidation in Acls4-knocked down cells and in cancer cells induced by Gpx4 inactivation (Byun et al., 2022; Doll et al., 2017; Lei et al., 2020).

To assess the impact of ferroptosis on neutrophil fate, we analyzed specific chemicals that modulate ferroptotic signaling in mouse blood neutrophils. Treatment with both Era and RSL3 increased neutrophil death rate to 80% compared to controls. Conversely, blocking ferroptosis with Fer, Rosiglitazone, Liproxstatin-1, and α-tocopherol (aTOC) at standard/physiologic concentrations protected neutrophils from ferroptosis. This suggests that ferroptosis modulates mature neutrophil numbers and may regulate neutrophil homeostasis and responses to injury.

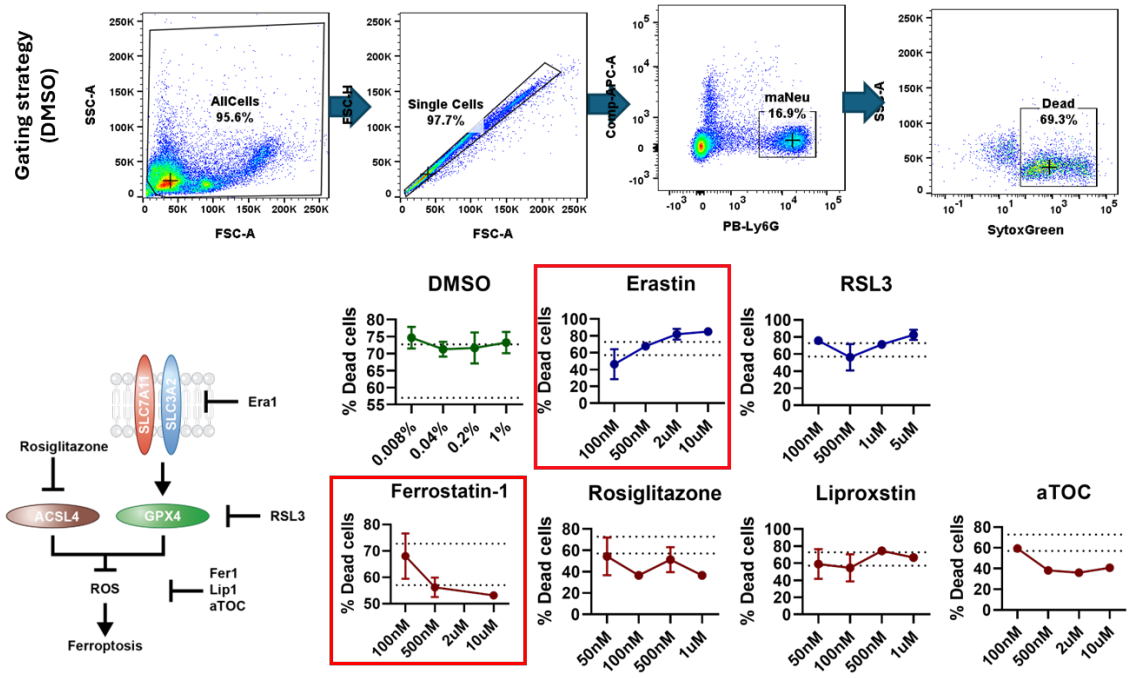

Figure 3.1.4 Induction and inhibition of ferroptosis in neutrophils. Isolated neutrophils were used for investigation of various chemicals to induce or block ferroptosis in neutrophils. SytoxGreen staining was used to quantify cell death via flow cytometry. Four different concentrations of each chemical

were tested in the assay and the entire assay was repeated three times for each condition. Erastin-1 and RSL3 were used to induce ferroptosis, while Ferrostain-1, Rosiglitazone, Liproxstatin, and aTOC were used as inhibitors.

Differentiated ER-Hoxb8 cells for 4 days with treatment of Era and Fer were harvested on each day to evaluate lipid peroxidation. Meanwhile, lactate dehydrogenase activity (LDH) released by damaged or dying cells from cytoplasm into extracellular medium were assessed by CytoTox-ONE™ Homogeneous Membrane Integrity Assay according to user's manual. Finally, we found oxidized BODIPY and LDH activity were low at first 3 days, while lower level of lipid oxidation was found in neutrophils with ferroptosis blockage. On day 3 and 4, LDH activity increased as mature neutrophil induced. Interestingly, Ferrostatin blocked LDH releasing in maturing neutrophils during the last 2 days. In contrast, Erastin significantly induced BODIPY intensity and LDH enzyme activity. Our data proved that neutrophil maturation happened gradually accompanied by ferroptosis, which can be reduced by chemical inhibition.

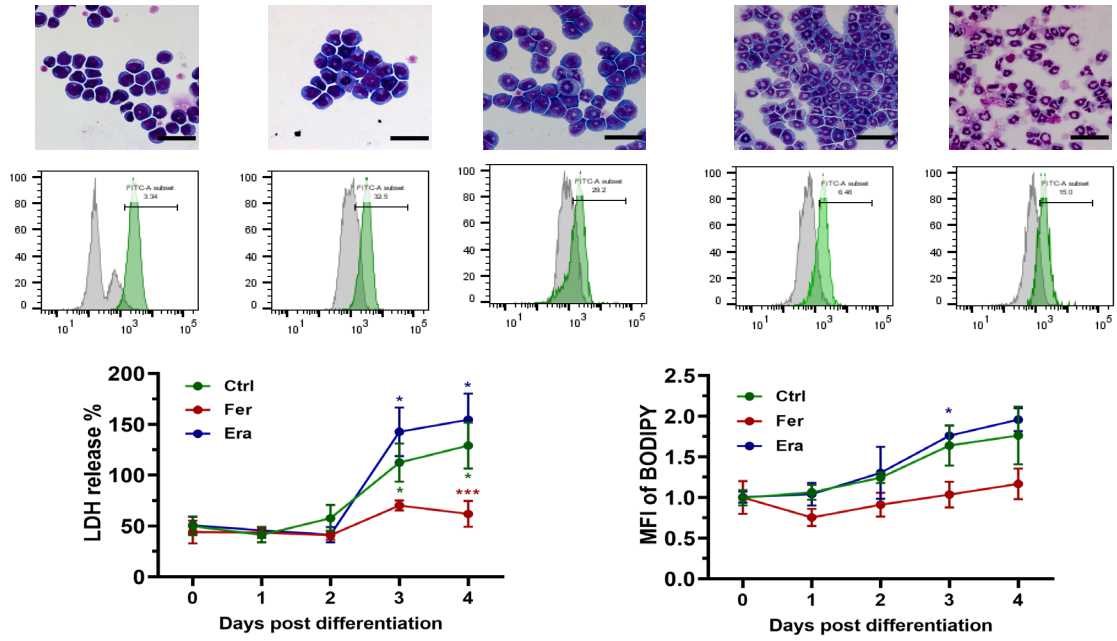

*Figure 3.1.5 Ferroptosis of differentiated neutrophils from ER-Hoxb8 cells. ER-Hoxb8 cells were collected day by day and stained for detection of viability and lipid peroxidation. LDH measurements were performed according to CytoTox-ONE™ Homogeneous Membrane Integrity Assay from Promega Co. To detect lipid peroxidation, BODIPYC11 was used for analyzing by flow cytometry. Dead cells were excluded from the analysis by LIVE/DEAD™ Fixable Near IR (780) dye. Each group contained 3 repeats and paired comparisons were carried out by ANOVA on each timepoint. * represents p-value less than 0.05; *** indicates p-value less than 0.001.*

3.2 Functional consequences of Ferroptotic Neutrophil in wound healing

3.2.1 Matrix Mobilization is Impaired by Ferroptosis Neutrophil.

Pre-labelling of the ECM on the surface of lung biopsy using FITC-conjugated NHS-ester dye has proven to be an ideal model for assessing ECM mobility ex vivo (Fischer et al., 2023). Neutrophils, as innate immune cells in first line of defense, have been shown to act as pre-existing matrix carriers post-wounding, supporting wound healing. Here, we applied a surface matrix migration model from lung biopsies to investigate the function of neutrophil clusters. In cultured lung biopsies, the pre-labelled surface matrix was demonstrated to migrate towards deeper tissue layers, as shown in the control group (PBS containing 0.1% DMSO). The distances of migration were measured by area of NHS-FITC labelled regions divided by the length of the biopsy section, using parameters measured by Fiji. When lung biopsies were co-cultured with neutrophils, matrix migration significantly increased, with an average of 13 mm (2nd Column, Figure 3.2.1) compared to the control groups average of 8 mm. Furthermore, ferroptotic neutrophils did not exhibit matrix mobilization. Inhibition of ferroptosis with Fer or α-TOC did not prevent matrix mobilization. Thus, neutrophil ferroptosis impacts matrix migration.

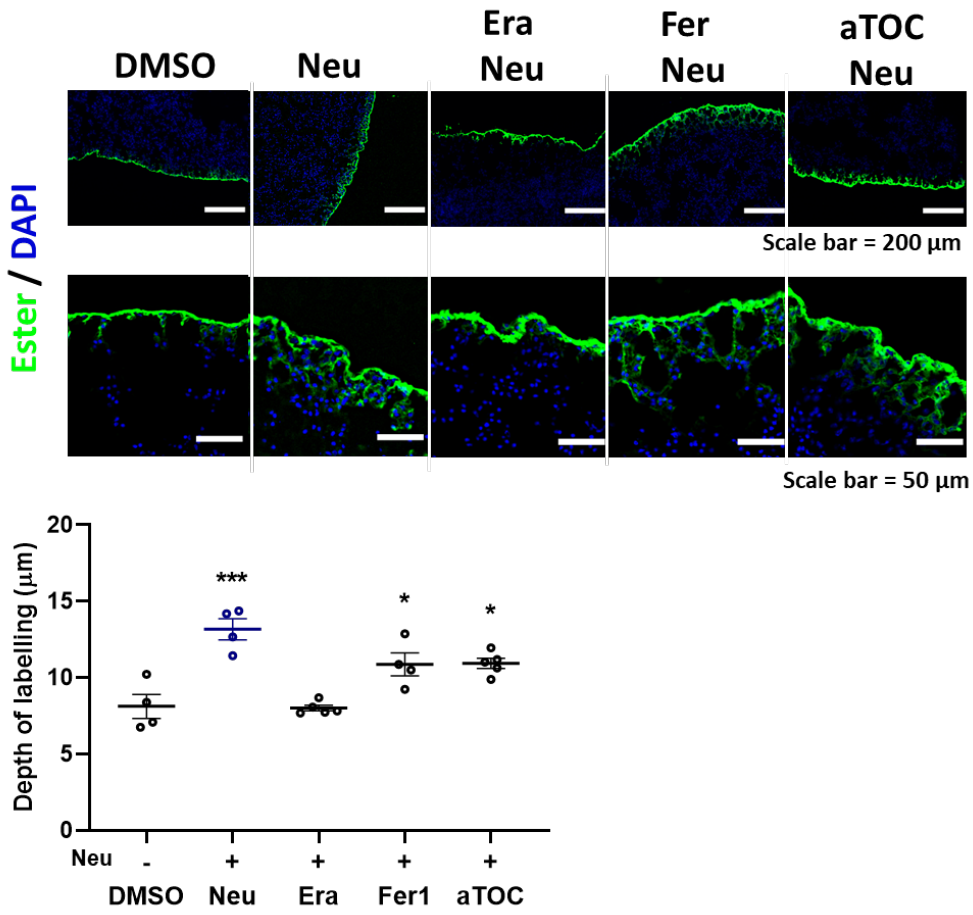

*Figure 3.2.1 Pre-exist matrix carried by neutrophil post wounding to support wound healing. Cultured lung biopsies post dissection from body were co-cultured with differentiated neutrophils from ER-Hoxb8 cells and modulated ferroptosis by drugs. NHS-FITC ester labelled extracellular matrix on the surfaces of lungs were pre-treated for tracking matrix migration post 48 hours. Migrated depth were measured by area of NHS-FITC labelled area divided by length of biopsy's section by parameters measured by Fiji. Each group contained 4 repeats and paired comparisons were carried out by ANOVA. * represents p-value less than 0.05; *** indicates p-value less than 0.001.*

3.2.2 Matrix Migration Caused by Primary Neutrophils.

Differentiation was induced in cultured ER-Hoxb8 cells for 4 days. As discussed in the previous section, the cells undergo differentiation from GMPs to precursor neutrophils on day 1, immature neutrophils on day 2, and mature neutrophils on day 4. We collected cells at different stages on the corresponding days to analyze their capacity to induce matrix migration by co-culturing the cells with 2 mm mouse lung biopsied as described above. Here, the average depth of labelled matrix gradually increased from 5 mm to 7 mm. In summary, we concluded that neutrophil carrier function was enhanced along with the maturation process.

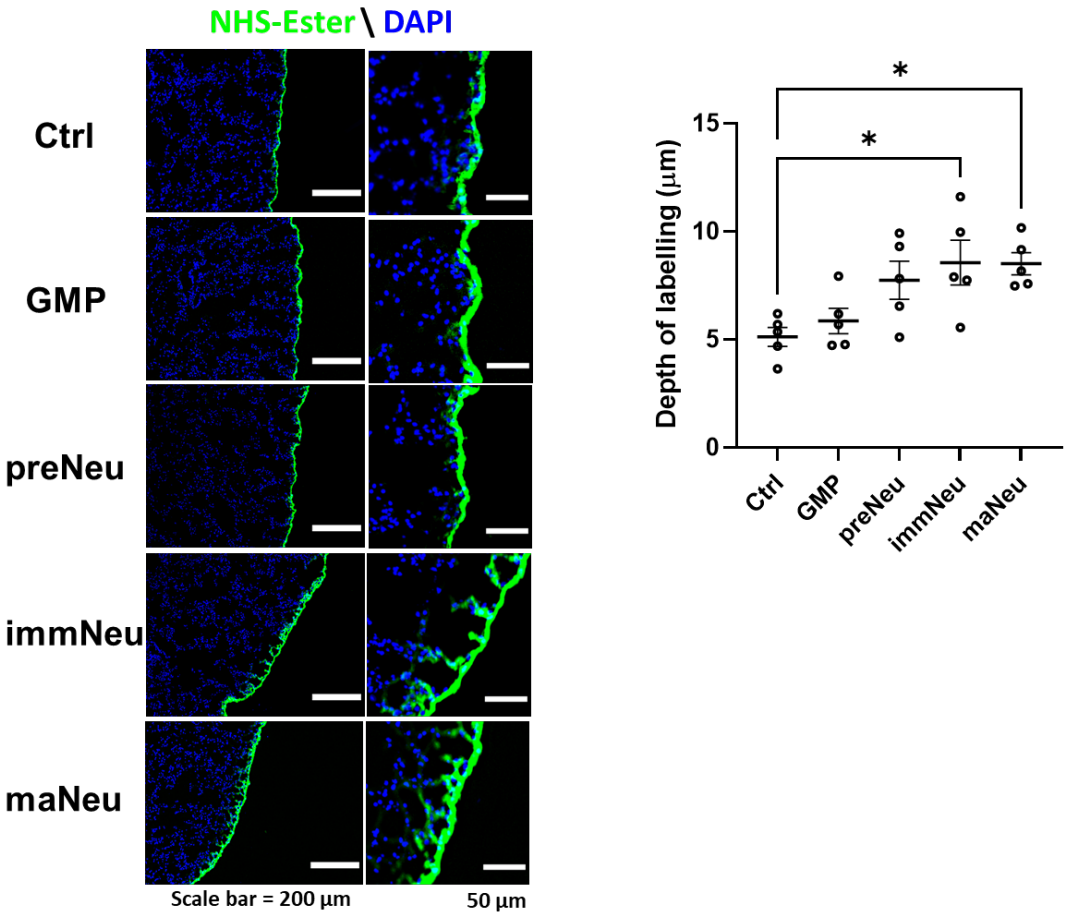

*Figure 3.2.2 Pre-exist matrix carried by mature neutrophil to support wound healing. Cultured lung biopsies were co-cultured with 4-days differentiated neutrophils from ER-Hoxb8 cells. NHS-FITC ester labelled extracellular matrix on the surfaces of lungs were pre-treated for tracking matrix migration post 48 hours. Migrated depth were measured by area of NHS-FITC labelled area divided by length of biopsy's section by parameters measured by Fiji. Each group contained 4 repeats and paired comparisons were carried out by ANOVA. * represents p-value less than 0.05; *** indicates p-value less than 0.001.*

3.2.3 Granular Proteins Dynamic Post Maturation

Here we also investigated the role of the granular protein cathepsin B (CSTB) in the process. Cathepsins, including CSTB, D, and G, are constituents of azurophilic granules and regulate neutrophil exocytosis (Fleit & Furie, 2014). Notably, CSTB possesses specific histone H3 protease activity implicated in ferroptosis (Nagakannan et al., 2021). To elucidate CSTB dynamics during neutrophil maturation, we performed Western blot analysis on differentiated ER-Hoxb8 neutrophils. Finally, our findings revealed increased pro-CSTB levels in the Era-treated group compared to the control and Fer group on day 4, suggesting that inhibiting ferroptosis in neutrophils prolongs granulopoiesis.

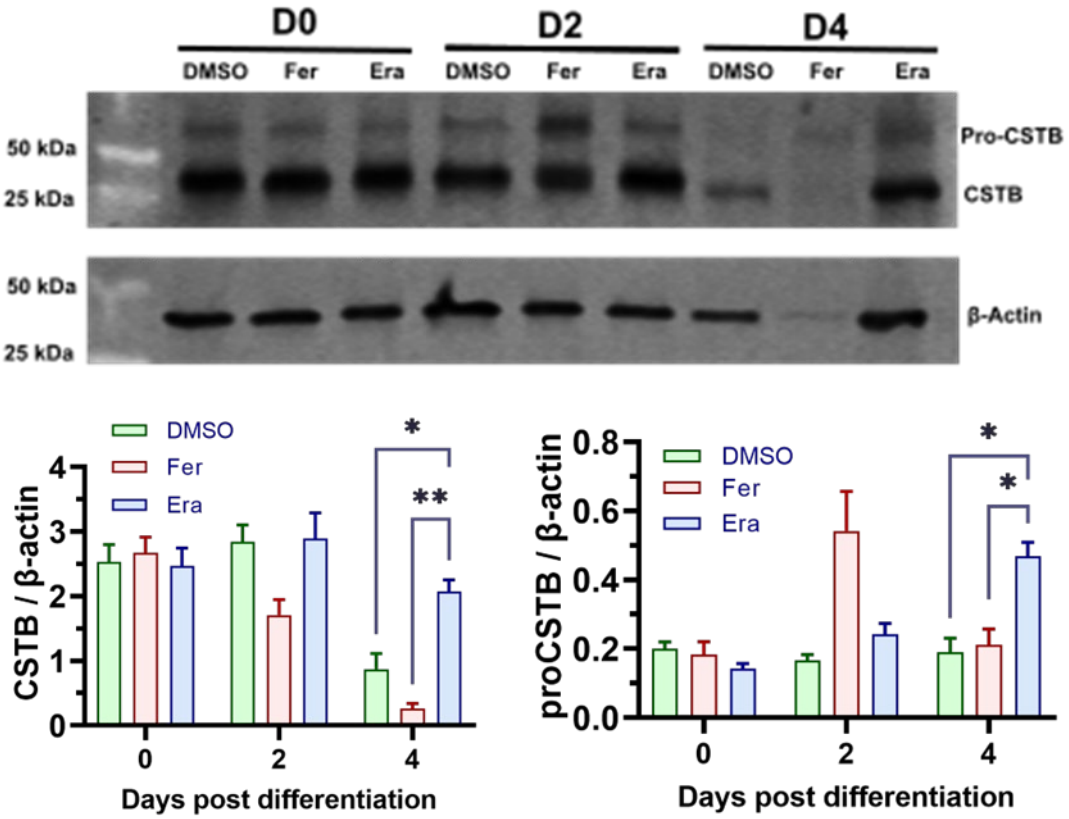

*Figure 3.2.3 Cathepsin B expression of differentiated neutrophils. ER-Hoxb8 cells were cultured 4 days to collected for western blotting analyses. β-actin were used as reference control. Each group contained 3 repeats and statistics comparison were carried out by ANOVA. * represents p-value less than 0.05; ** indicates p-value less than 0.01.*

3.3 Neutrophil Ferroptosis in Wound Repair and Surgical Adhesion

3.3.1 Ferroptosis Activity at Skin Wound.

To explore ferroptosis in wounds post-excisional injury, we adapted a 5-mm full-thickness excisional murine wound model, a standardized wound creation allowing controlled manipulation of the healing process. Prior to surgical operation, subcutaneous fasciae were labelled with NHS-FITC on days -3 and -1 as described in figure 3.3.1. Gpx4, identified as a master regulator in the ferroptosis process, converts lipid hydroperoxides (Doll et al., 2017). Hence, decreased Gpx4 implied accumulation of intracellular peroxides leading to ferroptosis. Wounds were harvested at 7 days post-wounding (dpw) and proceeded for cryosections. Immunofluorescence staining of Gpx4 showed high expression levels in the wound bed, highly co-localized with NHS-labelled fascia matrix (magnified squared region in figure 3.3.1). Our data implied that ferroptosis in fascia contributes to fascia matrix migration during wound healing.

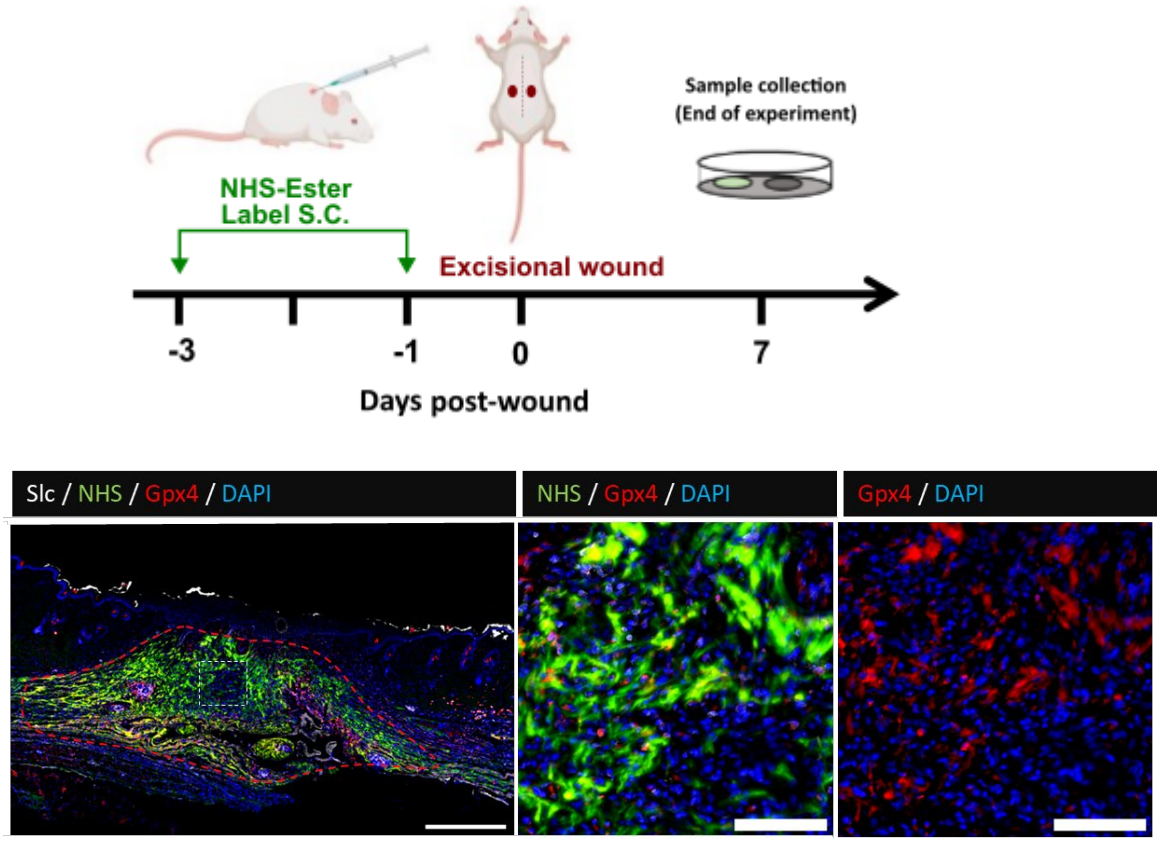

Figure 3.3.1 Detection ferroptosis activity on excisional wound. Wildtype mice were labelled with NHS-Ester via subcutaneous injection twice prior surgical excisional wound. On day 7, murine wound skin was dissected for immunostaining.

3.3.2 Neutrophil Ferroptosis in Diabetic Foot Ulcers

Inflammatory factors, ROS, and high level of blood glucose in diabetes progressively induce cellular death, including apoptosis and ferroptosis (Yang & Yang, 2022). Dysregulation of neutrophil ferroptosis is believed to be involved in the pathogenesis of diabetes, while inhibitors of ferroptosis benefit diabetes and its complications. To assess neutrophil cell death at the inflammation stage of wound healing, we analyzed transcriptomics of granulocytes from non-healing diabetic foot ulcers (DFU) extracted from a published scRNA-seq dataset (Theocharidis et al., 2022). Our analysis demonstrated defective recruitment of neutrophils and macrophages, leading to chronic inflammation. Granulocytes from DFU patients showed decreased GPX4 expression, a key inhibitor of GSH and ferroptosis suppression. Conversely, SLC3A2, a ferroptosis activator, was significantly elevated in granulocytes, suggesting enhanced iron uptake. These data suggest high ferroptosis stress in neutrophils.

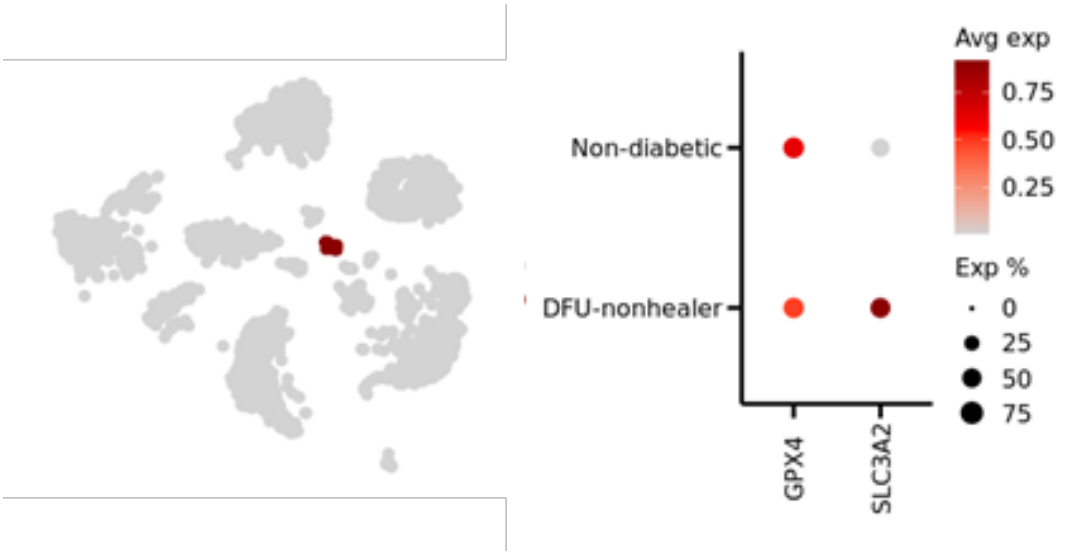

Figure 3.3.2 Ferroptosis activity of granulocytes from diabetic foot ulcer. Datasets were retrieved from GEO database. Granulocytes were extracted according to cell type clusters. Normalized gene expression was plotted to view.

3.3.3 Neutrophil Ferroptosis in Mouse Wound Model

At the late inflammatory stage of wound healing, macrophages accumulated at the wound site and take over inflammation process (Gay et al., 2020). However, we found neutrophils existed under skin wound from the whole dermis during injury (Correa-Gallegos et al., 2023). Here, we observed lower GPX4 expression in granulocytes compared to other cell types. Similarly, SLC7A11 was highly expressed in granulocyte clusters, which might imply pressure for suppressing ferroptosis.

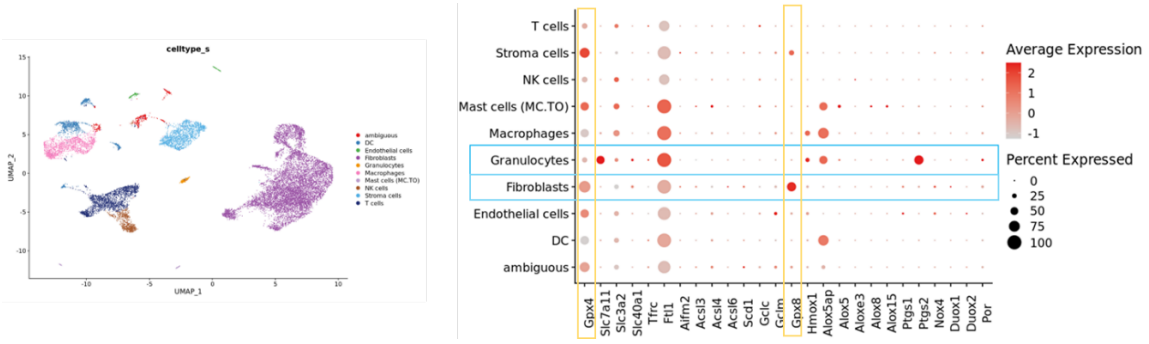

Figure 3.3.3 Ferroptosis activity of granulocytes from murine wound on day 18. Datasets were retrieved from GEO database. Granulocytes were extracted according to cell type clusters. Normalized gene expression was plotted to view.

3.4 Immune Cells at Murine Wound

3.4.1 Immune Cells Recruited into Wound.

Two full-thickness excisional wounds were created on the back of wildtype young mice using a 5 mm biopsy punch under anesthesia. On days 1, 3 and 7, post-wounding, the wounds were harvested and separated into fascia and dermis. Single-cell suspensions were prepared from the tissues and labelled with Cd45 and Ly6G antibodies for flow cytometric analysis to track neutrophils dynamics. The number of $Cd45^{+}Ly6G^{+}$ neutrophils peaked at 1 dpw, reaching 40% of total $Cd45^{+}$ immune cells. Subsequently, neutrophil numbers decreased, with 18% on day 3 and 5% at day 7 respectively.

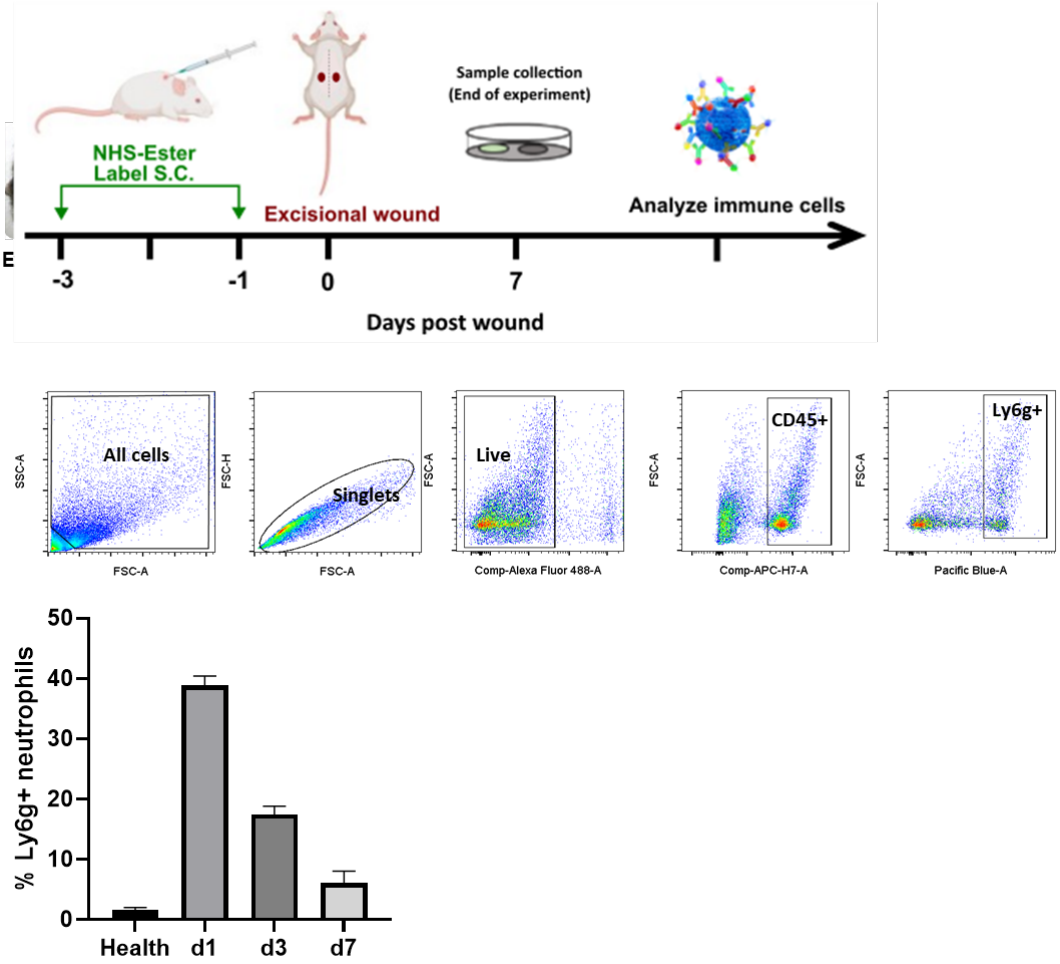

Figure 3.4.1 Immune cells recruited into wound post injury. Wildtype mice were performed excisional wound. On days 1, 3, and 7, wounded skin was dissected for immunostaining. Stained cells were analyzed by flow cytometry. Dead cells were excluded from analysis by SytoxGreen. Each group included 3 repeats from statistic comparison.

.

Subsequently, we sorted all Cd45^{+} immune cells via FACS and proceeded with library preparation for scRNA-sequencing analysis. The sequencing was performed on Illumina HiSeq 2500. Raw reads were aligned with mm10 genome from UCSC using the Cellranger toolkit.

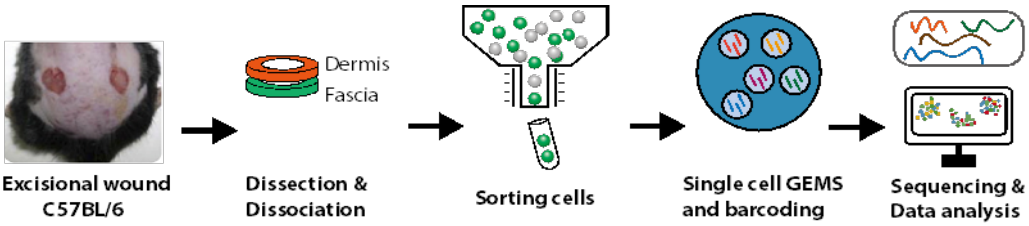

Figure 3.4.2 Scheme from immune cells sorting and single cell libraries preparation. Wildtype mice were performed excisional wound. On day 1 and 3, the wounded skin was dissected for sorting immune cells. Singlets were prepared from single cell sequencing. Dead cells were excluded from analysis by SytoxGreen.

3.4.2 Quality Control and Filtering of Single Cells

In our pre-processing workflow, we calculated quality metrics such as the number of genes and reads counts, as well as the percentages of mitochondrial, ribosomal, and hemoglobin genes per cell. A high percentage of mitochondrial genes represents poor-quality cells, suggesting that whole-cell transcripts were low possibly released extracellular. Hemoglobin genes signal blood cell contamination (Lun et al., 2016) Following the protocol from 10x Genomics, we included neutrophils for downstream analysis despite their low transcripts inputs, and used recommended Cellranger settings, including force-cells, including introns.

Here, cells from the dataset “Fascia from uninjured skin” contained fewer genes (n_genes_by_counts), and mapped reads (total_counts). Therefore, we applied a standard quality control approach, removing poor-quality cells with low number of genes and mapped reads. According to the QC results, we set a threshold of 200 to 6000 detected genes to filter out potential doublets, with less than 25% mitochondrial genes, more than 5% ribosomal genes, and less than 5% hemoglobin genes. We found cells distributed centroided very well in violin plots.

Finally, we demonstrated that neutrophils were preserved and well-annotated post filtering out low-quality reads as well as gene.

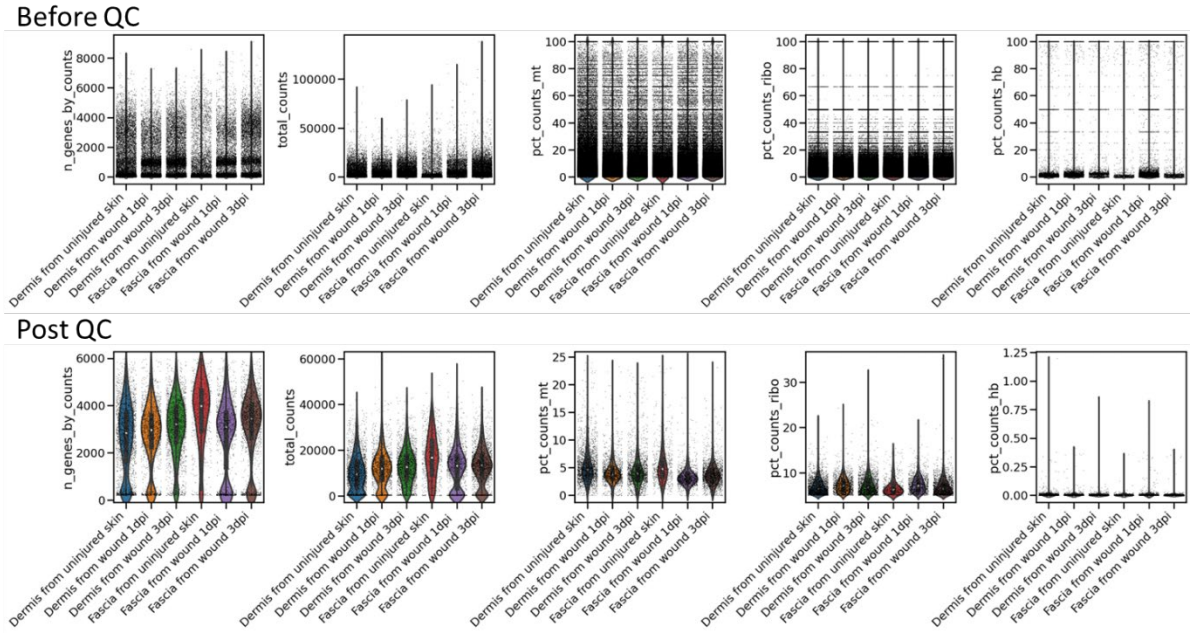

Figure 3.4.3 Quality control and filtering of low-quality cells. Quality metrics, gene number, reads counts, percentage of mitochondrial genes per cell, percentage of ribosomal genes per cell, and hemoglobin genes per cell were calculated for quality control. Low-quality cells were filtered out according to literatures.

3.4.3 High Variable Gene and Dimensional Reduction

To select highly variable genes and reduce computational burden, we normalized raw counts to a total of 10,000 counts per cell and log-transformed counts to standardized variance across cells. A total of 4595 highly variable genes were selected based on dispersion for dimensional reduction (Left plot in upper panel). PCA was used to calculate principal components, identifying meaningful genes for discerning cell types. An elbow plot assessed the cumulative explained variance by each component (2nd plot in upper panel). The first 4 components, plotted as PC1 vs. PC2 and PC3 vs PC4, effectively demonstrated sample overlap and dispersion (3rd and 4th plots in upper panel). While the first 3 components captured a substantial proportion of variance, the initial thirty components were retained to preserve potential biological information for further dimensional reduction using UMAP (2nd plot in upper panel). Subsequent visualization of gene loadings for each principal component revealed enrichment of collagen genes (Col3a1, Col1a2, Col5a2) in PC1 (1st plot in bottom panel), indicative of a fibroblast-like cellular component within the dataset. PC2 exhibited elevated expressions of Clec4e, Vegfa, and Cd14, suggesting potential immune cell populations. PC3 was associated with high MKi67 expression, potentially reflecting proliferative cell states, while PC4 displayed enrichment of Cebpb, characteristic of myeloid cell lineages.

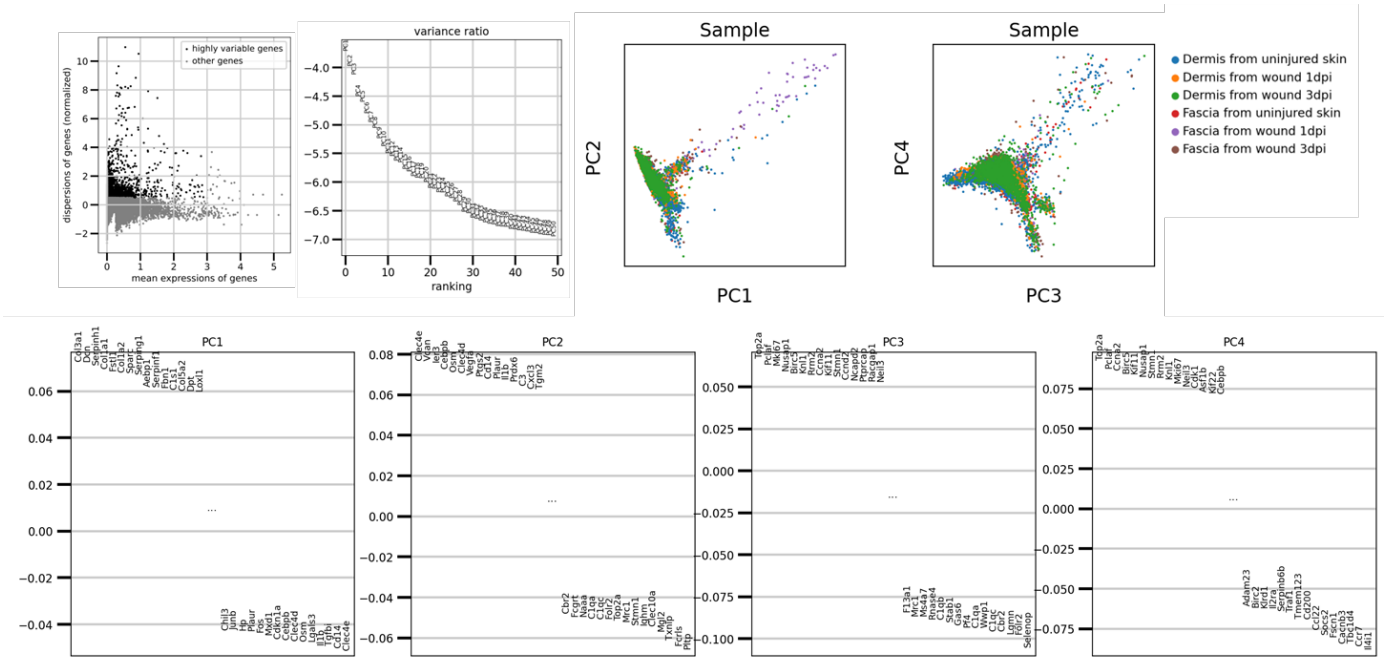

Figure 3.4.4 High variable genes were selected and performed PCA. High variables genes across original identities were found and 4595 genes used for dimensional reduction. The first 30 components of PCA were chosen for further processing.

3.4.4 Characteristics of Immune Cells at The Wound

The scRNA-seq datasets of mouse wound were detailed in subsequent plots. After quality control, we integrated datasets using the harmony algorithm (Korsunsky et al., 2019), projecting each cell according to its shared characteristics by cell type. Unsupervised clustering with UMAP was applied to detect cell clusters using harmony dimensions instead of PCA. Cell types were annotated using “Celltypist” with pre-trained mouse models and canonical marker genes. We identified 9 common immune cell types under wound conditions based on feature genes. All cell clusters present in both dermis and fascia across days post-injury.

Cell frequency was shown as the percentage of each cell type relative to the total cell amount. Neutrophils, which reside in low numbers in tissue, were most significantly accumulated cell type on day 1 post-wounding, reflecting their rapid activity. In dermis, a high percentage of neutrophils (~10%) were detected compared to 3 % in fascia initially, but their numbers decreased more slowly than fascia, possibly due to continuous inflammation. Monocytes remained at similar levels across all conditions, while macrophages decreased on day 1 and bounced back at day 3, implying a huge number of neutrophils at the wound bed. Mast cells appeared in the steady-state tissue but not in injured tissue due to their autoimmune role. Interestingly, type 1 DCs, characterized by Flt2, Cst3, and Clec9a, were

found but in low number. Adaptive immune cells, T cell and B cells, were low in the wound, suggesting they were not yet functional yet.

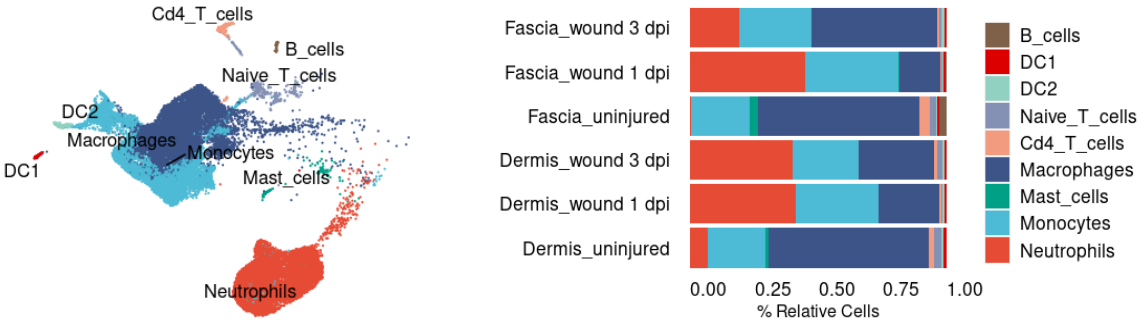

Figure 3.4.5 Immune cell annotation and fraction analysis. Leiden algorithms were utilized for cluster segmentation at resolution of 1.0. "Celltypist" together with pre-trained mouse models were tested in our mouse wound and cell type were inspected according to canonical marker genes manually.

The top 10 genes expressed in each cell type were identified, with neutrophils expressing S100a8/9, Cxcr2/Cxcl2 chemokines, G0s2, Il1b and Il1r2. While monocytes and macrophages shared markers such as Apoe, Clec4a1, Ctsc. Mast cells expressed Tpsb2, Mcpt3, Retnla, Cpa3 and Cma1. All DCs expressed Flt3 and Cst3, but Celc9a, Spet3, and Nup210 were specific to type 1, while Adcy6 and Socs2 were specific to type 2 (Ardouin et al., 2016). B cells were characterized by Ms4a1 and Cd79a/b.

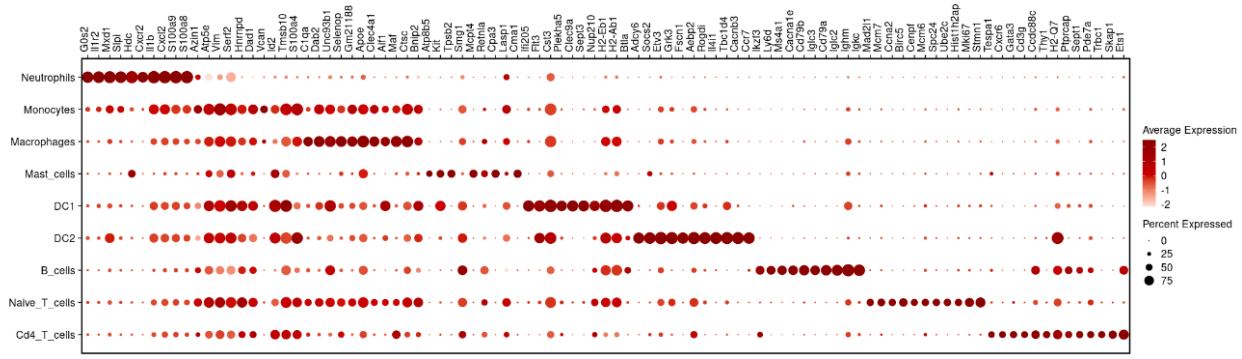

Figure 3.4.6 Potential cell markers were identified. Top expressed genes were identified by Scanpy and plotted by dot-plot.

3.4.5 scRNA-seq analysis of Ferroptosis of Wound infiltrated Immune Cells

To view cell distribution across tissues and treatments, we plotted cells in UMAP after quality control. Consistent with previous studies (Tsai et al., 2019), the percentage of neutrophils

peaked on day 1, while macrophage ratios slightly decreased compared to uninjured tissue, and monocyte levels slightly increased.

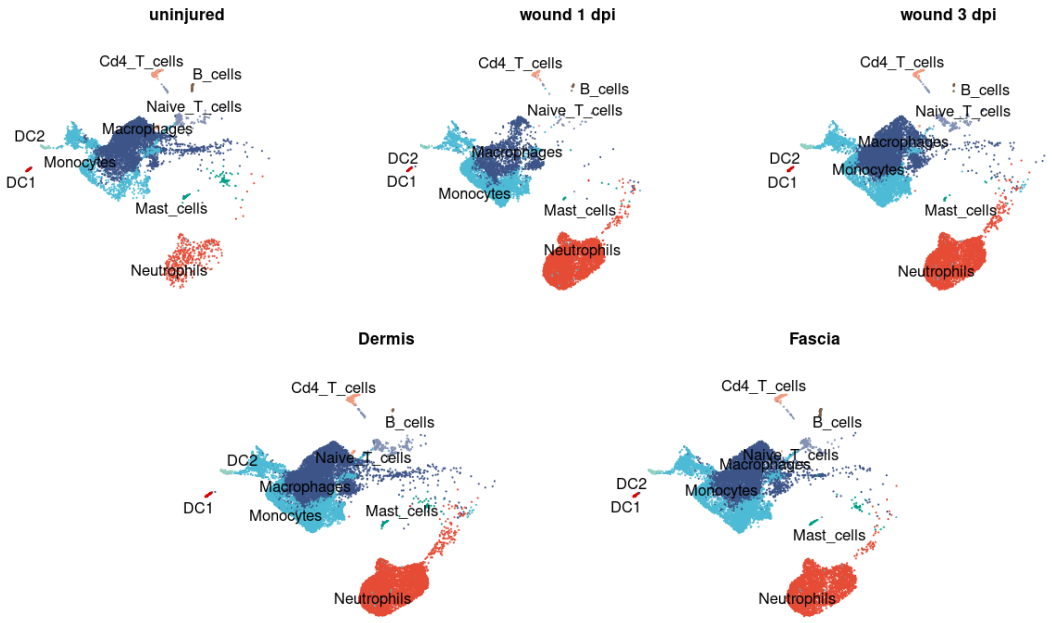

Figure 3.4.7 UMAP were adapted for cell heterogeneity.

Differentially expressed genes in each cell type were calculated using the FindAllMarkers function from Seurat, representing cell dynamics across time points. To explore immune cell death, gene sets were enriched with enrichGO embedded in ClusterProfile (Wu et al., 2021). Finally, neutrophil death was mainly attributed to ferroptosis and apoptosis, with genes such as Slc3a2 and Por highly expressed on day 1 and further increased on day 3. The ferroptosis score increased over time, aligning with our previous analysis.

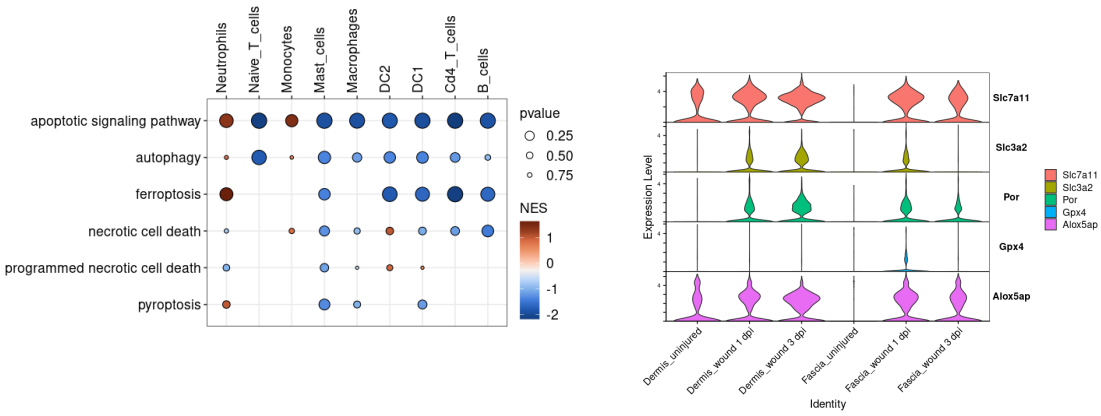

Figure 3.4.8 Different expressed genes of each cell type were enriched with enrichGO embedded in ClusterProfile. Top expressed genes in ferroptosis were plotted to inspect ferroptosis activity.

3.5 Ferroptosis in Neutrophils

3.5.1 Neutrophil Subsets in Wounds

Subsequently, we focused on the neutrophil populations within our dataset, distinguishing six subtypes (Neu_C1 through Neu_C6). Among these, the Neu_C2/3/4 constituted the predominant neutrophil proportions, likely corresponding to both immature and mature neutrophil states. Notably, Neu_C2 expressed Cxcr4 and Cstb, Neu_C4 expressed S100a8/9, and Neu_C3 expressed Cxcl2 and Nfkbia, indicating distinct molecular signatures.

In stacked bar plot, Neu_C1/2 were not detected in fascia and were low in the dermis, suggesting they represent neutrophil precursors. Neu_C3/4 presenting in a large population suggests their main function of homeostasis. But Neu_C3 decreased rapidly at day 1, indicating its emergency response role.

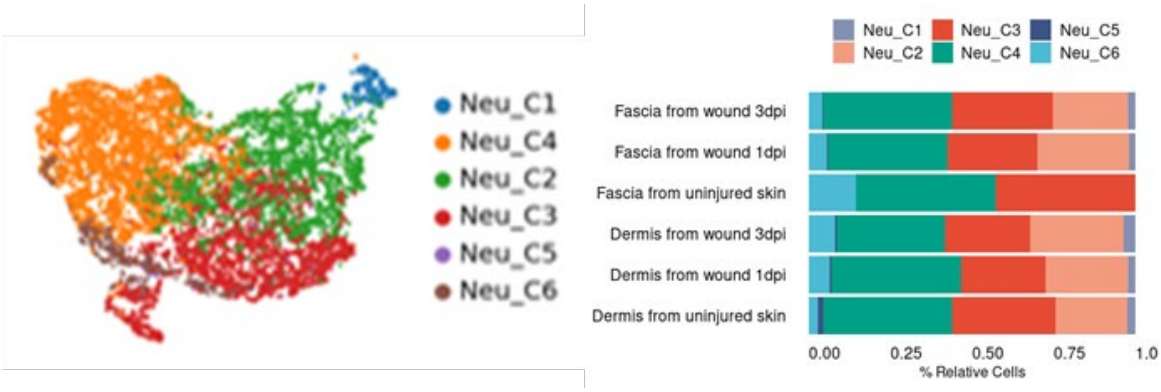

Figure 3.5.1 Neutrophil heterogeneity and percentage of each subtype neutrophil.

3.5.2 Dynamics of Neutrophil Subset Maturation

To track neutrophil maturation along its status, we performed RNA velocity analysis based on the estimation of spliced and unspliced mRNA variants in cells. Here we adapted scVelo, a computational tool inferring direction and speed of cell state transition (Bergen et al., 2020). Ordering of neutrophil in velocity pseudotime inferred root cells from right-top corner, Neu_C1 and arranged most of cells into a diffused population, to bottom and right side, Neu_C4. We supposed that neutrophil development and maturation during acute inflammation at wound were caused by cell death and clearance. Subpopulation kinetics in neutrophil were deducted into 3 distinct trajectories by estimating connectivity of each neutrophil subset. Cluster Neu_ C1, a root cell subset representing progenitors, expresses Cxcr4, a crucial chemokine receptor regulating neutrophils released from bone marrow.

Next, we analyzed the expression of key markers in status transition. Intricately, Neu_C2, expresses both Cxcr2 and Cxcr4, was identified as a transient intermediate state. Ly6g expression mainly exists in cluster Neu_C4, indicating their immature and maturate neutrophil nature. However, top-likelihood drivers in Neu_C3 were identified as Nfkbia, an inhibitor of NF-κB nuclear localization, which implied for an immunosuppressive neutrophil subset, but not working via inhibiting T cells activation and effector function.

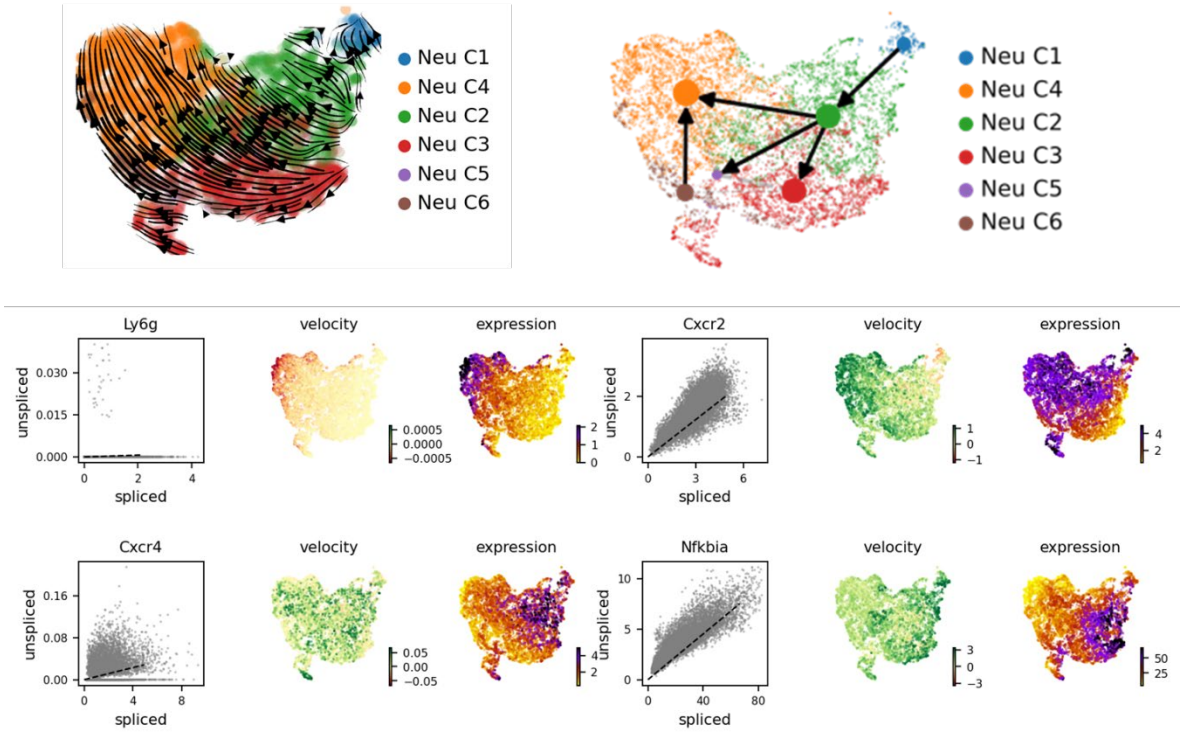

Figure 3.5.2 UMAP showed neutrophils mature dynamic. RNA velocity was analyzed by scVelo. Top regulators were plotted to view its velocity across cells.

3.5.3 Interaction Between Neutrophils and Fibroblasts

To investigate neutrophil interactions with fibroblasts, we performed Cellchat analysis, identifying chemokines as key regulators (Jin et al., 2021). Proinflammatory and proto-myofibroblast highly expressed Cxcl1/5, recruiting innate immune cells from peripheral blood via the Cxcl1/5-Cxcr2 axis.

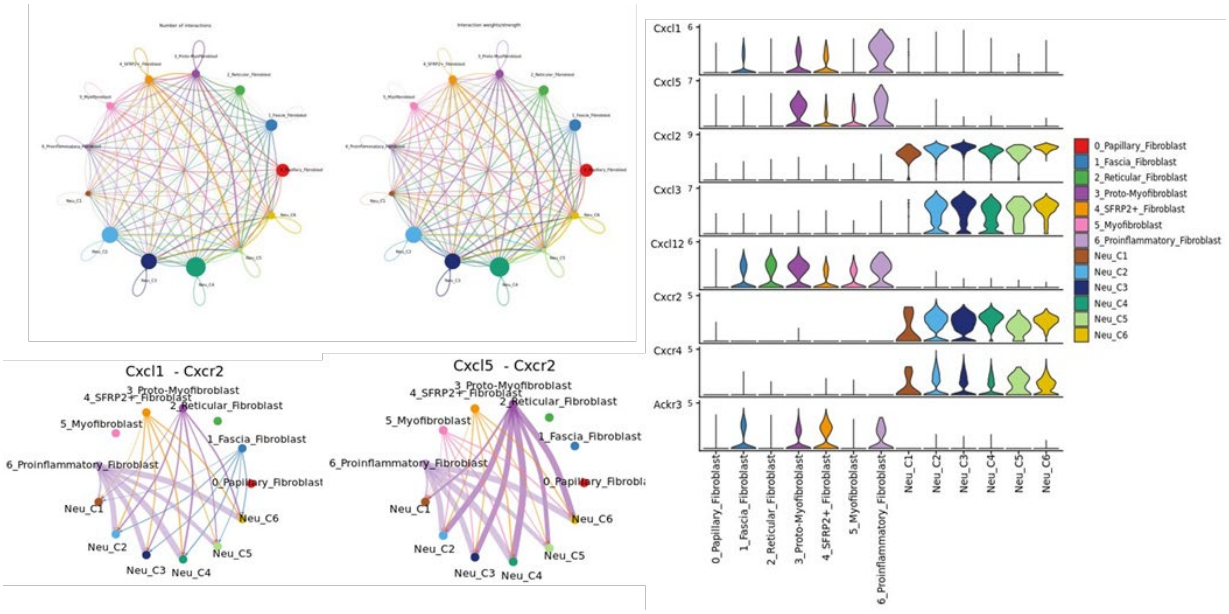

Figure 3.5.3 Cell interaction was evaluated by Cellchat. Neutrophils from our dataset and fibroblasts datasets were integrated for interaction analysis. Chemokines were identified by ranking signaling. Violinplot were used for top activity chemokines.

3.6 Ferroptosis in Neutrophils regulates Fascia Mobilization

3.6.1 Fascia Contraction with Neutrophil ferroptosis

Murine skin is composed of several consecutive layers, including the epidermis, dermis, subcutaneous fat, panniculus carnosus muscle, and subcutaneous fascia. The deepest fascia is fibroelastic and responsible for rapid wound repair, providing the possibility to characterize fascia in wound healing ex vivo (Rinkevich et al., 2022). Murine fascia of approximately 2 mm^3 excised from dorsal skin was cultured in a dish for 5 days to track tissue contraction. Notably, murine fascia treated with neutrophils with ferroptosis blocking showed slowed fascia contraction. However, inducing ferroptosis in neutrophils bypassed

the fascia contraction phases, reaching the terminal stage by day 3. Our data demonstrated that neutrophil ferroptosis slows down its contraction ex vivo.

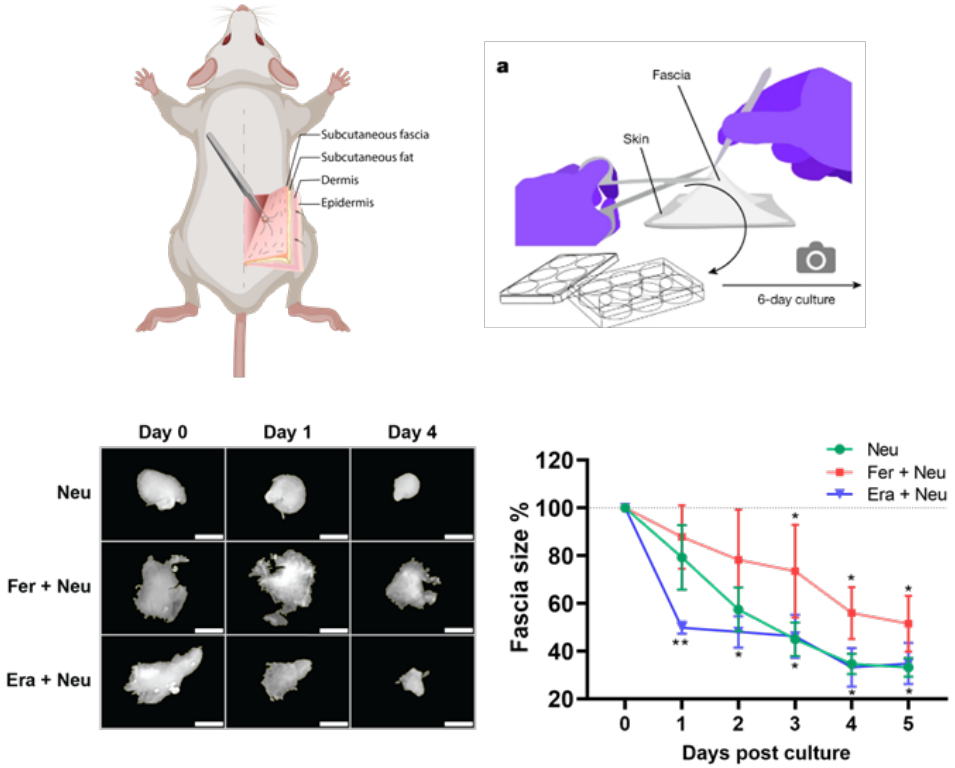

*Figure 3.6.1 Murine fascia contraction accelerated by ferroptotic neutrophil. Fasciae were dissected from dorsal skin and co-cultured with neutrophils and ferroptosis agents for 5 days. Each group included 4 repeats. The size of the cultured fascia explants was monitored daily by photography to assess their contractile activity. Contraction data was statistically analysed using ANOVA to compare the effects of contraction relative day 0. Statistical significance is indicated by p-values: * for $p < 0.05$ and ** for $p < 0.01$.*

The superficial fascia layers in humans are linked to the retinacula cutis superficialis, which extends the fascia layer into the dermis (Fede et al., 2023). Human fasciae were acquired from clinics according to guidelines. For the fascia contraction assay, the fascia was cultured in a dish for 8 days with neutrophils treated with ferroptosis blocker/inducers. Finally, we demonstrated that induced ferroptosis in neutrophils accelerated human fascia contraction during the first 2 days. Here we concluded that inhibiting ferroptotic neutrophil triggered gradual fascia contraction.

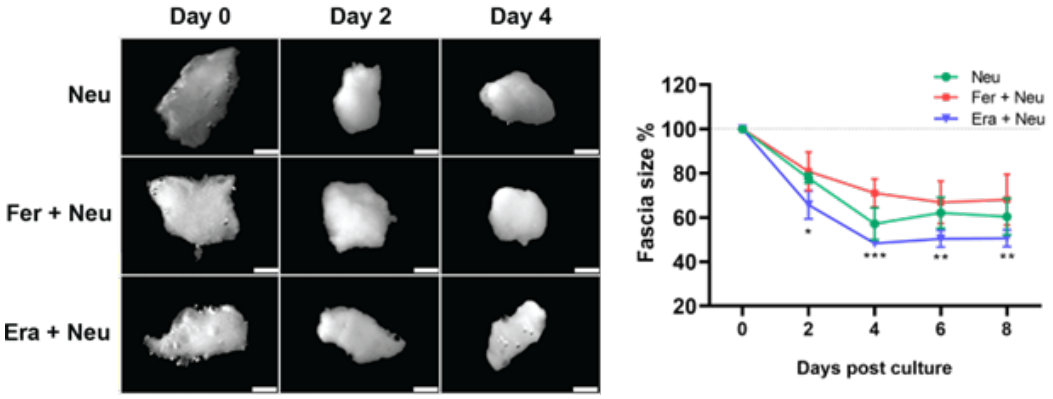

*Figure 3.6.3 Effects of ferroptosis induction and inhibition on human fascia contraction in vitro. Human fascia explants were harvested from patients and co-cultured with neutrophils and ferroptosis inducer/blocker in vitro for 8 days. The size of the cultured fascia explants was monitored daily by photography to assess their contractile activity. At least three independent replicates were performed for each treatment group relative day 0. Statistical significance is indicated by p-values: * for $p < 0.05$, ** for $p < 0.01$, and *** for $p < 0.001$.*

3.6.2 The Effect of Ferroptosis Inhibition on Wound Healing

Given that fascia contraction is regulated by ferroptotic neutrophil, we investigated the physiological effect of ferroptosis on wound healing in vivo. Excisional wounds were created on mouse back skin, and Era or Fer was locally injected around wound via subcutaneous injections. Wounds were harvested at 3, 5, and 7 dpw, proceeded for cryosections and subsequently stained Masson's trichrome. Wound areas were quantified using Fiji after scale calibration. Wound size was significantly decreased when treated with a ferroptosis blocker compared to controls or ferroptosis inducing treatment. Moreover, wounds treated with ferroptosis inducer showed prolonged inflammation with sustained high level of immune cell infiltration in the wound bed. These data suggest that blocking ferroptosis is beneficial for wound healing.

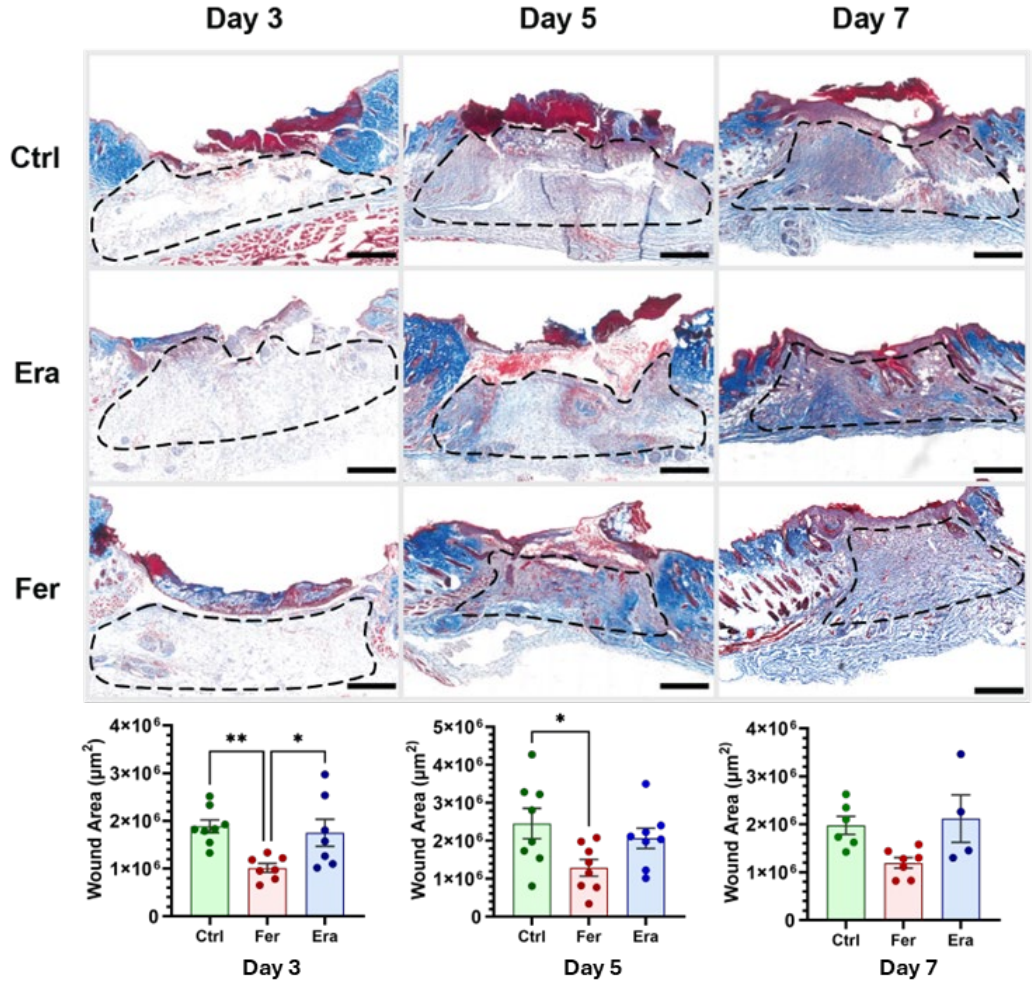

*Figure 3.6.4 Murine excisional wound was healed faster when blocking ferroptosis in vivo. Wildtype mice were carried out excisional wound and treated ferroptosis inducing and blocking chemicals via subcutaneous injection. On day 3,5 and 7, murine wound skin was dissected for trichrome staining. Each group includes at least 3 mice. Paired comparisons were performed by ANOVA. * represents that p value less than 0.05. ** represents that p value less than 0.01.*

3.6.3 Matrix Remodeling at Wound Site

As blocking ferroptosis benefits wound healing, we further investigated Gpx4 signaling after modulating the ferroptosis pathway. Murine skin samples were stained Gpx4 and Slc7a11, the upstream regulators that promote cystine uptake and glutathione biosynthesis. After 7 days, we found Gpx4 was highly expressed in the wound bed. However, Slc7a11 was overexpressed when the ferroptosis pathway blocked. Ideally, Gpx4 and Slc7a11 expressions in the Fer-treated group were lower than control and Era-treated group, implying that ferroptosis stress were alleviated after blocking ferroptosis. Our results align with the conclusion derived from development of skin lesion in homozygous Gpx4-reduction mice (P. Li et al., 2021).

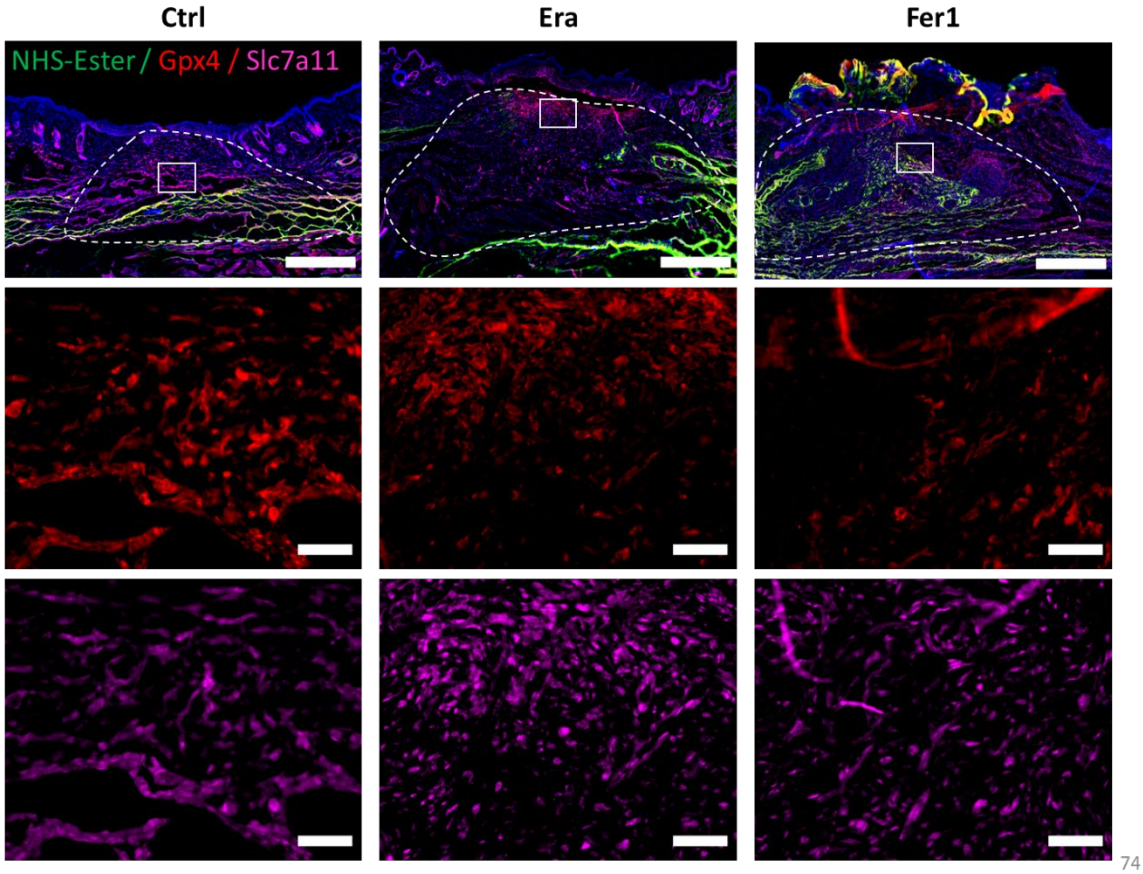

Figure 3.6.5 Murine excisional wound showed lower ferroptosis stress when blocking ferroptosis in vivo. Wildtype mice were carried out excisional wound and treated with ferroptosis inducing and blocking chemicals in vivo for 7 days.

4 Discussion

4.1 Maturation and Development of Neutrophils in Peripheral Tissue

Neutrophils are the main activist in immune system, especially in innate immune response, to induce inflammation and protect against infections (Nourshargh & Alon, 2014). Previously, maturation and development of neutrophils has been classified into several consecutive steps. Originally, neutrophils are conceived from hematopoietic stem cells, which happens in the bone marrow (Mackey et al., 2019). Upon inflammation, neutrophils extravasate from microvessels and migrate into the inflamed tissues after a short period of circulation in the peripheral blood, which including an amplification of the response that robust neutrophil infiltration followed by the first arrived signal (Ng, 2022). Finally, in distal or local tissue, the activities of neutrophils including phagocytosis, production of ROS, and release of granule proteins, contributing to the clearance of pathogens and the resolution of inflammation (Mayadas et al., 2014).

In peripheral blood, lifespan of neutrophils varies depending on lots of reasons, for example disease status, inflammation, tissue location, time periods. However, neutrophils have short half-life, approximately 6-8 hours in average (Pillay et al., 2013). The life span of tissue resident neutrophils are 6-15 times longer than that of blood neutrophils, which allow them to carry out more functions, such as carrying ECM, over an extended period. In our neutrophil ferroptosis assay, ~ 80 % neutrophil living after 16 hours when blocking ferroptosis with ferrostatin. Inverse, inducing ferroptosis promote ~30-40% more neutrophil death.

During neutrophil maturation, different granules are sequentially forming and CSTB is stored in azurophilic granules (Fleit & Furie, 2014). CSTB exists in an inactive pro-form within granules but is activated upon release to exert its cysteine protease activity. Western blot analysis revealed elevated levels of pro-CSTB/CSTB in Era-induced neutrophils compared to the control group and the Fer group. The activation and release of CSTB can partially act as a mediator of ferroptosis inversely (Nagakannan et al., 2021).

4.2 Interaction between Neutrophils and Fibroblasts

One potential interaction, excluding Cxcl1/Csf3, between neutrophils and fibroblasts in the progression of ascending thoracic aortic dissection (ATAD) is the Cxcl12-Cxcr4/Ackr3 axis (He et al., 2022). Cxcr4 and Ackr3 expressions were detected in fibroblasts of the adventitia and in neutrophils by IHC (He et al., 2022). Further, the downstream signaling of Cxcl12-

Cxcr4 activates JAK-STAT, ERK and so on, modulating cytokine production, chemotaxis, ROS production, cell differentiation, and apoptosis (Abdelouahab et al., 2017). However, here we identify neutrophils-regulated fascia contraction via interaction with fibroblasts, particularly proinflammatory fibroblast. Fibroblast transition from proinflammatory to proto-myofibroblast ultimately leads to tissue contraction. Interaction analysis, based bioinformatics, demonstrated the Cxcl1/5 – Cxcr2 axis as a main regulator.

A population of fibroblasts from gingival, activated to guide oral inflammation, was defined as AG fibroblasts, binding to infiltrated neutrophils and lymphocytes via its activated receptors and chemokines (Saczko et al., 2008). In mouse model of periodontitis, proinflammatory neutrophils were predominant in gingival lesion and expressed chemokine receptors such as Cxcr2, and G0/G1 switch gene 2 (G0s2), and Ccl/Cxcl chemokines (Kondo et al., 2023). Interaction between AG fibroblasts and neutrophils were proposed via Ccl8-Ccr1, Cxcl1-Cxcr2 and Cxcl12-Cxcr4 communications, which aligned with our findings. Our results suggest that fibroblasts and neutrophils interact and influence each other's functions in the context of not only gingival health and periodontitis but also wound healing.

In the development of immunofibrosis in Crohn's diseases, neutrophils interacted with intestinal fibroblasts via IFNα/JAK pathway in driving immunofibrotic process (Gavriilidis et al., 2023). The activated neutrophils were shown to promote a pro-fibrotic phenotype, by activating fibroblasts and inducing their differentiation, through NETs formation. IL-8, synthesized and released by intestinal fibroblasts, plays as a positive feedback signal, binding to receptors in neutrophils which sustain the signals (Gavriilidis et al., 2023). However, we did not get the chance to examine neutrophil-fibroblast crosstalk in the pathogenesis of wound healing, which required further in molecular and cellular assay.

Aberrant formation of NETs was explained as a reason of pathogenesis for systemic lupus erythematosus, psoriasis, and so on. Regarding the apparent neutrophil accumulation in synovial fluid from rheumatoid arthritis, NETs together with granular proteins decorated on chromatin, are sources of citrullinated autoantigens that stimulate invading fibroblast-like synoviocytes on cartilage (Khandpur et al., 2013). The interaction between NETs and fibroblasts-like cells in these studies were not included, while it may contribute by other complex mechanisms involving other immune cells, remaining to further study. Overall, interactions between fibroblasts and neutrophils can influence immune responses, tissue remodeling, and disease progression. Understanding the mechanisms and consequences of neutrophil-fibroblast interactions is crucial for elucidating the underlying processes in various diseases.

4.3 Heterogeneity of Neutrophils in Tissue

Recent studies highlighted the heterogeneity of neutrophils, both phenotype and function, caused by various factors, including maturation status, aging, and tissue microenvironment under homeostasis. Neutrophils, coming from bone marrow and characterized by Cd62L and Cxcr2, are reducing Cd62L dramatically and highly express Cxcr4, Cd11b, which is favor for migration from circulation into inflamed tissue (Jaillon et al., 2020). While, a subset of neutrophils, marked with interferon-stimulated genes, represent an anti-infection in mice and human, which were identified either in tumors (Zilionis et al., 2019). Our new findings observed the neutrophil subset present in wounds, specifically the Nfkbia+ subset of neutrophils.

In line with homeostasis, studies from inflammation, cancer, and periodontal disease discovered neutrophils with various phenotypes and functions in different contexts (Hirschfeld, 2019; Lecot et al., 2019; Rawat & Shrivastava, 2022). Tumor-burden mice were used to find neutrophil differentiation and maturation trajectories via using single-cell transcriptomics (Alshetaiwi et al., 2020). Myeloid-derived suppressor cells (MDSCs), in breast cancers, emerged from abnormally differentiated neutrophils and featured by Cd84 expression (Alshetaiwi et al., 2020). Similarly, unipotent-committed neutrophil progenitor (NeP) marked by Lin− Cd117+ Ly6A/E− were identified from healthy and cancer mouse model by CyTOF methods. NeP exists in human blood with low density but increased soon, from 1% to 9% in melanoma or in tumorigenesis (Zhu et al., 2018). As scRNA-seq technology greatly facilitates identification of a continuum of phenotype of neutrophils in human and mice, distinct neutrophil subsets such as Neu_C1(Csf1+Cxcr4+), Neu_C3(Nfkbia+), and Ly6g neutrophils were demonstrated that they present acute inflammatory phase of wound healing in mice.

While neutrophils heterogeneity was limited due to its short lifespan, more evidence provided their phenotypic heterogeneity and functional versatility (Ng, 2022). Regarding causing tissue damage, recruited neutrophils by Ltb4 and Cxcl2 to the sterile injury imply potential role in facilitating pre-exist matrix transfer, which represents a novel function performed by a distinct subset of neutrophil (Fischer et al., 2022).

In conclusion, neutrophils exhibit heterogeneity in both their phenotype and function. This heterogeneity has been observed in condition of inflammation, cancer, and periodontal disease. Understanding the heterogeneity of neutrophils is crucial for unravelling their diverse roles in health and disease, that will benefit for the development of targeted therapies.

4.4 Ferroptotic Neutrophil in Wound healing

Neutrophils exhibit a dual role in wound healing. Tissue damage and microbial infection leads to a quick swarming of resident neutrophils from distant region or peripheral blood to injury site, which amplified the recruitment signal further and covered site (Lämmermann et al., 2013). Same as macrophages, neutrophils modified its phenotype to acquiring responsible function associated with its local epithelial and connective tissue (Ballesteros et al., 2020). However, aberrant neutrophil activation, as observed when induced by IFN and autoantibodies, can damage its phagocytosis, aggregation of debris and pathogens, and accelerate cell death (P. Li et al., 2021). Notably, inhibiting neutrophil ferroptosis has demonstrated therapeutic potential by reducing neutrophil numbers and ameliorating disease severity, possibly through mechanisms linked to IFN modulation (P. Li et al., 2021).

Here we found that neutrophil alleviated fascia contraction when inhibiting ferroptosis in vitro and finally reflected a reduced wound size in vivo. While observed discrepancy in the duration of fascia contraction inhibition between mouse and human tissues following ferroptosis inhibition is intriguing. Previous studies have demonstrated that myofibroblast differentiation from proinflammatory fibroblast, a kye process of tissue contraction, is initiated later in the wound healing process (Correa-Gallegos et al., 2023). Thus, the timing of proinflammatory fibroblast activation and subsequent fascia contraction differing between mice and humans, potentially contribute to the observed disparity. In addition, the communication between subsets of neutrophils and fibroblasts through Cxcr2-Cxcl1/5 axis should be considered, while this pathway has been implicated in inflammatory phase of wound healing, it’s precise involvement in later stages and potential species-specific variations remain to be fully elucidated. The third factor is the impact of ferroptosis on the wound healing microenvironment. Emerging evidence suggests that ferroptosis can induce tissue damage through the release of proteases, potentially prolong the inflammation process (Wong et al., 2015). In the high-glucose environments, ferroptosis has been linked to accelerated neutrophils death and impaired wound closure (Lan et al., 2013).

In conclusion, neutrophils encompass both positive and negative effects on wound closure and scar formation. Factors in SLE, diabetes, tumor environments and so on, alert the function and phenotype of neutrophils in wound healing. Hence, further studies are essential to conclude diverse roles of neutrophils and the impact of ferroptosis on the wound healing.

5 Reference

Abdelouahab, H., Zhang, Y., Wittner, M., Oishi, S., Fujii, N., Besancenot, R., Plo, I., Ribrag, V., Solary, E., Vainchenker, W., Barosi, G., & Louache, F. (2017, Aug 15). CXCL12/CXCR4 pathway is activated by oncogenic JAK2 in a PI3K-dependent manner. *Oncotarget, 8*(33), 54082-54095. https://doi.org/10.18632/oncotarget.10789

Abdelsaid, K., Sudhahar, V., Harris, R. A., Das, A., Youn, S. W., Liu, Y., McMenamin, M., Hou, Y., Fulton, D., Hamrick, M. W., Tang, Y., Fukai, T., & Ushio-Fukai, M. (2022, Mar). Exercise improves angiogenic function of circulating exosomes in type 2 diabetes: Role of exosomal SOD3. *FASEB J, 36*(3), e22177. https://doi.org/10.1096/fj.202101323R

Alrobaiea, S. M., Ding, J., Ma, Z., & Tredget, E. E. (2016, Jul 1). A Novel Nude Mouse Model of Hypertrophic Scarring Using Scratched Full Thickness Human Skin Grafts. *Adv Wound Care (New Rochelle), 5*(7), 299-313. https://doi.org/10.1089/wound.2015.0670

Alshetaiwi, H., Pervolarakis, N., McIntyre, L. L., Ma, D., Nguyen, Q., Rath, J. A., Nee, K., Hernandez, G., Evans, K., Torosian, L., Silva, A., Walsh, C., & Kessenbrock, K. (2020, Feb 21). Defining the emergence of myeloid-derived suppressor cells in breast cancer using single-cell transcriptomics. *Sci Immunol, 5*(44). https://doi.org/10.1126/sciimmunol.aay6017

Ardestani, A., Yazdanparast, R., & Jamshidi, S. (2008, Sep). Therapeutic effects of Teucrium polium extract on oxidative stress in pancreas of streptozotocin-induced diabetic rats. *Journal Of Medicinal Food, 11*(3), 525-532. https://doi.org/10.1089/jmf.2006.0230

Ardouin, L., Luche, H., Chelbi, R., Carpentier, S., Shawket, A., Montanana Sanchis, F., Santa Maria, C., Grenot, P., Alexandre, Y., Gregoire, C., Fries, A., Vu Manh, T. P., Tamoutounour, S., Crozat, K., Tomasello, E., Jorquera, A., Fossum, E., Bogen, B., Azukizawa, H., Bajenoff, M., Henri, S., Dalod, M., & Malissen, B. (2016, Aug 16). Broad and Largely Concordant Molecular Changes Characterize Tolerogenic and Immunogenic Dendritic Cell Maturation in Thymus and Periphery. *Immunity, 45*(2), 305-318. https://doi.org/10.1016/j.immuni.2016.07.019

Baiula, M., Greco, R., Ferrazzano, L., Caligiana, A., Hoxha, K., Bandini, D., Longobardi, P., Spampinato, S., & Tolomelli, A. (2020). Integrin-mediated adhesive properties of neutrophils are reduced by hyperbaric oxygen therapy in patients with chronic non-healing wound. *PLoS One, 15*(8), e0237746. https://doi.org/10.1371/journal.pone.0237746

Ballesteros, I., Rubio-Ponce, A., Genua, M., Lusito, E., Kwok, I., Fernandez-Calvo, G., Khoyratty, T. E., van Grinsven, E., Gonzalez-Hernandez, S., Nicolas-Avila, J. A., Vicanolo, T., Maccataio, A., Benguria, A., Li, J. L., Adrover, J. M., Aroca-Crevillen, A., Quintana, J. A., Martin-Salamanca, S., Mayo, F., Ascher, S., Barbiera, G., Soehnlein, O., Gunzer, M., Ginhoux, F., Sanchez-Cabo, F., Nistal-Villan, E., Schulz, C., Dopazo, A., Reinhardt, C., Udalova, I. A., Ng, L. G., Ostuni, R., & Hidalgo, A. (2020, Oct 20). Co-option of Neutrophil Fates by Tissue Environments. *Cell*. https://doi.org/10.1016/j.cell.2020.10.003

Bergen, V., Lange, M., Peidli, S., Wolf, F. A., & Theis, F. J. (2020, Dec). Generalizing RNA velocity to transient cell states through dynamical modeling. *Nat Biotechnol, 38*(12), 1408-1414. https://doi.org/10.1038/s41587-020-0591-3

Boothby, I. C., Cohen, J. N., & Rosenblum, M. D. (2020, May 1). Regulatory T cells in skin injury: At the crossroads of tolerance and tissue repair. *Sci Immunol, 5*(47). https://doi.org/10.1126/sciimmunol.aaz9631

Brehm, M. A., Shultz, L. D., Luban, J., & Greiner, D. L. (2013, Nov). Overcoming current limitations in humanized mouse research. *J Infect Dis, 208 Suppl 2*(Suppl 2), S125-130. https://doi.org/10.1093/infdis/jit319

Brohem, C. A., Cardeal, L. B., Tiago, M., Soengas, M. S., Barros, S. B., & Maria-Engler, S. S. (2011, Feb). Artificial skin in perspective: concepts and applications. *Pigment Cell Melanoma Res, 24*(1), 35-50. https://doi.org/10.1111/j.1755-148X.2010.00786.x

Byun, J. K., Lee, S., Kang, G. W., Lee, Y. R., Park, S. Y., Song, I. S., Yun, J. W., Lee, J., Choi, Y. K., & Park, K. G. (2022, Mar 14). Macropinocytosis is an alternative pathway of cysteine acquisition and mitigates sorafenib-induced ferroptosis in hepatocellular carcinoma. *J Exp Clin Cancer Res, 41*(1), 98. https://doi.org/10.1186/s13046-022-02296-3

Canesso, M. C., Vieira, A. T., Castro, T. B., Schirmer, B. G., Cisalpino, D., Martins, F. S., Rachid, M. A., Nicoli, J. R., Teixeira, M. M., & Barcelos, L. S. (2014, Nov 15). Skin wound healing is accelerated and scarless in the absence of commensal microbiota. *J Immunol, 193*(10), 5171-5180. https://doi.org/10.4049/jimmunol.1400625

Casanova-Acebes, M., Dalla, E., Leader, A. M., LeBerichel, J., Nikolic, J., Morales, B. M., Brown, M., Chang, C., Troncoso, L., Chen, S. T., Sastre-Perona, A., Park, M. D., Tabachnikova, A., Dhainaut, M., Hamon, P., Maier, B., Sawai, C. M., Agullo-Pascual, E., Schober, M., Brown, B. D., Reizis, B., Marron, T., Kenigsberg, E., Moussion, C., Benaroch, P., Aguirre-Ghiso, J. A., & Merad, M. (2021, Jul). Tissue-resident macrophages provide a pro-tumorigenic niche to early NSCLC cells. *Nature, 595*(7868), 578-584. https://doi.org/10.1038/s41586-021-03651-8

Clarke, Z. A., Andrews, T. S., Atif, J., Pouyabahar, D., Innes, B. T., MacParland, S. A., & Bader, G. D. (2021, Jun). Tutorial: guidelines for annotating single-cell transcriptomic maps using automated and manual methods. *Nature Protocols, 16*(6), 2749-2764. https://doi.org/10.1038/s41596-021-00534-0

Correa-Gallegos, D., Ye, H., Dasgupta, B., Sardogan, A., Kadri, S., Kandi, R., Dai, R., Lin, Y., Kopplin, R., Shenai, D. S., Wannemacher, J., Ichijo, R., Jiang, D., Strunz, M., Ansari, M., Angelidis, I., Schiller, H. B., Volz, T., Machens, H. G., & Rinkevich, Y. (2023, Nov). CD201(+) fascia progenitors choreograph injury repair. *Nature, 623*(7988), 792-802. https://doi.org/10.1038/s41586-023-06725-x

Devalaraja, R. M., Nanney, L. B., Du, J., Qian, Q., Yu, Y., Devalaraja, M. N., & Richmond, A. (2000, Aug). Delayed wound healing in CXCR2 knockout mice. *Journal Of Investigative Dermatology, 115*(2), 234-244. https://doi.org/10.1046/j.1523-1747.2000.00034.x

Diller, R. B., & Tabor, A. J. (2022, Jul 1). The Role of the Extracellular Matrix (ECM) in Wound Healing: A Review. *Biomimetics (Basel), 7*(3). https://doi.org/10.3390/biomimetics7030087

Dixon, S. J., Lemberg, K. M., Lamprecht, M. R., Skouta, R., Zaitsev, E. M., Gleason, C. E., Patel, D. N., Bauer, A. J., Cantley, A. M., Yang, W. S., Morrison, B., 3rd, & Stockwell, B. R. (2012, May 25). Ferroptosis: an iron-dependent form of nonapoptotic cell death. *Cell, 149*(5), 1060-1072. https://doi.org/10.1016/j.cell.2012.03.042

Doll, S., Proneth, B., Tyurina, Y. Y., Panzilius, E., Kobayashi, S., Ingold, I., Irmler, M., Beckers, J., Aichler, M., Walch, A., Prokisch, H., Trumbach, D., Mao, G., Qu, F., Bayir, H., Fullekrug, J., Scheel, C. H., Wurst, W., Schick, J. A., Kagan, V. E., Angeli, J. P., & Conrad, M. (2017, Jan). ACSL4 dictates ferroptosis sensitivity by shaping cellular lipid composition. *Nature Chemical Biology, 13*(1), 91-98. https://doi.org/10.1038/nchembio.2239

Dolma, S., Lessnick, S. L., Hahn, W. C., & Stockwell, B. R. (2003, Mar). Identification of genotype-selective antitumor agents using synthetic lethal chemical screening in engineered human tumor cells. *Cancer Cell, 3*(3), 285-296. https://doi.org/10.1016/s1535-6108(03)00050-3

Dominguez Conde, C., Xu, C., Jarvis, L. B., Rainbow, D. B., Wells, S. B., Gomes, T., Howlett, S. K., Suchanek, O., Polanski, K., King, H. W., Mamanova, L., Huang, N., Szabo, P. A., Richardson, L., Bolt, L., Fasouli, E. S., Mahbubani, K. T., Prete, M., Tuck, L., Richoz, N., Tuong, Z. K., Campos, L., Mousa, H. S., Needham, E. J., Pritchard, S., Li, T., Elmentaite, R., Park, J., Rahmani, E., Chen, D., Menon, D. K., Bayraktar, O. A., James, L. K., Meyer, K. B., Yosef, N., Clatworthy, M. R., Sims, P. A., Farber, D. L., Saeb-Parsy, K., Jones, J. L., & Teichmann, S. A. (2022, May 13). Cross-tissue immune cell analysis reveals tissue-specific features in humans. *Science, 376*(6594), eabl5197. https://doi.org/10.1126/science.abl5197

Dovi, J. V., He, L. K., & DiPietro, L. A. (2003, Apr). Accelerated wound closure in neutrophil-depleted mice. *J Leukoc Biol, 73*(4), 448-455. https://doi.org/10.1189/jlb.0802406

Duverger, O., & Morasso, M. I. (2014, Jan-Feb). To grow or not to grow: hair morphogenesis and human genetic hair disorders. *Semin Cell Dev Biol, 25-26*, 22-33. https://doi.org/10.1016/j.semcdb.2013.12.006

Evrard, M., Kwok, I. W. H., Chong, S. Z., Teng, K. W. W., Becht, E., Chen, J., Sieow, J. L., Penny, H. L., Ching, G. C., Devi, S., Adrover, J. M., Li, J. L. Y., Liong, K. H., Tan, L., Poon, Z., Foo, S., Chua, J. W., Su, I. H., Balabanian, K., Bachelerie, F., Biswas, S. K., Larbi, A., Hwang, W. Y. K., Madan, V., Koeffler, H. P., Wong, S. C., Newell, E. W., Hidalgo, A., Ginhoux, F., & Ng, L. G. (2018, Feb 20). Developmental Analysis of Bone Marrow Neutrophils Reveals Populations Specialized in Expansion, Trafficking, and Effector Functions. *Immunity, 48*(2), 364-379 e368. https://doi.org/10.1016/j.immuni.2018.02.002

Fede, C., Petrelli, L., Pirri, C., Tiengo, C., De Caro, R., & Stecco, C. (2023, Jul 18). Detection of Mast Cells in Human Superficial Fascia. *International Journal Of Molecular Sciences, 24*(14). https://doi.org/10.3390/ijms241411599

Fischer, A., Correa-Gallegos, D., Wannemacher, J., Christ, S., Machens, H. G., & Rinkevich, Y. (2023, Aug 9). In vivo fluorescent labeling and tracking of extracellular matrix. *Nature Protocols*. https://doi.org/10.1038/s41596-023-00867-y

Fischer, A., Wannemacher, J., Christ, S., Koopmans, T., Kadri, S., Zhao, J., Gouda, M., Ye, H., Muck-Hausl, M., Krenn, P. W., Machens, H. G., Fassler, R., Neumann, P. A., Hauck, S. M., & Rinkevich, Y. (2022, Apr). Neutrophils direct preexisting matrix to initiate repair in damaged tissues. *Nat Immunol, 23*(4), 518-531. https://doi.org/10.1038/s41590-022-01166-6

Fleit, H., & Furie, M. (2014). Phagocytes in Inflammation.

Fulton, C., Anderson, G. M., Zasloff, M., Bull, R., & Quinn, A. G. (1997, Dec 13). Expression of natural peptide antibiotics in human skin. *Lancet, 350*(9093), 1750-1751. https://doi.org/10.1016/S0140-6736(05)63574-X

Gavriilidis, E., Divolis, G., Natsi, A.-M., Kafalis, N., Kogias, D., Antoniadou, C., Synolaki, E., Pavlos, E., Koutsi, M. A., Didaskalou, S., Tsironidou, V., Gavriil, A., Papadopoulos, V., Agelopoulos, M., Tsilingiris, D., Koffa, M., Giatromanolaki, A., Kouklakis, G., Ritis, K., & Skendros, P. (2023). Neutrophil-fibroblast crosstalk drives immunofibrosis in Crohn's disease through IFNα pathway. *medRxiv*. https://doi.org/10.1101/2023.09.08.23295281

Gay, D., Ghinatti, G., Guerrero-Juarez, C. F., Ferrer, R. A., Ferri, F., Lim, C. H., Murakami, S., Gault, N., Barroca, V., Rombeau, I., Mauffrey, P., Irbah, L., Treffeisen, E., Franz, S., Boissonnas, A., Combadiere, C., Ito, M., Plikus, M. V., & Romeo, P. H. (2020, Mar). Phagocytosis of Wnt

inhibitor SFRP4 by late wound macrophages drives chronic Wnt activity for fibrotic skin healing. *Sci Adv, 6*(12), eaay3704. https://doi.org/10.1126/sciadv.aay3704

Gray, R. D., Hardisty, G., Regan, K. H., Smith, M., Robb, C. T., Duffin, R., Mackellar, A., Felton, J. M., Paemka, L., McCullagh, B. N., Lucas, C. D., Dorward, D. A., McKone, E. F., Cooke, G., Donnelly, S. C., Singh, P. K., Stoltz, D. A., Haslett, C., McCray, P. B., Whyte, M. K. B., Rossi, A. G., & Davidson, D. J. (2018, Feb). Delayed neutrophil apoptosis enhances NET formation in cystic fibrosis. *Thorax, 73*(2), 134-144. https://doi.org/10.1136/thoraxjnl-2017-210134

Grinnell, F. (1984). Fibronectin and wound healing. *Journal Of Cellular Biochemistry, 26*(2), 107-116. https://doi.org/10.1002/jcb.240260206

Guénet, J.-L., Orth, A., & Bonhomme, F. (2012). Origins and Phylogenetic Relationships of the Laboratory Mouse. 3-20. https://doi.org/10.1016/b978-0-12-382008-2.00001-5

Guo, S., & Dipietro, L. A. (2010, Mar). Factors affecting wound healing. *Journal Of Dental Research, 89*(3), 219-229. https://doi.org/10.1177/0022034509359125

Gurtner, G. C., Werner, S., Barrandon, Y., & Longaker, M. T. (2008, May 15). Wound repair and regeneration. *Nature, 453*(7193), 314-321. https://doi.org/10.1038/nature07039

Halim, A. S., Khoo, T. L., & Mohd Yussof, S. J. (2010, Sep). Biologic and synthetic skin substitutes: An overview. *Indian J Plast Surg, 43*(Suppl), S23-28. https://doi.org/10.4103/0970-0358.70712

He, L., & Marneros, A. G. (2013, Jun). Macrophages are essential for the early wound healing response and the formation of a fibrovascular scar. *Am J Pathol, 182*(6), 2407-2417. https://doi.org/10.1016/j.ajpath.2013.02.032

He, Y. B., Jin, H. Z., Zhao, J. L., Wang, C., Ma, W. R., Xing, J., Zhang, X. B., Zhang, Y. Y., Dai, H. D., Zhao, N. S., Zhang, J. F., Zhang, G. X., & Zhang, J. (2022, Dec 19). Single-cell transcriptomic analysis reveals differential cell subpopulations and distinct phenotype transition in normal and dissected ascending aorta. *Molecular Medicine, 28*(1), 158. https://doi.org/10.1186/s10020-022-00584-4

Hidalgo, A., Chilvers, E. R., Summers, C., & Koenderman, L. (2019). The Neutrophil Life Cycle. *Trends in Immunology*. https://doi.org/10.1016/j.it.2019.04.013

Hirschfeld, J. (2019). Neutrophil Subsets in Periodontal Health and Disease: A Mini Review. *Front Immunol, 10*, 3001. https://doi.org/10.3389/fimmu.2019.03001

Hosseini Mansoub, N. (2021). The role of keratinocyte function on the defected diabetic wound healing. *Int J Burns Trauma, 11*(6), 430-441. https://www.ncbi.nlm.nih.gov/pubmed/35111377

Hosseini Mansoub, N. (2022). The role of keratinocyte function on the defected diabetic wound healing. *Clinical Diabetology*. https://doi.org/10.5603/DK.a2022.0004

Hu, Y., Bojanowski, C. M., Britto, C. J., Wellems, D., Song, K., Scull, C., Jennings, S., Li, J., Kolls, J. K., & Wang, G. (2023, Jan 25). Aberrant Immune Programming in Neutrophils in Cystic Fibrosis. *medRxiv*. https://doi.org/10.1101/2023.01.22.23284619

Ionescu, A. M., Chato-Astrain, J., Cardona Perez, J. C., Campos, F., Perez Gomez, M., Alaminos, M., & Garzon Bello, I. (2020, May). Evaluation of the optical and biomechanical properties of bioengineered human skin generated with fibrin-agarose biomaterials. *Journal Of Biomedical Optics, 25*(5), 1-16. https://doi.org/10.1117/1.JBO.25.5.055002

Jagdeo, J., & Shumaker, P. R. (2017, Mar 1). Traumatic Scarring. *JAMA Dermatol, 153*(3), 364. https://doi.org/10.1001/jamadermatol.2016.5232

Jaillon, S., Ponzetta, A., Di Mitri, D., Santoni, A., Bonecchi, R., & Mantovani, A. (2020, Sep). Neutrophil diversity and plasticity in tumour progression and therapy. *Nature Reviews Cancer, 20*(9), 485-503. https://doi.org/10.1038/s41568-020-0281-y

Jia, Y., Subramanian, K. K., Erneux, C., Pouillon, V., Hattori, H., Jo, H., You, J., Zhu, D., Schurmans, S., & Luo, H. R. (2007, Sep). Inositol 1,3,4,5-tetrakisphosphate negatively regulates phosphatidylinositol-3,4,5- trisphosphate signaling in neutrophils. *Immunity, 27*(3), 453-467. https://doi.org/10.1016/j.immuni.2007.07.016

Jiang, D., Christ, S., Correa-Gallegos, D., Ramesh, P., Kalgudde Gopal, S., Wannemacher, J., Mayr, C. H., Lupperger, V., Yu, Q., Ye, H., Muck-Hausl, M., Rajendran, V., Wan, L., Liu, J., Mirastschijski, U., Volz, T., Marr, C., Schiller, H. B., & Rinkevich, Y. (2020, Nov 6). Injury triggers fascia fibroblast collective cell migration to drive scar formation through N-cadherin. *Nat Commun, 11*(1), 5653. https://doi.org/10.1038/s41467-020-19425-1

Jiang, D., Correa-Gallegos, D., Christ, S., Stefanska, A., Liu, J., Ramesh, P., Rajendran, V., De Santis, M. M., Wagner, D. E., & Rinkevich, Y. (2018, Apr). Two succeeding fibroblastic lineages drive dermal development and the transition from regeneration to scarring. *Nature Cell Biology, 20*(4), 422-431. https://doi.org/10.1038/s41556-018-0073-8

Jiang, D., & Rinkevich, Y. (2021, Aug 20). Furnishing Wound Repair by the Subcutaneous Fascia. *International Journal Of Molecular Sciences, 22*(16). https://doi.org/10.3390/ijms22169006

Jin, S., Guerrero-Juarez, C. F., Zhang, L., Chang, I., Ramos, R., Kuan, C. H., Myung, P., Plikus, M. V., & Nie, Q. (2021, Feb 17). Inference and analysis of cell-cell communication using CellChat. *Nat Commun, 12*(1), 1088. https://doi.org/10.1038/s41467-021-21246-9

Jin, Z., Sun, J., Song, Z., Chen, K., Nicolas, Y. S. M., Kc, R., Ma, Q., Liu, J., & Zhang, M. (2020, Oct 30). Neutrophil extracellular traps promote scar formation in post-epidural fibrosis. *NPJ Regen Med, 5*(1), 19. https://doi.org/10.1038/s41536-020-00103-1

Johnson, T. R., Gomez, B. I., McIntyre, M. K., Dubick, M. A., Christy, R. J., Nicholson, S. E., & Burmeister, D. M. (2018, Sep 11). The Cutaneous Microbiome and Wounds: New Molecular Targets to Promote Wound Healing. *International Journal Of Molecular Sciences, 19*(9). https://doi.org/10.3390/ijms19092699

Khandpur, R., Carmona-Rivera, C., Vivekanandan-Giri, A., Gizinski, A., Yalavarthi, S., Knight, J. S., Friday, S., Li, S., Patel, R. M., Subramanian, V., Thompson, P., Chen, P., Fox, D. A., Pennathur, S., & Kaplan, M. J. (2013, Mar 27). NETs are a source of citrullinated autoantigens and stimulate inflammatory responses in rheumatoid arthritis. *Sci Transl Med, 5*(178), 178ra140. https://doi.org/10.1126/scitranslmed.3005580

Khiao In, M., Richardson, K. C., Loewa, A., Hedtrich, S., Kaessmeyer, S., & Plendl, J. (2019, May). Histological and functional comparisons of four anatomical regions of porcine skin with human abdominal skin. *Anat Histol Embryol, 48*(3), 207-217. https://doi.org/10.1111/ahe.12425

Kim, R., Hashimoto, A., Markosyan, N., Tyurin, V. A., Tyurina, Y. Y., Kar, G., Fu, S., Sehgal, M., Garcia-Gerique, L., Kossenkov, A., Gebregziabher, B. A., Tobias, J. W., Hicks, K., Halpin, R. A., Cvetesic, N., Deng, H., Donthireddy, L., Greenberg, A., Nam, B., Vonderheide, R. H., Nefedova, Y., Kagan, V. E., & Gabrilovich, D. I. (2022, Dec). Ferroptosis of tumour neutrophils causes immune suppression in cancer. *Nature, 612*(7939), 338-346. https://doi.org/10.1038/s41586-022-05443-0

Kolaczkowska, E., & Kubes, P. (2013, Mar). Neutrophil recruitment and function in health and inflammation. *Nat Rev Immunol, 13*(3), 159-175. https://doi.org/10.1038/nri3399

Kondo, T., Gleason, A., Okawa, H., Hokugo, A., & Nishimura, I. (2023, Jul 24). Mouse gingival single-cell transcriptomic atlas: An activated fibroblast subpopulation guides oral barrier immunity in periodontitis. *bioRxiv*. https://doi.org/10.1101/2023.04.13.536751

Korkmaz, H. I., Ulrich, M. M. W., Vogels, S., de Wit, T., van Zuijlen, P. P. M., Krijnen, P. A. J., & Niessen, H. W. M. (2017, Aug). Neutrophil extracellular traps coincide with a pro-coagulant status of microcirculatory endothelium in burn wounds. *Wound Repair Regen, 25*(4), 609-617. https://doi.org/10.1111/wrr.12560

Korsunsky, I., Millard, N., Fan, J., Slowikowski, K., Zhang, F., Wei, K., Baglaenko, Y., Brenner, M., Loh, P. R., & Raychaudhuri, S. (2019, Dec). Fast, sensitive and accurate integration of single-cell data with Harmony. *Nature Methods, 16*(12), 1289-1296. https://doi.org/10.1038/s41592-019-0619-0

Kotwal, G. J., & Chien, S. (2017). Macrophage Differentiation in Normal and Accelerated Wound Healing. *Results Probl Cell Differ, 62*, 353-364. https://doi.org/10.1007/978-3-319-54090-0_14

Kwok, I., Becht, E., Xia, Y., Ng, M., Teh, Y. C., Tan, L., Evrard, M., Li, J. L. Y., Tran, H. T. N., Tan, Y., Liu, D., Mishra, A., Liong, K. H., Leong, K., Zhang, Y., Olsson, A., Mantri, C. K., Shyamsunder, P., Liu, Z., Piot, C., Dutertre, C. A., Cheng, H., Bari, S., Ang, N., Biswas, S. K., Koeffler, H. P., Tey, H. L., Larbi, A., Su, I. H., Lee, B., St John, A., Chan, J. K. Y., Hwang, W. Y. K., Chen, J., Salomonis, N., Chong, S. Z., Grimes, H. L., Liu, B., Hidalgo, A., Newell, E. W., Cheng, T., Ginhoux, F., & Ng, L. G. (2020, Jun 22). Combinatorial Single-Cell Analyses of Granulocyte-Monocyte Progenitor Heterogeneity Reveals an Early Uni-potent Neutrophil Progenitor. *Immunity*. https://doi.org/10.1016/j.immuni.2020.06.005

Lämmermann, T., Afonso, P. V., Angermann, B. R., Wang, J. M., Kastenmüller, W., Parent, C. A., & Germain, R. N. (2013). Neutrophil swarms require LTB4 and integrins at sites of cell death in vivo. *Nature, 498*(7454), 371-375. https://doi.org/10.1038/nature12175

Lan, F., Lee, A. S., Liang, P., Sanchez-Freire, V., Nguyen, P. K., Wang, L., Han, L., Yen, M., Wang, Y., Sun, N., Abilez, O. J., Hu, S., Ebert, A. D., Navarrete, E. G., Simmons, C. S., Wheeler, M., Pruitt, B., Lewis, R., Yamaguchi, Y., Ashley, E. A., Bers, D. M., Robbins, R. C., Longaker, M. T., & Wu, J. C. (2013, Jan 3). Abnormal calcium handling properties underlie familial hypertrophic cardiomyopathy pathology in patient-specific induced pluripotent stem cells. *Cell Stem Cell, 12*(1), 101-113. https://doi.org/10.1016/j.stem.2012.10.010

Lansdown, A. B., Mirastschijski, U., Stubbs, N., Scanlon, E., & Agren, M. S. (2007, Jan-Feb). Zinc in wound healing: theoretical, experimental, and clinical aspects. *Wound Repair Regen, 15*(1), 2-16. https://doi.org/10.1111/j.1524-475X.2006.00179.x

Lecot, P., Sarabi, M., Pereira Abrantes, M., Mussard, J., Koenderman, L., Caux, C., Bendriss-Vermare, N., & Michallet, M. C. (2019). Neutrophil Heterogeneity in Cancer: From Biology to Therapies. *Front Immunol, 10*, 2155. https://doi.org/10.3389/fimmu.2019.02155

Lei, G., Zhang, Y., Koppula, P., Liu, X., Zhang, J., Lin, S. H., Ajani, J. A., Xiao, Q., Liao, Z., Wang, H., & Gan, B. (2020, Feb). The role of ferroptosis in ionizing radiation-induced cell death and tumor suppression. *Cell Research, 30*(2), 146-162. https://doi.org/10.1038/s41422-019-0263-3

Lei, P., Bai, T., & Sun, Y. (2019). Mechanisms of Ferroptosis and Relations With Regulated Cell Death: A Review. *Front Physiol, 10*, 139. https://doi.org/10.3389/fphys.2019.00139

Leoni, G., Neumann, P. A., Sumagin, R., Denning, T. L., & Nusrat, A. (2015, Sep). Wound repair: role of immune-epithelial interactions. *Mucosal Immunol, 8*(5), 959-968. https://doi.org/10.1038/mi.2015.63

Li, P., Jiang, M., Li, K., Li, H., Zhou, Y., Xiao, X., Xu, Y., Krishfield, S., Lipsky, P. E., Tsokos, G. C., & Zhang, X. (2021, Sep). Glutathione peroxidase 4-regulated neutrophil ferroptosis induces systemic autoimmunity. *Nat Immunol, 22*(9), 1107-1117. https://doi.org/10.1038/s41590-021-00993-3

Li, S., Li, Y., Wu, Z., Wu, Z., & Fang, H. (2021, Oct 1). Diabetic ferroptosis plays an important role in triggering on inflammation in diabetic wound. *Am J Physiol Endocrinol Metab, 321*(4), E509-E520. https://doi.org/10.1152/ajpendo.00042.2021

Li, S., Luo, X., Zhang, S., Su, Y., Deng, M., Zhu, Y., Zhang, P., Wu, R., & Zhao, M. (2023, Jan 29). Ferroptosis Activation Contributes to the Formation of Skin Lesions in Psoriasis Vulgaris. *Antioxidants (Basel), 12*(2). https://doi.org/10.3390/antiox12020310

Lima, M. H., Caricilli, A. M., de Abreu, L. L., Araujo, E. P., Pelegrinelli, F. F., Thirone, A. C., Tsukumo, D. M., Pessoa, A. F., dos Santos, M. F., de Moraes, M. A., Carvalheira, J. B., Velloso, L. A., & Saad, M. J. (2012). Topical insulin accelerates wound healing in diabetes by enhancing the AKT and ERK pathways: a double-blind placebo-controlled clinical trial. *PLoS One, 7*(5), e36974. https://doi.org/10.1371/journal.pone.0036974

Lin, C. H., Chiu, P. Y., Hsueh, Y. Y., Shieh, S. J., Wu, C. C., Wong, T. W., Chuong, C. M., & Hughes, M. W. (2019, Apr). Regeneration of rete ridges in Lanyu pig (Sus scrofa): Insights for human skin wound healing. *Experimental Dermatology, 28*(4), 472-479. https://doi.org/10.1111/exd.13875

Liu, L., Lian, N., Shi, L., Hao, Z., & Chen, K. (2022). Ferroptosis: Mechanism and connections with cutaneous diseases. *Front Cell Dev Biol, 10*, 1079548. https://doi.org/10.3389/fcell.2022.1079548

Liu, M., Kong, X. Y., Yao, Y., Wang, X. A., Yang, W., Wu, H., Li, S., Ding, J. W., & Yang, J. (2022, Mar). The critical role and molecular mechanisms of ferroptosis in antioxidant systems: a narrative review. *Ann Transl Med, 10*(6), 368. https://doi.org/10.21037/atm-21-6942

Ljubimov, A. V., & Saghizadeh, M. (2015, Nov). Progress in corneal wound healing. *Prog Retin Eye Res, 49*, 17-45. https://doi.org/10.1016/j.preteyeres.2015.07.002

Lun, A. T., McCarthy, D. J., & Marioni, J. C. (2016). A step-by-step workflow for low-level analysis of single-cell RNA-seq data with Bioconductor. *F1000Res, 5*, 2122. https://doi.org/10.12688/f1000research.9501.2

Ma, T., Du, J., Zhang, Y., Wang, Y., Wang, B., & Zhang, T. (2022, Oct 30). GPX4-independent ferroptosis-a new strategy in disease's therapy. *Cell Death Discov, 8*(1), 434. https://doi.org/10.1038/s41420-022-01212-0

Mackey, S., Allgaier, N., Chaarani, B., Spechler, P., Orr, C., Bunn, J., Allen, N. B., Alia-Klein, N., Batalla, A., Blaine, S., Brooks, S., Caparelli, E., Chye, Y. Y., Cousijn, J., Dagher, A., Desrivieres, S., Feldstein-Ewing, S., Foxe, J. J., Goldstein, R. Z., Goudriaan, A. E., Heitzeg, M. M., Hester, R., Hutchison, K., Korucuoglu, O., Li, C. R., London, E., Lorenzetti, V., Luijten, M., Martin-Santos, R., May, A., Momenan, R., Morales, A., Paulus, M. P., Pearlson, G., Rousseau, M. E., Salmeron, B. J., Schluter, R., Schmaal, L., Schumann, G., Sjoerds, Z., Stein, D. J., Stein, E. A., Sinha, R., Solowij, N., Tapert, S., Uhlmann, A., Veltman, D., van Holst, R., Whittle, S., Wright, M. J., Yucel, M., Zhang, S., Yurgelun-Todd, D., Hibar, D. P., Jahanshad, N., Evans, A., Thompson, P. M., Glahn, D. C., Conrod, P., Garavan, H., & Group, E. A. W. (2019, Feb 1).

Mega-Analysis of Gray Matter Volume in Substance Dependence: General and Substance-Specific Regional Effects. *Am J Psychiatry, 176*(2), 119-128. https://doi.org/10.1176/appi.ajp.2018.17040415

Martinez, A. M., Kim, A., & Yang, W. S. (2020). Detection of Ferroptosis by BODIPY 581/591 C11. *Methods Mol Biol, 2108*, 125-130. https://doi.org/10.1007/978-1-0716-0247-8_11

Martinod, K., & Wagner, D. D. (2014, May 1). Thrombosis: tangled up in NETs. *Blood, 123*(18), 2768-2776. https://doi.org/10.1182/blood-2013-10-463646

Mayadas, T. N., Cullere, X., & Lowell, C. A. (2014). The multifaceted functions of neutrophils. *Annu Rev Pathol, 9*, 181-218. https://doi.org/10.1146/annurev-pathol-020712-164023

McDaniel, J. C., Roy, S., & Wilgus, T. A. (2013, May-Jun). Neutrophil activity in chronic venous leg ulcers--a target for therapy? *Wound Repair Regen, 21*(3), 339-351. https://doi.org/10.1111/wrr.12036

Misic, A. M., Gardner, S. E., & Grice, E. A. (2014, Jul 1). The Wound Microbiome: Modern Approaches to Examining the Role of Microorganisms in Impaired Chronic Wound Healing. *Adv Wound Care (New Rochelle), 3*(7), 502-510. https://doi.org/10.1089/wound.2012.0397

Nagakannan, P., Islam, M. I., Conrad, M., & Eftekharpour, E. (2021, Mar). Cathepsin B is an executioner of ferroptosis. *Biochim Biophys Acta Mol Cell Res, 1868*(3), 118928. https://doi.org/10.1016/j.bbamcr.2020.118928

Ng, L. G. (2022, Apr). Neutrophils guide pre-existing matrix into injured organs to initiate tissue repair. *Nat Immunol, 23*(4), 472-473. https://doi.org/10.1038/s41590-022-01173-7

Ng, W. L., Qi, J. T. Z., Yeong, W. Y., & Naing, M. W. (2018, Jan 23). Proof-of-concept: 3D bioprinting of pigmented human skin constructs. *Biofabrication, 10*(2), 025005. https://doi.org/10.1088/1758-5090/aa9e1e

Nourshargh, S., & Alon, R. (2014, Nov 20). Leukocyte migration into inflamed tissues. *Immunity, 41*(5), 694-707. https://doi.org/10.1016/j.immuni.2014.10.008

Nowak, M., Mehrholz, D., Baranska-Rybak, W., & Nowicki, R. J. (2022, Jun). Wound debridement products and techniques: clinical examples and literature review. *Postepy Dermatol Alergol, 39*(3), 479-490. https://doi.org/10.5114/ada.2022.117572

Ohl, K., Rauen, T., & Tenbrock, K. (2021, Nov 11). Dysregulated neutrophilic cell death in SLE: a spotlight on ferroptosis. *Signal Transduct Target Ther, 6*(1), 392. https://doi.org/10.1038/s41392-021-00804-z

Paratz, J. D., Stockton, K., Plaza, A., Muller, M., & Boots, R. J. (2012, Jul). Intensive exercise after thermal injury improves physical, functional, and psychological outcomes. *J Trauma Acute Care Surg, 73*(1), 186-194. https://doi.org/10.1097/TA.0b013e31824baa52

Pillay, J., Tak, T., Kamp, V. M., & Koenderman, L. (2013, Oct). Immune suppression by neutrophils and granulocytic myeloid-derived suppressor cells: similarities and differences. *Cell Mol Life Sci, 70*(20), 3813-3827. https://doi.org/10.1007/s00018-013-1286-4

Proksch, E., Brandner, J. M., & Jensen, J. M. (2008, Dec). The skin: an indispensable barrier. *Experimental Dermatology, 17*(12), 1063-1072. https://doi.org/10.1111/j.1600-0625.2008.00786.x

Quigley, D. A., To, M. D., Perez-Losada, J., Pelorosso, F. G., Mao, J. H., Nagase, H., Ginzinger, D. G., & Balmain, A. (2009, Mar 26). Genetic architecture of mouse skin inflammation and tumour susceptibility. *Nature, 458*(7237), 505-508. https://doi.org/10.1038/nature07683

Ranamukhaarachchi, S. A., Lehnert, S., Ranamukhaarachchi, S. L., Sprenger, L., Schneider, T., Mansoor, I., Rai, K., Hafeli, U. O., & Stoeber, B. (2016, Aug 25). A micromechanical comparison of human and porcine skin before and after preservation by freezing for medical device development. *Sci Rep, 6*, 32074. https://doi.org/10.1038/srep32074

Rawat, K., & Shrivastava, A. (2022, Dec). Neutrophils as emerging protagonists and targets in chronic inflammatory diseases. *Inflammation Research, 71*(12), 1477-1488. https://doi.org/10.1007/s00011-022-01627-6

Ren, Y., Mao, X., Xu, H., Dang, Q., Weng, S., Zhang, Y., Chen, S., Liu, S., Ba, Y., Zhou, Z., Han, X., Liu, Z., & Zhang, G. (2023, Aug 19). Ferroptosis and EMT: key targets for combating cancer progression and therapy resistance. *Cell Mol Life Sci, 80*(9), 263. https://doi.org/10.1007/s00018-023-04907-4

Rinkevich, Y., Correa-Gallegos, D., Ye, H., Dasgupta, B., Sardogan, A., Ichijo, R., Strunz, M., Ansari, M., Angelidis, I., Schiller, H., Volz, T., & Machens, H.-G. (2022). CD201+ fascia progenitors choreograph injury repair. https://doi.org/10.21203/rs.3.rs-2009916/v1

Roca, C. P., Burton, O. T., Gergelits, V., Prezzemolo, T., Whyte, C. E., Halpert, R., Kreft, L., Collier, J., Botzki, A., Spidlen, J., Humblet-Baron, S., & Liston, A. (2021, May 17). AutoSpill is a principled framework that simplifies the analysis of multichromatic flow cytometry data. *Nat Commun, 12*(1), 2890. https://doi.org/10.1038/s41467-021-23126-8

Saczko, J., Dominiak, M., Kulbacka, J., Chwilkowska, A., & Krawczykowska, H. (2008). A simple and established method of tissue culture of human gingival fibroblasts for gingival augmentation. *Folia Histochem Cytobiol, 46*(1), 117-119. https://doi.org/10.2478/v10042-008-0017-4

Stockwell, B. R. (2022, Jul 7). Ferroptosis turns 10: Emerging mechanisms, physiological functions, and therapeutic applications. *Cell, 185*(14), 2401-2421. https://doi.org/10.1016/j.cell.2022.06.003

Takagi, N., Kawakami, K., Kanno, E., Tanno, H., Takeda, A., Ishii, K., Imai, Y., Iwakura, Y., & Tachi, M. (2017, Feb). IL-17A promotes neutrophilic inflammation and disturbs acute wound healing in skin. *Experimental Dermatology, 26*(2), 137-144. https://doi.org/10.1111/exd.13115

Tang, D., Chen, X., Kang, R., & Kroemer, G. (2021, Feb). Ferroptosis: molecular mechanisms and health implications. *Cell Research, 31*(2), 107-125. https://doi.org/10.1038/s41422-020-00441-1

Tang, Y., Zhu, L., Cho, J. S., Li, X. Y., & Weiss, S. J. (2022, Feb 4). Matrix remodeling controls a nuclear lamin A/C-emerin network that directs Wnt-regulated stem cell fate. *Dev Cell*. https://doi.org/10.1016/j.devcel.2022.01.015

Teichert, A. E., Elalieh, H., Elias, P. M., Welsh, J., & Bikle, D. D. (2011, Nov). Overexpression of hedgehog signaling is associated with epidermal tumor formation in vitamin D receptor-null mice. *Journal Of Investigative Dermatology, 131*(11), 2289-2297. https://doi.org/10.1038/jid.2011.196

Theocharidis, G., Thomas, B. E., Sarkar, D., Mumme, H. L., Pilcher, W. J. R., Dwivedi, B., Sandoval-Schaefer, T., Sirbulescu, R. F., Kafanas, A., Mezghani, I., Wang, P., Lobao, A., Vlachos, I. S., Dash, B., Hsia, H. C., Horsley, V., Bhasin, S. S., Veves, A., & Bhasin, M. (2022, Jan 10). Single cell transcriptomic landscape of diabetic foot ulcers. *Nat Commun, 13*(1), 181. https://doi.org/10.1038/s41467-021-27801-8

Tsai, J. M., Shoham, M., Fernhoff, N. B., George, B. M., Marjon, K. D., McCracken, M. N., Kao, K. S., Sinha, R., Volkmer, A. K., Miyanishi, M., Seita, J., Rinkevich, Y., & Weissman, I. L. (2019, Sep

24). Neutrophil and monocyte kinetics play critical roles in mouse peritoneal adhesion formation. *Blood Adv, 3*(18), 2713-2721. https://doi.org/10.1182/bloodadvances.2018024026

Vats, K., Kruglov, O., Mizes, A., Samovich, S. N., Amoscato, A. A., Tyurin, V. A., Tyurina, Y. Y., Kagan, V. E., & Bunimovich, Y. L. (2021, Nov). Keratinocyte death by ferroptosis initiates skin inflammation after UVB exposure. *Redox Biol, 47*, 102143. https://doi.org/10.1016/j.redox.2021.102143

Wan, L., Jiang, D., Correa-Gallegos, D., Ramesh, P., Zhao, J., Ye, H., Zhu, S., Wannemacher, J., Volz, T., & Rinkevich, Y. (2021, Mar). Connexin43 gap junction drives fascia mobilization and repair of deep skin wounds. *Matrix Biology, 97*, 58-71. https://doi.org/10.1016/j.matbio.2021.01.005

Wang, G. G., Calvo, K. R., Pasillas, M. P., Sykes, D. B., Hacker, H., & Kamps, M. P. (2006, Apr). Quantitative production of macrophages or neutrophils ex vivo using conditional Hoxb8. *Nature Methods, 3*(4), 287-293. https://doi.org/10.1038/nmeth865

Wang, Z., Qi, F., Luo, H., Xu, G., & Wang, D. (2022). Inflammatory Microenvironment of Skin Wounds. *Front Immunol, 13*, 789274. https://doi.org/10.3389/fimmu.2022.789274

Whyte, J. L., Smith, A. A., & Helms, J. A. (2012, Aug 1). Wnt signaling and injury repair. *Cold Spring Harb Perspect Biol, 4*(8), a008078. https://doi.org/10.1101/cshperspect.a008078

Wong, C., Odom, S. L., Hume, K. A., Cox, A. W., Fettig, A., Kucharczyk, S., Brock, M. E., Plavnick, J. B., Fleury, V. P., & Schultz, T. R. (2015, Jul). Evidence-Based Practices for Children, Youth, and Young Adults with Autism Spectrum Disorder: A Comprehensive Review. *Journal Of Autism And Developmental Disorders, 45*(7), 1951-1966. https://doi.org/10.1007/s10803-014-2351-z

Wu, T., Hu, E., Xu, S., Chen, M., Guo, P., Dai, Z., Feng, T., Zhou, L., Tang, W., Zhan, L., Fu, X., Liu, S., Bo, X., & Yu, G. (2021, Aug 28). clusterProfiler 4.0: A universal enrichment tool for interpreting omics data. *Innovation (Camb), 2*(3), 100141. https://doi.org/10.1016/j.xinn.2021.100141

Yang, X. D., & Yang, Y. Y. (2022). Ferroptosis as a Novel Therapeutic Target for Diabetes and Its Complications. *Front Endocrinol (Lausanne), 13*, 853822. https://doi.org/10.3389/fendo.2022.853822

Yee, P. P., Wei, Y., Kim, S. Y., Lu, T., Chih, S. Y., Lawson, C., Tang, M., Liu, Z., Anderson, B., Thamburaj, K., Young, M. M., Aregawi, D. G., Glantz, M. J., Zacharia, B. E., Specht, C. S., Wang, H. G., & Li, W. (2020, Oct 27). Neutrophil-induced ferroptosis promotes tumor necrosis in glioblastoma progression. *Nat Commun, 11*(1), 5424. https://doi.org/10.1038/s41467-020-19193-y

Youn, C., Archer, N. K., & Miller, L. S. (2020, Aug). Research Techniques Made Simple: Mouse Bacterial Skin Infection Models for Immunity Research. *Journal Of Investigative Dermatology, 140*(8), 1488-1497 e1481. https://doi.org/10.1016/j.jid.2020.04.012

Zeng, N., Ma, L., Cheng, Y., Xia, Q., Li, Y., Chen, Y., Lu, Z., Lu, Q., Jiang, F., & Luo, D. (2021). Construction of a Ferroptosis-Related Gene Signature for Predicting Survival and Immune Microenvironment in Melanoma Patients. *Int J Gen Med, 14*, 6423-6438. https://doi.org/10.2147/IJGM.S327348

Zhang, Q., Tang, S., Huang, G., & Liu, H. (2022, Jul). Cigarettes, a skin killer! Cigarette smoke may cause ferroptosis in female skin. *J Cosmet Dermatol, 21*(7), 3085-3094. https://doi.org/10.1111/jocd.14559

Zhang, X., Ma, Y., Lv, G., & Wang, H. (2023). Ferroptosis as a therapeutic target for inflammation-related intestinal diseases. *Front Pharmacol, 14*, 1095366. https://doi.org/10.3389/fphar.2023.1095366

Zhou, Q., Yang, L., Li, T., Wang, K., Huang, X., Shi, J., & Wang, Y. (2022). Mechanisms and inhibitors of ferroptosis in psoriasis. *Front Mol Biosci, 9*, 1019447. https://doi.org/10.3389/fmolb.2022.1019447

Zhu, Y. P., Padgett, L., Dinh, H. Q., Marcovecchio, P., Blatchley, A., Wu, R., Ehinger, E., Kim, C., Mikulski, Z., Seumois, G., Madrigal, A., Vijayanand, P., & Hedrick, C. C. (2018, Aug 28). Identification of an Early Unipotent Neutrophil Progenitor with Pro-tumoral Activity in Mouse and Human Bone Marrow. *Cell Rep, 24*(9), 2329-2341 e2328. https://doi.org/10.1016/j.celrep.2018.07.097

Zilionis, R., Engblom, C., Pfirschke, C., Savova, V., Zemmour, D., Saatcioglu, H. D., Krishnan, I., Maroni, G., Meyerovitz, C. V., Kerwin, C. M., Choi, S., Richards, W. G., De Rienzo, A., Tenen, D. G., Bueno, R., Levantini, E., Pittet, M. J., & Klein, A. M. (2019, May 21). Single-Cell Transcriptomics of Human and Mouse Lung Cancers Reveals Conserved Myeloid Populations across Individuals and Species. *Immunity, 50*(5), 1317-1334 e1310. https://doi.org/10.1016/j.immuni.2019.03.009

6 Abbreviations

Abbreviation	Definition
3D	Three dimensions
ACLS4	Long-chain-fatty-acid—CoA ligase 4
ADSCS	Adipose tissue-derived stem cells
AF488	Alexa fluor 488
AKT	A serine/threonine protein kinase, protein kinase b
AMPK	Adenosine monophosphate activated protein kinase
ANOVA	Analysis of variance
ARDS	Acute respiratory distress syndrome
ATAD	Ascending thoracic aortic dissection
ATP	Adenosine triphosphate
BODIPY	Boron dipyrromethene fluorophore, difluoro[2-[(3,5-dimethyl-2h-pyrrol-2-ylidene-n) phenylmethyl]-3,5-dimethyl-1h-pyrrolato-n**] BORON**
BPD	Bronchopulmonary dysplasia
COPD	Chronic obstructive pulmonary disease
COX	Cox proportional hazards model
CR	Calorie restriction
CSTB	Cathepsin b
CYTOF	Cytometry by time of flight
DAMPS	Damage-associated molecular patterns
DAPI	4′,6-diamidino-2-phenylindole
DC	Dendritic cells
DFU	Non-healing foot ulcers
DMSO	Dimethyl sulfoxide
DNA	Deoxyribonucleic acid

DPBS	Dulbecco's phosphate buffered saline
ECM	Extracellular matrix
EDTA	Ethylenediaminetetraacetic acid
EMT	Epithelial-mesenchymal transition
ER	Estrogen receptor
ERA	Erastin
ERK	Extracellular-signal-regulated kinase
FAP-A	Fibroblast activation protein α
FBS	Fetal bovine serum
FER	Ferrostatin-1
FGF-1	Fibroblast growth factor 1
GEO	Gene expression omnibus
GM-CSF	Granulocyte-macrophage colony-stimulating factor
GMP	Granulocyte-monocyte progenitor
GPX4	Glutathione peroxidase 4
GSH	Glutathione
GSSG	Glutathione disulfide
HA	Hyaluronan
HBD1	Human beta defensin 1
HBOT	Hyperbaric oxygen therapy
HMGB1	High-mobility group box protein-1
HOXB8	Homeobox b8
HRT	Hormone replacement therapy
HSP47	Heat shock protein 47
IFN	Interferons

IL-1	Interleukin-1
IL-17A	Interleukin-17a
IL-6	Interleukin-6
IL-8	Interleukin-8
LASSO	Least absolute shrinkage and selection operator
LDH	Lactate dehydrogenase
MDSCS	Myeloid-derived suppressor cells
MM10	Mus musculus reference genome assembly version 10
MMP	Matrix metalloproteinase
MSC	Mesenchymal stem cells
NEP	Unipotent-committed neutrophil progenitor
NETS	Neutrophil extracellular traps
NHS-FITC	5/6-CARBOXYFLUORESCEIN SUCCINIMIDYL ESTER
OCT	Optimal cutting temperature
PAMPS	Pathogen-associated molecular patterns
PCA	PRINCIPAL COMPONENT ANALYSIS
PCR	Polymerase chain reaction
PDGF	Platelet-derived growth factor
PFUAS	POLYUNSATURATED FATTY ACIDS
PRFM	Platelet-rich fibrin matrix
PRP	Platelet-rich plasma
QC	Quality control
RNASEQ	RNA sequencing
ROS	Reactive oxygen species
RPMI1640	Roswell Park memorial institute 1640 medium

SCAD	Scar-like tissue in a dish
SCF	Stem cell factor
SCRNA	Single cells RNA sequencing
SDF-1	Stromal cell-derived factor-1
SLE	Systemic lupus erythematosus
SRA	Sequence read archive database
TAE	Tris-acetate-EDTA
TF	Transcription factor
TGF	Transforming growth factor
TLR4	Toll-like receptor 4
TNF-A	Tumor necrosis factor-alpha
UCSC	University of California, santa cruz
UMAP	Uniform manifold approximation and projection
UV	Ultraviolet
UVB	Ultraviolet b radiation
VEGF	Vascular endothelial growth factor
A-SMA	A-smooth muscle actin
ATOC	α-tocopherol

Acknowledgment

Arriving at this point has been a challenging journey, and the realization that time waits for no one has dawned upon me. As I conclude the final chapter, gratitude floods my thoughts for the multitude of individuals who supported, guided, and propelled me throughout my doctoral study. I feel compelled to express my sincere appreciation to each person who played a role in my academic endeavor.

Foremost, I extend my heartfelt thanks to my supervisor, Professor Dr. med. Jürgen Behr, a mentor of unparalleled kindness at Medizinische Klinik und Poliklinik V, Ludwigs-Maximilian University of Munich, Germany. It was under his guidance that I embarked on my journey in Human Biology (Dr. rer. biol. hum.). I am deeply grateful for his acceptance and the unwavering support provided, alongside the invaluable assistance from my co-supervisor, Dr. Yuval Rinkevich, the successful scientist at the Helmholtz Institute. Their dedication to this esteemed international research institute has been truly commendable.

Appreciation extends to all my colleagues in our lab, with special mention to Mrs. Sandra Schiener, Dr. Rinkevich's secretary, and Dr. Juliane Wannemacher and Mrs. Natalja Ring, our laboratory manager. Their generosity in offering assistance, whether related to work or personal matters, has been consistently remarkable. I also express gratitude to Dr. Dongsheng Jiang, my dear lab colleague, whose support in part of this project. Special thanks to Dr. Haifeng Ye, and Ms Ruoxuan Dai, Ms Yue Lin, Mr. Jin Xu, Ms Ruiji Guo and Ms Xiangyu Zhang for their contributions to the experimental aspects. To all other members, Dr. Donovon Correa Gallegos, Dr Adrian Fisher, Dr. Martin, Dr. Safoune Kardri … in our lab and institute, a sincere "Thank you!"

We express our gratitude to Dr. Conrad Marcus from Helmholtz Munich Centre Mice for providing $GPX4^{fl/fl}$. Our appreciation extends to Dr. Markus Sperandio from the Biomedical Centre of LMU for generously providing Catchup mice. Special thanks are also extended to Dr. David Sykes from Harvard Medical School for granting ER-Hoxb8 cells.

Crucially, I cannot overlook the vital support extended by the Chinese Scholarship Council & LMU Grant. Their acceptance as a doctoral candidate and financial

support allowed me to fully immerse myself in my studies. Their generosity has instilled in me a desire to contribute to the community, fostering a hope that I can one day assist others in achieving their aspirations.

Lastly, my deepest and most profound gratitude goes to my family—my wife and daughter—for their unwavering support. They have been my pillars, alleviating the pressures and accompanying me through the highs and lows of my academic and daily life. This achievement would not have been possible without their constant presence and encouragement.

Publications

1. **Connexin43 gap junction drives fascia mobilization and repair of deep skin wounds.**

   Wan L, Jiang D, Correa-Gallegos D, Ramesh P, **Zhao J**, Ye H, Zhu S, Wannemacher J, Volz T, Rinkevich Y.

   Matrix Biol. 2021. 97: 58-71

2. **Neutrophils direct preexisting matrix to initiate repair in damaged tissues.**

   Fischer A, Wannemacher J, Christ S, Koopmans T, Kadri S, **Zhao J**, Gouda M, Ye H, Muck-Hausl M, Krenn PW, Machens HG, Fassler R, Neumann PA, Hauck SM, Rinkevich Y.

   Nat Immunol. 2022. 23: 518-31

3. **Wound infiltrating adipocytes are not myofibroblasts.**

   Kalgudde Gopal S, Dai R, Stefanska AM, Ansari M, **Zhao J**, Ramesh P, Bagnoli JW, Correa-Gallegos D, Lin Y, Christ S, Angelidis I, Lupperger V, Marr C, Davies LC, Enard W, Machens HG, Schiller HB, Jiang D, Rinkevich Y.

   Nat Commun. 2023. 14: 3020

Affidavit

Zhao, Jiakuan

Surname, first name

I hereby declare, that the submitted thesis entitled

Neutrophils drive fascia matrix mobilization and regulate wound healing through ferroptosis

is my own work. I have only used the sources indicated and have not made unauthorised use of services of a third party. Where the work of others has been quoted or reproduced, the source is always given.

I further declare that the dissertation presented here has not been submitted in the same or similar form to any other institution for the purpose of obtaining an academic degree.

6,11,2024 Munich

Place, Date

Jiakuan Zhao

Signature doctoral candidate